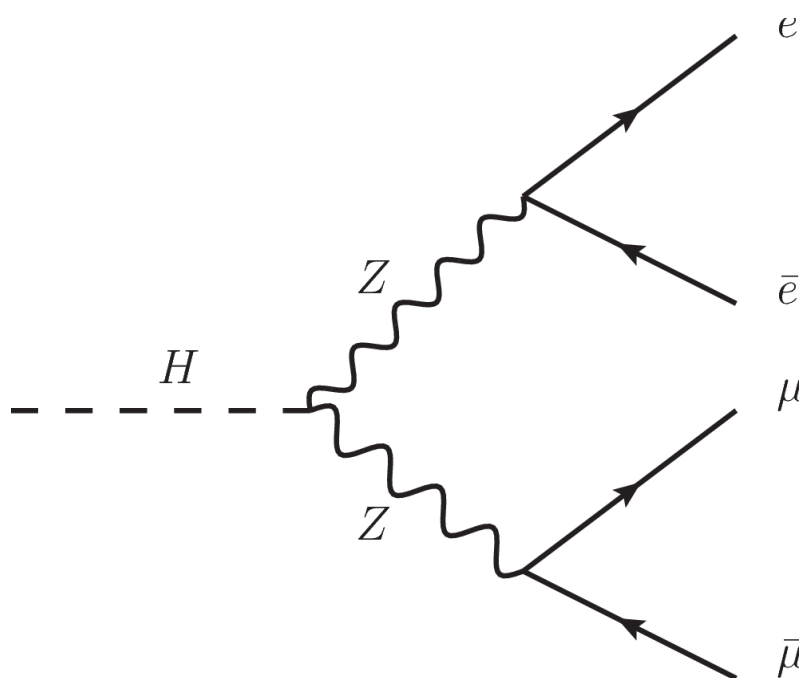# Theoretical predictions for Higgs boson decay into four leptons

Stefano Boselli

Tesi per il conseguimento del titolo

Università degli Studi di Pavia
Dipartimento di Fisica

DOTTORATO DI RICERCA IN FISICA – XXIX CICLO

Theoretical predictions for Higgs boson decay into four leptons

Stefano Boselli

Submitted to the Graduate School in Physics in partial
fulfilment of the requirements for the degree of
DOTTORE DI RICERCA IN FISICA
DOCTOR OF PHILOSPHY IN PHYSICS
at the University of Pavia

Supervisor: Fulvio Piccinini

Theoretical predictions for Higgs boson decay into four leptons

Stefano Boselli

Contents

Introduction

The Standard Model (SM) of particle physics represents one of the most important breakthroughs in the understanding of the fundamental interactions of Nature. On general grounds, the SM is a quantum field theory which incorporates the Electroweak (EW) theory, proposed by Glashow, Salam and Weinberg, to describe the electromagnetic and weak interactions among leptons and quarks in a unified way [1, 2, 3], and Quantum Chromodynamics (QCD), the theory of strong interactions among colored quarks [4, 5, 6]. The phenomenon of Electroweak Symmetry Breaking (EWSB) is a cornerstone of the theory [7, 8, 9, 10, 11, 12]. In a nutshell, the EWSB is a mechanism which allows to generate weak boson masses in a way that preserves the renormalizability [13, 14, 15] and unitarity [16, 17, 18, 19] of the theory. The Higgs boson can be thought as a leftover of this mechanism, and its discovery represented for many years one of the most challenging tests of the SM. Ever since the SM took its present form in the 1970s, a multitude of experiments has been performed to test its reliability: from the discovery of the weak neutral currents by the Gargamelle experiment [20, 21, 22] up to the precision measurements carried out over the decades at LEP, SLC, Tevatron and nowadays at LHC, the excellent agreement between SM predictions and experimental results has established that the SM provides a faithful description of strong and electroweak interactions, at least up to the accessible energy scales. Then, with the discovery by ATLAS [23] and CMS [24] collaborations, of a spin-0 neutral boson, whose properties closely resemble those of the Higgs boson, the last missing piece of the SM puzzle has been eventually found. The discovery of a particle compatible with the SM Higgs boson marks the beginning of a new era for high energy physics, where the EWSB sector can be finally probed by the experiments. After the discovery, many efforts have been devoted to the study of the Higgs boson properties, such as mass, spin, parity, and couplings [25, 26, 27, 28]. From the point of view of

Higgs searches at the LHC, a Higgs boson mass of about 125 GeV represents a very lucky coincidence. In fact, for this mass value, ATLAS and CMS are able to observe the Higgs boson in several production and decay channels, some of them allowing for a precise reconstruction of the invariant mass. Nowadays, the most precise estimate of the Higgs boson mass is provided by the combined analysis of the data collected by ATLAS and CMS during the LHC Run-1 [29],

$$M_H = 125.09 \pm 0.21 \,(\text{stat.}) \pm 0.11 \,(\text{sys.}) \,\text{GeV.}$$

Regarding the spin-parity properties, the data analyzed by ATLAS and CMS strongly favor the scalar nature $J^P = 0^+$ of the observed particle, rejecting other non-standard hypothesis $\left(J^P = 0^-, 1^\pm, 2^\pm \right)$ or the possibility of CP mixtures [30, 31]. Last but not least, the ATLAS and CMS combined measurements of Higgs boson production and decay rates, as well as the constraints on its couplings to vector bosons and fermions, are consistent with the SM predictions [32]. Although the present data are in agreement with the SM hypothesis, one of the main tasks of the LHC program for the next years will be the precise determination of the Higgs profile and the unraveling of the EWSB mechanism. The main production modes, *i.e.* the loop induced gluon-gluon fusion, the vector boson fusion, the associate Higgs production with a W or a Z boson and the associate production with a $t\bar{t}$ pair, have to be thoroughly investigated, either in the most accessible decay channels, as the $H \to \gamma\gamma$, $H \to 4\ell$ and $H \to 2\ell 2\nu_\ell$, or in those channels, as $H \to \tau\tau$ and $H \to b\bar{b}$, where the unfavorable signal to background ratios are compensated by larger decay rates. Finally, the measurement of the Higgs self coupling would allow for the complete determination of the Higgs potential.

The precise determination of the Higgs properties is of great importance also for New Physics searches. Since no tantalizing hints of new particles have emerged so far, it is reasonable to assume that the scale of new physics is too heavy to be directly probed at the LHC. In this scenario, the best chance to find evidence of new physics would lie in the discovery of discrepancies between experimental data and theoretical predictions in SM processes. For instance, higher-order corrections due to heavy particles would give rise to anomalous couplings among SM particles, with consequent deviations from SM predictions at the level of total rates and differential distributions. Concerning the Higgs sector, more accurate measurements of the Higgs couplings to fermions and gauge bosons will be then mandatory to unveil effects of new physics, if additional ingredients beyond those of the SM are involved. This is particularly true in weakly interacting theories such as Supersymmetric

theories (SUSY) in which the quantum effects are expected to be small if the scale of mass of new particles is sufficiently light. At present, in order to improve the sensitivity to New Physics, a large increase of the integrated luminosity at the LHC is the option on which there is a wide consensus in the community. According to the High Luminosity LHC project (HL-LHC), an integrated luminosity of 3 ab^{-1} per experiment should be the goal for the next decade. The prospects for Higgs physics in the HL-LHC project have been discussed in Refs. [33, 34, 35].

My PhD project has been developed in view of the precise theoretical predictions which are necessary to explore the Higgs sector with continuously increasing detail. In particular, I have focused my attention on the Higgs boson decay into four charged leptons. This decay channel plays a particularly relevant rôle, as it provides the cleanest experimental signature, given by a peak in the four lepton invariant mass spectrum on top of a flat and small background. The $H \to 4\ell$ decay mode allows to derive a precise mass measurement in the different combinations of lepton final states, to assess the spin-parity quantum numbers using sensitive angular distributions and to perform precision tests of the SM at the level of differential cross sections.

As a first step, the full set of Next-to-Leading Order (NLO) electroweak corrections to $H \to Z^{(*)}Z^{(*)} \to 4\ell$, with $4\ell = 4e, 4\mu, 2e2\mu$ has been calculated. The calculation is publicly available in a new event generator, `Hto4l` [36]. A preliminary study on the impact of the gauge-invariant NLO and higher-order leading-logarithmic (LL) QED corrections to the determination of the Higgs boson mass in the $H \to 4\ell$ decay was performed in Refs. [37, 38]. The NLO electroweak and QCD corrections to the Higgs decay into four fermions have been calculated in Refs. [39, 40] and are available in the Monte Carlo (MC) program `Prophecy4f` [41, 42], which is used in the context of Higgs studies at the LHC [25, 26, 27] for the precision calculation of the branching ratios of the decays $H \to Z^{(*)}Z^{(*)}/W^{(*)}W^{(*)} \to 4$ fermions, including all the leptonic, semi-leptonic and hadronic channels. Then, as a sanity check, a tuned comparison of the two codes was performed, finding an excellent agreement. Once the NLO accuracy was achieved, the NLO corrections have been matched with a QED PS, in order to simulate multiphoton emission exclusively, providing final results at NLOPS electroweak accuracy[1]. In the treatment of higher-order QED corrections, the present calculation differs from the one implemented in `Prophecy4f`, where multiphoton effects are taken into account in terms of QED collinear Structure Functions. Once the NLOPS accuracy was achieved, an interesting develop-

---

[1]NLOPS accuracy is the precision level of a calculation which includes the virtues of a NLO calculation with the ones of a PS simulation.

ment of the work has been identified in the inclusion of New Physics (NP) effects in the $H \to 4\ell$ decay width. In particular, an Effective Field Theory (EFT) framework has been adopted for a model independent parametrization of NP effects. The main motivation is that, given the absence of any direct or indirect signal of new physics, it is reasonable to assume that the scale where new particles would eventually appear is at least in the TeV range and consequently the low energy effects of new physics are well described by an EFT Lagrangian. Moreover, the particularly clean signature and the non-trivial kinematics make the $H \to 4\ell$ an important channel for searching indirect evidence of new physics. The EFT Lagrangian can be understood as arising from integrating out the new heavy degrees of freedom, so that the different terms in the Lagrangian are obtained from a systematic expansion in the inverse power of the NP scale. Interactions with arbitrary mass dimension D larger than four are allowed in this framework and the leading order term in the expansion is the SM Lagrangian with operators up to $D = 4$.

This dissertation is organized as follows: in Chapter 1 a general introduction to Electroweak Theory is given. In particular, we illustrate the problem of building a massive theory for electroweak interactions and we describe the solution provided by the EWSB mechanism. Since one of the building blocks of the work is the computation of $\mathcal{O}(\alpha)$ EW corrections to the $H \to 4\ell$ decay channel, a sizeable part of the chapter is devoted to the illustration of the on-shell renormalization scheme. Furthermore, in order to treat the finite width effects of unstable particles in a consistent way, the complex-mass scheme, introduced in Ref. [43] and adopted in our calculation, is also described. Chapter 2 deals with the problem of infrared divergences arising in QED virtual and real higher-order corrections and their cancellation. The remaining part of the chapter is devoted to the problem of collinear enhancement in QED. In particular, a general introduction to the collinear factorization problem in QED is given. Then, the structure function for the electron and the related Altarelli-Parisi equations are derived. Finally, we describe the main features of the Parton Shower algorithm in QED, which is one of the main ingredients of the calculation. Chapter 3 provides a general overview on the Higgs searches at the LHC: the main Higgs production and decay mechanisms are reviewed, with a special attention to the state of the art of theoretical calculations and related numerical tools. Then, the main aspects of the Higgs particle discovery and the current efforts in the determination of Higgs boson properties are summarized. In Chapter 4 we detail the calculation of $\mathcal{O}(\alpha)$ EW corrections to the Higgs decay into four charged leptons and the matching scheme for the consistent inclusion of a Parton Shower on top of the NLO calculation. The calculation has been implemented in `Hto4l`, a new Monte Carlo event generator which describes the Higgs boson decay

into four charged leptons up to NLOPS accuracy. In Chapter 5 we show and discuss the numerical results which have been obtained with `Hto4l`. First, we show the comparison of our NLO predictions with the ones obtained with `Prophecy4f`. Then, our best predictions at NLOPS accuracy are described. In particular, since the full calculation can be split in different contributions, a critical discussion on the impact of higher-order corrections is performed for some observables of particular interest in experimental analysis. In Chapter 6 we describe the EFT approach that we have adopted for the study of BSM effects on the Higgs decay into four charged leptons and we show and discuss some preliminary results. Finally, in the last chapter, we draw our conclusions.

The main features of the calculation described in Chapter 4 and the results presented in Chapter 5 have been published in the Journal of High Energy Physics in 2015 (see Ref. [36]) and will appear in the CERN Yellow Report 4 [28]. A paper on the BSM effects on the Higgs decay into four charges leptons, studied in Chapter 6, is in preparation and will be submitted to a peer-reviewed journal in the next weeks.

Chapter 1

The Standard Model of Electroweak interactions

The SM of particle physics is a quantum field theory which describes in a unified framework the electromagnetic, weak and strong interactions between leptons and quarks at the quantum level. It can be thought as the combination of QCD [4, 5, 6], the theory of strong interactions, and the Glashow-Salam-Weinberg electroweak (EW) theory [1, 2, 3].

The purpose of this chapter is to provide a short introduction to the EW sector of the SM. In Sec. 1.1 we introduce a massless Yang-Mills Lagrangian that is locally invariant under the symmetry group $SU(2)_L \otimes U(1)_Y$ of left isospin and hypercharge and we will show that a naive incorporation of mass terms for weak gauge bosons and fermions leads to a violation of the gauge symmetry. On the other side, from the short-range nature of weak interactions it follows that the related gauge bosons have to be massive. In Sec. 1.2 we introduce the EWSB mechanism [7, 8, 9, 10, 11, 12] as a clever solution of generating weak boson masses in a gauge invariant way. In particular, we introduce a gauge invariant Lagrangian for a scalar doublet and we describe how a non-zero vacuum expectation value for this field breaks the $SU(2)_L \otimes U(1)_Y$ symmetry down to electromagnetic $U(1)_{em}$ gauge invariance, leading weak bosons to acquire mass. Of the new four degrees of freedom, three are absorbed in the longitudinal components of the massive weak bosons, while the remaining one is a physical field. The spin-0 particle associated to this field is the Higgs boson. Fermion masses are generated by coupling fermions to the Higgs field in a gauge invariant way through Yukawa interaction terms.

We dedicate the remaining sections to the renormalization of the EW theory, which is necessary for the treatment of the UV divergences arising in

7

the calculations of higher-order corrections. The formal proof that a Yang-Mills theory in presence of spontaneous symmetry breaking, such as the SM, is renormalizable, was given by 't Hooft in Ref. [13]. In Sec. 1.3 we introduce the problem of gauge-fixing and we introduce the renormalizable 't Hooft-Feynman gauge according to the Faddeev-Popov procedure [44]. In Sec. 1.4 we describe the on-shell renormalization scheme, proposed in Ref. [45] and widely used in electroweak precision calculations. Finally, in Sec. 1.5 we take into account the problems arising when finite width effects are included in the calculations of scattering amplitudes and we introduce the complex-mass scheme, which allows to include such effects without running into gauge dependent results.

1.1 A massless theory of Electroweak interactions

Before starting to deal with the EWSB mechanism, it is worthwhile to give a hint of the puzzling dilemma the theoretical community was facing in the mid-sixties. To this end we start with the development of a massless Lagrangian for the electroweak interactions. In this Lagrangian quarks and leptons are organized in three generations of left-handed and right-handed chiral fermionic fields $f_{L,R} = \frac{1}{2} \left(1 \mp \gamma_5 \right) f$. Left-handed fermions are in weak isodoublets, while right-handed ones are in weak isosinglets

$$
\begin{aligned}
L_1 &= \begin{pmatrix} \nu_e \\ e \end{pmatrix}_L, & e_{R_1} &= e_R^-, & Q_1 &= \begin{pmatrix} u \\ d \end{pmatrix}_L, & u_{R_1} &= u_R, & d_{R_1} &= d_R, \\
L_2 &= \begin{pmatrix} \nu_\mu \\ \mu \end{pmatrix}_L, & e_{R_2} &= \mu_R^-, & Q_2 &= \begin{pmatrix} c \\ s \end{pmatrix}_L, & u_{R_2} &= c_R, & d_{R_2} &= s_R, \quad (1.1) \\
L_3 &= \begin{pmatrix} \nu_\tau \\ \tau \end{pmatrix}_L, & e_{R_3} &= \tau_R^-, & Q_3 &= \begin{pmatrix} t \\ b \end{pmatrix}_L, & u_{R_3} &= t_R, & d_{R_3} &= b_R,
\end{aligned}
$$

with $I_{L,Q}^3 = \pm(1/2)$ and $I_{R_i}^3 = 0$. Assuming that the unified theory for weak and electromagnetic interactions must account for electric charge conservation, the hypercharge quantum numbers are derived by the Gell-Mann-Nishijima formula,

$$
Y_f = 2(Q_f - I_f^3), \tag{1.2}
$$

where the electric charge Q_f is expressed in terms of the proton charge $+e$. From Eq. (1.2) it follows

$$Y_{L_i} = -1, \quad Y_{e_{R_i}} = -2, \quad Y_{Q_i} = \frac{1}{3}, \quad Y_{u_{R_i}} = \frac{4}{3}, \quad Y_{d_{R_i}} = -\frac{2}{3}. \qquad (1.3)$$

The Lagrangian for free fermionic fields containing only the kinetic terms

$$\mathcal{L}_{kin} = i \sum_{j=1}^{3} \left(\bar{L}_j \slashed{\partial} L_j + \bar{e}_{R_j} \slashed{\partial} e_{R_j} + \bar{Q}_j \slashed{\partial} Q_j + \bar{u}_{R_j} \slashed{\partial} u_{R_j} + \bar{d}_{R_j} \slashed{\partial} d_{R_j} \right) \qquad (1.4)$$

is invariant under a global $SU(2)_L \otimes U(1)_Y$ transformation

$$L_i \rightarrow L'_i = e^{(i\alpha_a T^a + i\beta Y)} L_i, \qquad R_i \rightarrow R'_i = e^{i\beta Y} R_i, \qquad (1.5)$$

where T^a are the generators of the $SU(2)$ group defined by the commutation relations

$$\left[T^a, T^b \right] = i f^{abc} T^c. \qquad (1.6)$$

These generators are equivalent to $T^a = \frac{1}{2}\tau^a$, where τ^a are the 2x2 Pauli matrices

$$\tau_1 = \begin{pmatrix} 0 & 1 \\ 1 & 0 \end{pmatrix}, \quad \tau_2 = \begin{pmatrix} 0 & -i \\ i & 0 \end{pmatrix}, \quad \tau_3 = \begin{pmatrix} 1 & 0 \\ 0 & -1 \end{pmatrix}. \qquad (1.7)$$

In order to obtain an interacting Lagrangian invariant under local symmetry transformations, namely when α and β are functions of the spacetime coordinates, we need to incorporate in the Lagrangian as many spin-1 bosonic fields as the number of the generators of the symmetry group. In other words, we have to introduce three W_μ^a fields associated with the $SU(2)$ generators T^a and a B_μ field associated with the Y generator. The fermionic fields are minimally coupled to the gauge fields by replacing ∂_μ with the covariant derivative D_μ, defined as

$$D_\mu = \partial_\mu - i g_2 T_a W_\mu^a - i g_1 \frac{Y}{2} B_\mu. \qquad (1.8)$$

The Lagrangian that we obtain with this substitution is invariant under $SU(2)_L \otimes U(1)_Y$ gauge symmetry group if the local version of the transformation in Eq. (1.5) is followed by the following transformations of the gauge fields:

$$\vec{W}_\mu(x) \rightarrow \vec{W}_\mu(x) - \frac{1}{g_2} \partial_\mu \vec{\alpha}(x) - \vec{\alpha}(x) \times \vec{W}_\mu(x) \qquad (1.9a)$$

$$B_\mu(x) \rightarrow B_\mu(x) - \frac{1}{g_1} \partial_\mu \beta(x). \qquad (1.9b)$$

Finally, we have to include a gauge invariant Lagrangian for the kinetic terms of the gauge fields. The field-strength tensors for W^a and B fields can be derived by the commutator of covariant derivatives, from which the Feynman rules for gauge-bosons self-interactions can be also derived. Since the covariant derivative has been introduced in order to have

$$D_\mu\psi \to e^{i\alpha(x)}D_\mu\psi, \tag{1.10}$$

also the commutator of the covariant derivative must be invariant. For the EW case it follows that,

$$[D_\mu, D_\nu] = -ig_2 W^a_{\mu\nu} - ig_1\frac{Y}{2}B_{\mu\nu}, \tag{1.11}$$

where

$$W^a_{\mu\nu} = \partial_\mu W^a_\nu - \partial_\nu W^a_\mu + g_2\epsilon^{abc}W^b_\mu W^c_\nu, \tag{1.12a}$$

$$B_{\mu\nu} = \partial_\mu B_\nu - \partial_\nu B_\mu, \tag{1.12b}$$

are respectively the W and B field-strength tensors. The pure bosonic part of the EW Lagrangian can be written as

$$\mathcal{L}_{gauge} = -\frac{1}{4}W^a_{\mu\nu}W^{\mu\nu,a} - \frac{1}{4}B_{\mu\nu}B^{\mu\nu}. \tag{1.13}$$

The first term of Eq. (1.13) contains trilinear and quartic self interactions of the W fields which are proportional to the structure constants of the $SU(2)$ Lie algebra, and thus directly linked to the non-Abelian structure of the symmetry group.

The theory we have described so far is not suitable to describe short-ranged weak interactions. A gauge-boson mass term of the form $\frac{1}{2}M_V^2 V_\mu V^\nu$ violates local $SU(2)\otimes U(1)$ gauge invariance. For the sake of clearness we show the easier case of QED, where a mass term for the photon field would transform under a $U(1)_{em}$ gauge transformation as

$$\frac{1}{2}M_A^2 A_\mu A^\mu \to \frac{1}{2}M_A^2\left(A_\mu - \frac{1}{e}\partial_\mu\alpha\right)\left(A^\mu - \frac{1}{e}\partial^\mu\alpha\right) \neq \frac{1}{2}M_A^2 A_\mu A^\nu. \tag{1.14}$$

On the other hand, in spite of the QED case, also mass terms for fermions lead to gauge invariance violations. In fact, a mass term of the form $-m_f\bar{f}f$ can be rewritten as

$$-m_f \bar{f} f = m_f \bar{f} \left(\frac{1}{2} \left(1 - \gamma_5 \right) + \frac{1}{2} \left(1 + \gamma_5 \right) \right) f = -m_f \left(\bar{f}_R f_L + \bar{f}_L f_R \right), \quad (1.15)$$

which is not invariant under isospin transformation.

Now that we have shown why a trivial inclusion of mass terms in the SM Lagrangian is not an available option, the terms of the problem should be evident. Is there a chance to include mass terms for weak bosons and fermions without giving up with gauge invariance?

1.2 The electroweak symmetry breaking in the Standard Model

Since a massive spin-1 particle can be found in three polarization states, we need to introduce at least three new degrees of freedom, two for the charged $W^\pm$ bosons and one for the neutral Z boson, while the photon has to remain massless. In the Brout-Englert-Higgs (BEH) mechanism of EWSB [7, 8, 9] four additional degrees of freedom are provided by the complex doublet

$$\Phi = \begin{pmatrix} \varphi^+ \\ \varphi^0 \end{pmatrix}, \qquad Y_\Phi = +1, \quad (1.16)$$

which is minimally coupled to the gauge fields through the Lagrangian

$$\mathcal{L}_{Higgs} = \left(D^\mu \Phi \right)^\dagger \left(D_\nu \Phi \right) - V \left(\Phi \right), \quad (1.17)$$

where the potential includes a mass and a self-interaction term:

$$V \left(\Phi \right) = -\mu^2 \Phi^\dagger \Phi + \frac{\lambda}{4} \left(\Phi^\dagger \Phi \right)^2. \quad (1.18)$$

Assuming $\lambda > 0$ (otherwise the potential would not be bounded from below) and $\mu^2 > 0$, the potential has a minimum for a non-vanishing energy and the Φ field develops a Vacuum Expectation Value (vev),

$$\langle \Phi \rangle_0^2 = \left| \langle 0 | \Phi | 0 \rangle \right|^2 = \frac{v^2}{2} = \frac{2\mu^2}{\lambda}. \quad (1.19)$$

Since the vacuum has to be electrically neutral in order to preserve the $U(1)_e$ QED symmetry, the ground state is

$$\Phi_0 = \begin{pmatrix} 0 \\ \frac{v}{\sqrt{2}} \end{pmatrix}, \quad (1.20)$$

while small excitations from the ground state can be parametrized by the formula

$$\Phi = \frac{1}{\sqrt{2}} \begin{pmatrix} \varphi_2 + i\varphi_1 \\ v + H - i\varphi_3 \end{pmatrix} = \begin{pmatrix} \varphi^+ \\ \frac{1}{\sqrt{2}} (v + H + i\chi) \end{pmatrix}, \qquad (1.21)$$

where H is the Higgs field with mass $\sqrt{2}\mu$, while $\varphi^+ = \frac{1}{\sqrt{2}} (\varphi_2 + i\varphi_1)$ and $\chi = -\varphi_3$ are unphysical Goldstone fields. A generic state for the Φ field can be obtained by a $SU(2)$ transformation of a gauge equivalent state where only the Higgs field is present:

$$\Phi(x) = \begin{pmatrix} \varphi(x)^+ \\ \frac{1}{\sqrt{2}} (v + H(x) + i\chi(x)) \end{pmatrix} = \exp\left(i\frac{\varphi_a(x)\tau^a}{v} \right) \begin{pmatrix} 0 \\ \frac{1}{\sqrt{2}} (v + H(x)) . \end{pmatrix}$$
$$(1.22)$$

Therefore, since the φ_i can be regarded as parameters of local gauge transformations, they cannot be physical fields, we can adopt the so called unitary gauge where the would-be Goldstone bosons are not present. In order to see how weak bosons acquire mass we expand the derivative term in (1.17):

$$|D_\mu \Phi|^2 = \frac{1}{\sqrt{2}} (\partial_\mu H)^2 + \frac{1}{8} g_2^2 (v + H)^2 |W_\mu^1 + iW_\mu^2|^2 + \frac{1}{8} (v + H)^2 |g_2 W_\mu^3 - g_1 B_\mu|^2.$$
$$(1.23)$$

From Eq. (1.23) we can derive the transformations for the expressions of the physical $W_\mu^\pm$, Z_μ and A_μ fields as a superposition of the gauge fields W_μ^i and B_μ. In fact, identifying the mass terms as those proportional to v^2, we define

$$W^\pm = \frac{1}{\sqrt{2}} \left(W_\mu^1 \mp iW_\mu^2 \right) \qquad (1.24)$$

$$\begin{pmatrix} Z_\mu \\ A_\mu \end{pmatrix} = \begin{pmatrix} c_W & s_W \\ -s_W & c_W \end{pmatrix} \begin{pmatrix} W_\mu^3 \\ B_\mu \end{pmatrix}, \qquad (1.25)$$

where

$$c_W = \cos\theta_W = \frac{g_2}{\sqrt{g_1^2 + g_2^2}}, \qquad s_W = \sin\theta_W, \qquad (1.26)$$

and θ_W is the weak mixing angle. The W and Z masses are:

$$M_W = \frac{1}{2} v g_2 \qquad M_Z = \frac{1}{2} v \sqrt{g_1^2 + g_2^2}, \qquad (1.27)$$

while the photon remains massless as it has to be. Replacing the couplings in (1.26) with the boson masses we derive the relation:

$$c_W^2 = \frac{M_W^2}{M_Z^2}, \qquad s_W^2 = 1 - \frac{M_W^2}{M_Z^2} \qquad (1.28)$$

while the transformation (1.25) in the gauge Lagrangian (1.13) and the identification of the electric charge e with the coupling of the photon field A_μ to the lepton currents yields:

$$e = \frac{g_1 g_2}{\sqrt{g_1^2 + g_2^2}}, \qquad g_1 = \frac{e}{c_W}, \qquad g_2 = \frac{e}{s_W}. \tag{1.29}$$

We still have to incorporate gauge invariant mass terms for the fermions in the EW Lagrangian. This can be done by introducing the most general gauge invariant Lagrangian for the interactions between the Higgs doublet and the fermion fields. To this end we introduce the charge conjugate of the Higgs field

$$\tilde{\Phi} = i\tau_2 \Phi^*, \tag{1.30}$$

and the Yukawa Lagrangian

$$\mathcal{L}_{Yukawa} = -\sum_{i=1}^{3} \left(\bar{L}'_i G_{ij}^l e'_{R,j} \Phi + \bar{Q}'_i G_{ij}^d d'_{R,j} \Phi + \bar{Q}'_i G_{ij}^u u'_{R,i} \tilde{\Phi} + \text{h.c.} \right), \tag{1.31}$$

where prime denotes interactions eigenstates and h.c. stands for the hermitian conjugate of the terms in Eq. (1.31). The Yukawa couplings are complex 3x3 matrices in generation space. In order to isolate the mass terms for fermions we express the interaction eigentstates in terms of (unprimed) mass eigenstates through the relations:

$$\bar{\psi}_{L,i} = \sum_{j=1}^{3} U_{L,ij} \psi_{L,j} \qquad \bar{\psi}_{R,i} = \sum_{j=1}^{3} U_{R,ij} \psi_{R,j}, \tag{1.32}$$

where ψ represents both quark and lepton fields. Then, by picking up the vev in the Higgs field, we get

$$m_{ij} = \delta_{ij} \frac{v}{\sqrt{2}} \sum_{k,l=1}^{3} U_{L,ik} G_{kl} U_{L,lj}^\dagger. \tag{1.33}$$

For leptons and neutrinos we can set the transformation matrices equal to the identity. The absence of a term coupling the lepton fields to $\tilde{\Phi}$ leaves the neutrino massless, as it must be if neutrino oscillations are neglected. On the other hand, we have to consider the quark mixing in the charged current interactions, parametrised by the Cabibbo-Kobayashi-Maskawa (CKM) matrix [46, 47], which can be written as:

$$U_L^u U_L^{d\dagger} = V_{CKM} = \begin{pmatrix} V_{ud} & V_{us} & V_{ub} \\ V_{cd} & V_{cs} & V_{cb} \\ V_{td} & V_{ts} & V_{tb} \end{pmatrix}. \tag{1.34}$$

It can be easily shown that quark mixing appears only in the charged currents. Since V_{CKM} can be parametrized by three angles and a complex phase we can say that quark mixing takes into account CP violation effects.

1.3   Gauge fixing and ghost fields

In the previous section we have isolated the mass terms for weak bosons and fermions from the classical Lagrangian

$$\mathcal{L}_C = \mathcal{L}_{kin} + \mathcal{L}_{gauge} + \mathcal{L}_{Higgs} + \mathcal{L}_{Yukawa}. \tag{1.35}$$

In principle, from Eq. (1.35) it is possible to derive all the couplings for the interactions between classical fields. However, in order to derive the expressions for the field propagators we have to define a gauge-fixing procedure. As anticipated in the previous section, in the unitary gauge the gauge fixing condition is chosen in order to get rid of the would-be Goldstone bosons. The explicit expressions for gauge-boson propagators read:

$$\Delta_V^{\mu\nu}(k) = \frac{-ig^{\mu\nu} + ik^{\mu}k^{\nu}/M_V^2}{k^2 - M_V^2}. \tag{1.36}$$

Although the unitary gauge has the virtue to leave only the physical fields in the Lagrangian, it is preferable to work in a gauge where the gauge-boson propagators behave as k^{-2} for large momenta. For this reason we adopt the so called R_{ξ} gauge. According to the Faddeev-Popov (FP) procedure [44], the gauge-fixing condition is chosen in order to remove the mixing terms $V_{\mu}\partial^{\mu}\varphi$ between gauge bosons and would-be Goldstone bosons which give rise to non-diagonal propagators. To this end we introduce the gauge-fixing Lagrangian

$$\mathcal{L}_{fix} = -\frac{1}{2}\left[\left(C^A\right)^2 + \left(C^Z\right)^2 + 2\left(C^+C^-\right)\right], \tag{1.37}$$

where the gauge fixing operators C^V are

$$C^A = \frac{1}{\sqrt{\xi_1^A}}\partial^{\mu}A_{\mu},$$

$$C^Z = \frac{1}{\sqrt{\xi_1^Z}}\partial^{\mu}Z_{\mu} - \sqrt{\xi_2^Z}M_Z\chi, \tag{1.38}$$

$$C^{\pm} = \frac{1}{\sqrt{\xi_1^W}}\partial^{\mu}W_{\mu}^{\pm} \mp iM_W\sqrt{\xi_2^W}\varphi^{\pm}.$$

The mixing terms $V_{\mu}\partial^{\mu}\varphi$ in the classical Lagrangian are cancelled by the mixing terms in Eq. (1.37), while the quadratic terms in the gauge fields lead to the following expressions for the gauge-boson propagators:

$$\Delta_V^{\mu\nu}(k) = \frac{-i}{k^2 - M_V^2} \left(g^{\mu\nu} - \left(1 - \xi_2^V\right) \frac{k^\mu k^\nu}{k^2 - \xi_2^V M_V^2} \right). \qquad (1.39)$$

The transverse parts of the propagators are independent of the gauge parameters, whereas the longitudinal component are gauge dependent and thus have to disappear in S-matrix elements. Furthermore, the quadratic terms of the form $\xi_2^W M_W^2$ and $\xi_2^Z M_Z^2$ can be identified as mass terms for the would-be Goldstone bosons. Then, the Goldstone-boson propagator take the form

$$\Delta_\varphi^V(k) = \frac{i}{k^2 - \xi_2^V M_V^2}. \qquad (1.40)$$

It just remains to consider the Lagrangian for the FP ghost fields,

$$\mathcal{L}_{FP} = -\int d^4y d^4z\, \bar{u}^a(x) \left(\frac{\delta C^a(x)}{\delta V_\nu^c(z)} \frac{\delta V_\nu^c(z)}{\delta \theta^b(y)} + \frac{\delta C^a(x)}{\delta \varphi^c(z)} \frac{\delta \varphi^c(z)}{\delta \theta^b(y)} \right) u^b(y), \quad (1.41)$$

where $\delta\theta^i$ represents an infinitesimal gauge transformation. The coupling of the Faddeev-Popov ghost fields $u^\pm$, u^Z, u^A with gauge fields and would-be Goldstone bosons can be derived by inserting the gauge-fixing operators in Eq. (1.41), whereas from the bilinear terms we get the expressions for the ghost propagators

$$\Delta_u^V(k) = \frac{i}{k^2 - \xi_V M_V^2}. \qquad (1.42)$$

We note that ghost and Goldstone propagators have the same ξ_V dependence of the corresponding gauge-boson longitudinal components. This is necessary to remove the unphysical poles in the S-matrix elements. The unitary gauge can be recovered by taking the limit $\xi_a \to \infty$, so that the masses of unphysical bosons become infinite and the latter decouple from the rest of the theory. In this work we adopt the 't Hooft-Feynman gauge, corresponding to $\xi_V = 1$, so that the longitudinal components of weak bosons are absent and the propagators of unphysical particles have the same poles of the corresponding gauge bosons.

1.4 Renormalization

Eventually, after the inclusion of gauge fixing through the Faddeev-Popov procedure the complete renormalizable Lagrangian for the electroweak interactions reads

$$\mathcal{L}_{SM} = \mathcal{L}_C + \mathcal{L}_{fix} + \mathcal{L}_{FP}, \qquad (1.43)$$

whence the Feynman rules can be derived and measurable quantities for a given process can be in principle calculated at any order of the perturbative expansion (in this work we use the Feynman rules summarized in Appendix A of Ref. [48]). In order to produce theoretical predictions we need as many experimental inputs as the free parameters of the Lagrangian. For the EW theory they can be chosen as the electromagnetic coupling constant, the mass of the particles and the CKM matrix elements,

$$e, \quad M_W, \quad M_Z, \quad M_H, \quad m_f, \quad V_{CKM}. \tag{1.44}$$

All the other parameters can be derived from this set. For instance, the value of the weak mixing angle is fixed through the relation in Eq. (1.28). The calculation of next-to-leading order (NLO) corrections to a generic process proceeds through the evaluation of the virtual diagrams where a closed loop has to be connected to each vertex, internal and external lines. The corresponding integral over the unconstrained loop momentum q may not be finite in the high momentum region and the ultraviolet (UV) divergences, which may arise, would forbid any physical interpretation of the (bare) parameters appearing in Eq. (1.43). However, if a theory is renormalizable all UV divergences drop out in the relations that express physical observables in terms of measurable quantities[1]. The proof that a non-abelian gauge theory in presence of spontaneous symmetry breaking, and thus the SM, is renormalizable was given by 't Hooft in Ref. [14]. On general grounds, in the counterterm approach the fields and the parameters are split into a finite, renormalized part and a divergent counterterm, so that the bare Lagrangian can be written as

$$\mathcal{L}_0 = \mathcal{L} + \mathcal{L}_{\mathrm{CT}}. \tag{1.45}$$

The renormalized Lagrangian $\mathcal{L}$ has the same form of $\mathcal{L}_0$ with bare parameters and fields replaced by renormalized ones, while from $\mathcal{L}_{\mathrm{CT}}$ we can derive the Feynman rules for the counterterms which have to be taken into account in the calculation of higher-order corrections.

The counterterms and the renormalized parameters are fixed through appropriate renormalization conditions, and the values of renormalized quantities are determined through experimental inputs. Throughout this work we adopt the on-shell renormalization scheme, developed by Ross and Tayor [45] and widely used in electroweak higher-order calculations. In this section we summarize the renormalization procedure outlined in Ref. [48], to which the reader can refer for further details. In this scheme the set of independent

---

[1]In the evaluation of one-loop integrals infrared divergences (IR) may also arise. The problem of IR divergences and the relative cancellations will be investigated thoroughly in the next chapter.

parameters is the one listed in (1.44). The bare parameters are split into renormalized parameters and counterterms

$$e_0 = (1 + \delta Z_e)e, \tag{1.46a}$$

$$M_{W,0}^2 = M_W^2 + \delta M_W^2, \tag{1.46b}$$

$$M_{Z,0}^2 = M_Z^2 + \delta M_Z^2, \tag{1.46c}$$

$$M_{H,0}^2 = M_H^2 + \delta M_H^2, \tag{1.46d}$$

$$m_{f,i,0} = m_{f,i} + \delta m_{f,i}, \tag{1.46e}$$

$$V_{ij,0} = V_{ij} + \delta V_{ij}, \tag{1.46f}$$

where the subscript $'0'$ denotes the bare parameters. In addition we fix the condition that the renormalized vev is the physical one, *i.e.* it is given by the minimum of the Higgs potential. This condition is equivalent to the condition on the renormalized tadpole

$$t = t_0 + \delta t = 0, \tag{1.47}$$

where $t = v^2 \left(\mu^2 - \frac{\lambda}{4} v^2 \right)$. With this condition tadpole contributions have not to be considered in practical calculations.

Finally, although the counterterms introduced so far are sufficient to guarantee finite S-matrix elements we introduce the renormalization for the SM fields

$$W_0^\pm = \sqrt{Z_W} W^\pm = \left(1 + \frac{1}{2} \delta Z_W \right) W^\pm, \tag{1.48a}$$

$$\begin{pmatrix} Z_0 \\ A_0 \end{pmatrix} = \begin{pmatrix} \sqrt{Z_{ZZ}} & \sqrt{Z_{ZA}} \\ \sqrt{Z_{AZ}} & \sqrt{Z_{AA}} \end{pmatrix} \begin{pmatrix} Z \\ A \end{pmatrix} = \begin{pmatrix} 1 + \frac{1}{2} \delta Z_{ZZ} & \frac{1}{2} \delta Z_{ZA} \\ \frac{1}{2} \delta Z_{AZ} & 1 + \frac{1}{2} \delta Z_{AA} \end{pmatrix} \begin{pmatrix} Z \\ A \end{pmatrix}, \tag{1.48b}$$

$$H_0 = \sqrt{Z_H} H = \left(1 + \frac{1}{2} \delta Z_H \right) H, \tag{1.48c}$$

$$f_{i,0}^L = \sqrt{Z_{ij}^{f,L}} f_j^L = \left(\delta_{ij} + \frac{1}{2} \delta Z_{ij}^{f,L} \right) f_j^L, \tag{1.48d}$$

$$f_{i,0}^R = \sqrt{Z_{ij}^{f,R}} f_j^R = \left(\delta_{ij} + \frac{1}{2} \delta Z_{ij}^{f,R} \right) f_j^R, \tag{1.48e}$$

which are necessary to render all the Green functions finite.

1.4.1 The on-shell renormalization conditions

The on-shell scheme gets its name by the fact that the renormalization conditions are formulated for external fields on their mass shell. All the parameters

have a direct physical interpretation and can be measured with great precision in suitable experiments. Since for our purposes we can safely neglect quark mixing effects, in the following we will always assume $V_{CKM} = 1$. Then, besides the renormalization of the vev which has been introduced in the previous section, we have to define the renormalization conditions for the particle masses, the fields and the electric charge.

The renormalized masses of SM particles are required to be equal to the physical ones. This amounts to say that they are equal to the real part of the poles of the corresponding propagators, or equivalently, to the zeros of the renormalized one-particle irreducible two-point functions, projected on physical states

$$\left. \operatorname{Re} \hat{\Gamma}_{\mu\nu}^{VV}(k)\, \varepsilon^\nu(k) \right|_{k^2 = M_V^2} = 0, \qquad VV = WW, ZZ, AA \tag{1.49a}$$

$$\left. \operatorname{Re} \hat{\Gamma}_{\mu\nu}^{AZ}(k)\, \varepsilon^\nu(k) \right|_{k^2 = M_Z^2} = 0 \tag{1.49b}$$

$$\left. \operatorname{Re} \hat{\Gamma}_{\mu\nu}^{AZ}(k)\, \varepsilon^\nu(k) \right|_{k^2 = 0} = 0 \tag{1.49c}$$

$$\left. \operatorname{Re} \hat{\Gamma}^{H}(k) \right|_{k^2 = M_H^2} = 0, \tag{1.49d}$$

$$\left. \operatorname{Re} \hat{\Gamma}^{ff}(p)\, u_f(p) \right|_{p^2 = m_f^2} = 0, \tag{1.49e}$$

where the symbol (ˆ) denotes renormalized quantities and it is understood that $M_A = 0$. The expressions for the mass counterterms can be greatly simplified by a suitable choice of the renormalization conditions for the SM fields. These are fixed by imposing that on-shell particles do not mix with each other. The further condition that the propagator of a given particle has residue 1 at the pole mass leads to the following expressions:

$$\lim_{k^2 \to M_V^2} \frac{1}{k^2 - M_V^2} \operatorname{Re} \hat{\Gamma}_{\mu\nu}^{VV}(k)\, \varepsilon^\nu(k) = -i\varepsilon_\mu(k), \quad V = W, A, Z, \tag{1.50a}$$

$$\lim_{k^2 \to M_H^2} \frac{1}{k^2 - M_H^2} \operatorname{Re} \hat{\Gamma}^{H}(k) = i, \tag{1.50b}$$

$$\lim_{p^2 \to m_f^2} \frac{\slashed{p} + m_f}{p^2 - m_f^2} \operatorname{Re} \hat{\Gamma}^{ff}(p)\, u_f(p) = i u_f(p). \tag{1.50c}$$

In the 't Hooft-Feynman gauge the one-particle irreducible two-point functions are defined as follows

$$\hat{\Gamma}_{\mu\nu}^{VV'}\left(k\right) = -ig_{\mu\nu}\left(k^2 - M_V^2\right)\delta^{VV'}$$
$$- i\left(g_{\mu\nu} - \frac{k_\mu k_\nu}{k^2}\right)\hat{\Sigma}_T^{VV'}\left(k^2\right) - i\frac{k_\mu k_\nu}{k^2}\hat{\Sigma}_L^{VV'}\left(k^2\right), \qquad (1.51\text{a})$$

$$\hat{\Gamma}^H\left(k\right) = i\left(k^2 - M_H^2\right) + i\hat{\Sigma}^H\left(k^2\right), \qquad (1.51\text{b})$$

$$\hat{\Gamma}^{ff}\left(p\right) = i\left(\not{p} - m_f\right)$$
$$+ i\left[\not{p}\omega_-\hat{\Sigma}_L^f\left(p^2\right) + \not{p}\omega_+\hat{\Sigma}_R^f\left(p^2\right) + \left(m_f\omega_- + m_f\omega_+\right)\Sigma_S^f\left(p^2\right)\right], \qquad (1.51\text{c})$$

where we have introduced the shorthand notation $\omega_\pm = \frac{1}{2}\left(1 \pm \gamma_5\right)$. The renormalization conditions in Eqs. (1.49- 1.50) are thus equivalent to the following conditions on the renormalized self energies in the bosonic sector:

$$\text{Re}\,\hat{\Sigma}_T^{WW}\left(M_W^2\right) = 0, \qquad \text{Re}\left.\frac{\partial\hat{\Sigma}_T^{WW}\left(k^2\right)}{\partial k^2}\right|_{k^2 = M_W^2} = 0, \qquad (1.52\text{a})$$

$$\text{Re}\,\hat{\Sigma}_T^{ZZ}\left(M_Z^2\right) = 0, \qquad \text{Re}\left.\frac{\partial\hat{\Sigma}_T^{ZZ}\left(k^2\right)}{\partial k^2}\right|_{k^2 = M_Z^2} = 0, \qquad (1.52\text{b})$$

$$\text{Re}\,\hat{\Sigma}_T^{AA}\left(0\right) = 0, \qquad \text{Re}\left.\frac{\partial\hat{\Sigma}_T^{AA}\left(k^2\right)}{\partial k^2}\right|_{k^2 = 0} = 0, \qquad (1.52\text{c})$$

$$\text{Re}\,\hat{\Sigma}_T^{AZ}\left(M_Z^2\right) = 0, \qquad (1.52\text{d})$$
$$\text{Re}\,\hat{\Sigma}_T^{AZ}\left(0\right) = 0, \qquad (1.52\text{e})$$

$$\text{Re}\,\hat{\Sigma}^H\left(M_H^2\right) = 0, \qquad \text{Re}\left.\frac{\partial\hat{\Sigma}_T^H\left(k^2\right)}{\partial k^2}\right|_{k^2 = M_H^2} = 0. \qquad (1.52\text{f})$$

$$(1.52\text{g})$$

We remark that from the contraction with the polarization vectors ε^ν only the transverse parts of $\hat{\Sigma}_T$ enter the renormalization conditions. For fermions we get

$$m_f \text{Re} \, \hat{\Sigma}^f_L \left(m^2_f \right) + m_f \text{Re} \, \hat{\Sigma}^f_S \left(m^2_f \right) = 0, \tag{1.53a}$$

$$m_f \text{Re} \, \hat{\Sigma}^f_R \left(m^2_f \right) + m_f \text{Re} \, \hat{\Sigma}^f_S \left(m^2_f \right) = 0, \tag{1.53b}$$

$$2m^2_f \frac{\partial}{\partial p^2} \left(\text{Re} \, \hat{\Sigma}^f_L \left(p^2 \right) + \text{Re} \, \hat{\Sigma}^f_R \left(p^2 \right) + 2\text{Re} \, \hat{\Sigma}^f_S \left(p^2 \right) \right) \Bigg|_{p^2 = m^2_f} = 0. \tag{1.53c}$$

The explicit form for the counterterms can be derived by substituting the renormalized self energies with their expressions written in terms of the unrenormalized ones and the counterterms, which read

$$\hat{\Sigma}^{WW}_T \left(k^2 \right) = \Sigma^{WW}_T \left(k^2 \right) + \left(k^2 - M^2_W \right) \delta Z_W - \delta M^2_W, \tag{1.54a}$$

$$\hat{\Sigma}^{ZZ}_T \left(k^2 \right) = \Sigma^{ZZ}_T \left(k^2 \right) + \left(k^2 - M^2_Z \right) \delta Z_{ZZ} - \delta M^2_Z, \tag{1.54b}$$

$$\hat{\Sigma}^{AZ}_T \left(k^2 \right) = \Sigma^{AZ}_T \left(k^2 \right) + \frac{1}{2} k^2 \delta Z_{AZ} + \frac{1}{2} \left(k^2 - M^2_Z \right) \delta Z_{ZA}, \tag{1.54c}$$

$$\hat{\Sigma}^{AA}_T \left(k^2 \right) = \Sigma^{AA}_T \left(k^2 \right) + k^2 \delta Z_{AA}, \tag{1.54d}$$

$$\hat{\Sigma}^{H} \left(k^2 \right) = \Sigma^{H} \left(k^2 \right) + \left(k^2 - M^2_H \right) \delta Z_H - \delta M^2_H, \tag{1.54e}$$

$$\hat{\Sigma}^f_\sigma \left(p^2 \right) = \Sigma^f_\sigma \left(p^2 \right) + \delta Z^\sigma_f, \qquad \sigma = L, R, \tag{1.54f}$$

$$\hat{\Sigma}^f_S \left(p^2 \right) = \Sigma^f_S \left(p^2 \right) - \delta Z^f_L - \delta Z^f_R - \frac{\delta m^2_f}{m^2_f}. \tag{1.54g}$$

The explicit expressions for the unrenormalized self energies can be found in Appendix B of Ref. [48]. Inserting these expressions in the renormalization conditions we finally get

$$\delta M_W^2 = \operatorname{Re} \Sigma_T^{WW} \left(M_W^2 \right), \tag{1.55a}$$

$$\delta M_Z^2 = \operatorname{Re} \Sigma_T^{ZZ} \left(M_Z^2 \right), \tag{1.55b}$$

$$\delta M_H^2 = \operatorname{Re} \Sigma^H \left(M_H^2 \right), \tag{1.55c}$$

$$\delta Z_W = -\operatorname{Re} \left. \frac{\partial \Sigma_T^{WW} \left(k^2 \right)}{\partial k^2} \right|_{k^2 = M_W^2}, \tag{1.55d}$$

$$\delta Z_{ZZ} = -\operatorname{Re} \left. \frac{\partial \Sigma_T^{ZZ} \left(k^2 \right)}{\partial k^2} \right|_{k^2 = M_Z^2}, \tag{1.55e}$$

$$\delta Z_{AZ} = -2\operatorname{Re} \frac{\Sigma_T^{AZ} \left(M_Z^2 \right)}{M_Z^2}, \tag{1.55f}$$

$$\delta Z_{ZA} = 2 \frac{\Sigma_T^{AZ} \left(0 \right)}{M_Z^2}, \tag{1.55g}$$

$$\delta Z_{AA} = -\operatorname{Re} \left. \frac{\partial \Sigma_T^{AA} \left(k^2 \right)}{\partial k^2} \right|_{k^2 = 0}, \tag{1.55h}$$

$$\delta Z_H = -\operatorname{Re} \left. \frac{\partial \Sigma^H \left(k^2 \right)}{\partial k^2} \right|_{k^2 = M_H^2} \tag{1.55i}$$

$$\delta m_f = \frac{m_f}{2} \operatorname{Re} \left(\Sigma_L^f \left(m_f^2 \right) + \Sigma_R^f \left(m_f^2 \right) + 2\Sigma_S^f \left(m_f^2 \right) \right), \tag{1.55j}$$

$$\delta Z_F^L = -\operatorname{Re} \Sigma_F^L \left(m_f^2 \right) - m_f^2 \frac{\partial}{\partial p^2} \operatorname{Re} \left[\Sigma_L^f \left(p^2 \right) + \Sigma_R^f \left(p^2 \right) + 2\Sigma_S^f \left(p^2 \right) \right]_{p^2 = m_f^2}, \tag{1.55k}$$

$$\delta Z_F^R = -\operatorname{Re} \Sigma_F^R \left(m_f^2 \right) - m_f^2 \frac{\partial}{\partial p^2} \operatorname{Re} \left[\Sigma_L^f \left(p^2 \right) + \Sigma_R^f \left(p^2 \right) + 2\Sigma_S^f \left(p^2 \right) \right]_{p^2 = m_f^2}. \tag{1.55l}$$

We still have to renormalize the electric charge e. In the on-shell scheme e is defined as the coupling of the full on-shell $e^+ e^- \gamma$ vertex in the Thomson limit, *i.e.* for vanishing momentum transfer of the photon. This renormalization condition can be expressed in terms of the one-particle irreducible vertex function $\hat{\Gamma}_\mu^{ee\gamma}$ as follows:

$$\bar{u}(p) \, i\hat{\Gamma}_\mu^{ee\gamma} \left(k = 0, p, p \right) u \left(p \right) \Big|_{p^2 = m_e^2} = ie \, \bar{u}(p) \gamma_\mu u \left(p \right). \tag{1.56}$$

From this expression the counterterm δZ_e can be determined (see Ref. [48]

for details). The final results is

$$\delta Z_e = -\frac{1}{2}\delta Z_{AA} - \frac{s_W}{2c_W}\delta Z_{ZA} = \frac{1}{2}\Pi^{AA}(0) - \frac{s_W}{c_W}\frac{\Sigma_T^{AZ}(0)}{M_Z^2}, \qquad (1.57)$$

where

$$\Pi^{AA}\left(k^2\right) = \frac{\partial \Sigma_T^{AA}\left(k^2\right)}{\partial k^2} \qquad (1.58)$$

is the photon vacuum polarization. We conclude this section with the introduction of the counterterms for the weak mixing angle

$$s_{W,0} = s_W + \delta s_W \qquad c_{W,0} = c_W + \delta c_W \qquad (1.59)$$

which are rather convenient in higher-order computations because of their direct relation with the counterterms of the gauge-boson masses

$$\frac{\delta c_W}{c_W} = -\frac{s_W^2}{c_W^2}\frac{\delta s_W}{s_W} = \frac{1}{2}\mathrm{Re}\left(\frac{\Sigma_T^{WW}\left(M_W^2\right)}{M_W^2} - \frac{\Sigma_T^{ZZ}\left(M_Z^2\right)}{M_Z^2}\right). \qquad (1.60)$$

1.4.2   The $\alpha_{\mathbf{G}_\mu}$-scheme

In the previous section we have shown that in the on-shell scheme the renormalized parameters are equal to the physical ones to all orders in perturbation theory. The latter have to be extracted by experimental data. In particular, the electric charge is fixed in the Thomson limit, namely for vanishing photon transferred momentum. This specific condition defines the so called $\alpha(0)$ scheme ($\alpha = e/4\pi$ is the fine structure constant). The counterterm of the electric charge introduces universal logarithmic corrections $\propto \log\left(m_f^2/s\right)$ in the S-matrix calculations (s is a generic scale characterizing the process). These contributions arise from hadronic contributions to photon vacuum polarization. The sensitivity to light-quark masses of the hadronic contribution to the photon vacuum polarization represents a serious conceptual problem. In fact, although in the SM Lagrangian quarks are treated as free particles, the non-perturbative nature of QCD at low energy confines them in colourless bound states and therefore no straightforward definition for free quarks masses is available. In this section we present an alternative definition of the electromagnetic coupling that allows to bypass the definition of quark masses in the calculation of higher-order corrections, as far as one considers processes without external photons (in the case of external photons the logarithms of fermion masses appearing in δZ_e are canceled by the photon wave function renormalization).

In the "G_μ-scheme" the electromagnetic coupling constant is derived from the muon lifetime. Adopting the Fermi theory and including the $\mathcal{O}(\alpha)$ QED corrections the following expression has been derived in Refs. [49, 50]:

$$\frac{1}{\tau_\mu} = \frac{G_\mu m_\mu^5}{192\pi^3} \left(1 - 8\frac{m_e^2}{m_\mu^2}\right) \left[1 + \frac{\alpha}{2\pi}\left(\frac{25}{4} - \pi^2\right)\right]. \tag{1.61}$$

This equation is used as definition of the Fermi constant G_μ. The muon lifetime τ_μ can be calculated also in the full SM. In particular, the result of the NLO calculation in the on-shell scheme reads

$$\begin{aligned}
G_\mu &= \frac{\pi\alpha}{\sqrt{2}s_W^2 M_W^2} \left\{1 + \delta Z_e - \frac{\delta s_W^2}{s_W^2} - \frac{\delta M_W^2}{M_W^2} + \frac{\Sigma_T^{WW}(0)}{M_W^2} + \delta\right\} \\
&= \frac{\pi\alpha}{\sqrt{2}s_W^2 M_W^2} \left(1 + \Delta r\right).
\end{aligned} \tag{1.62}$$

Δr includes W boson self-energy, vertex and box contributions (collectively represented by δ) and counterterms, while the QED corrections included in Eq (1.61) have been subtracted. After having inserted the explicit expressions of the counterterms and after having performed the calculation of one-loop contributions we get

$$\begin{aligned}
\Delta r = {} & \Pi^{AA}(0) + \frac{\Sigma_T^{WW}(0) - \mathrm{Re}\,\Sigma_T^{WW}(M_W^2)}{M_W^2} \\
& - \frac{c_W^2}{s_W^2}\mathrm{Re}\left(\frac{\Sigma_T^{ZZ}(M_Z^2)}{M_Z^2} - \frac{\Sigma_T^{WW}(M_W^2)}{M_W^2}\right) \\
& + 2\frac{c_W}{s_W}\frac{\Sigma_T^Z(0)}{M_Z^2} + \frac{\alpha}{4\pi s_W^2}\left(6 + \frac{7 - 4s_W^2}{2s_W^2}\log\frac{M_W^2}{M_Z^2}\right).
\end{aligned} \tag{1.63}$$

From the presence of gauge-boson self-energies it follows that Δr depends on all the EW parameters. In particular, we can isolate the leading $\mathcal{O}(\alpha)$ corrections due to the presence of light quarks circulating in the W and Z boson self-energy diagrams. In the limit $m_q \ll M_W^2$, valid for $q = u, d, s, c, b$ we can calculate the contribution of light fermion doublets, getting the following expression:

$$\Delta r_{l.f.} = \frac{\alpha}{3\pi} \sum_{f=u,d} \left[Q_f\left(\log\frac{M_Z^2}{m_f^2} - \frac{5}{3}\right) - \frac{c_W^2 - s_W^2}{8s_W^4}\log c_W^2\right]. \tag{1.64}$$

The first term arises from the renormalization of the electromagnetic coupling and becomes large for light-fermion doublets, accounting for the running of

the electromagnetic coupling from the light-fermion mass scale ($q^2 \to 0$) to the electroweak scale ($q^2 \to M_Z^2$). Therefore the first term in Eq. (1.64) can be related to the UV finite quantity

$$\Delta\alpha\left(M_Z^2\right) = \Pi^{AA}(0) - \operatorname{Re}\Pi^{AA}\left(M_Z^2\right) \tag{1.65}$$

We still have to consider the effects of the third quark generation in the self energies. In this case the dominant correction originates from the large mass difference between b and t quarks. It can be shown that in presence of doublet with a light quark and a heavy one, the only term in Eq. (1.63) which gives rise to enhanced corrections is:

$$\operatorname{Re}\left(\frac{\Sigma_T^{ZZ}\left(M_Z^2\right)}{M_Z^2} - \frac{\Sigma_T^{WW}\left(M_W^2\right)}{M_W^2}\right), \tag{1.66}$$

which is related to the higher-order corrections to the ρ parameter

$$\rho = \frac{M_W^2}{M_Z^2 c_W^2}. \tag{1.67}$$

The ρ parameter is exactly one at tree-level according to the weak mixing angle definition in the on-shell scheme. From this relation it follows that higher-order corrections to the ρ parameter originate from the renormalization of c_W^2. It can be demonstrated that the contribution of the top-bottom doublet is

$$\Delta r_{t,b} = -\frac{c_W^2}{s_W^2}\frac{3\alpha m_t^2}{16\pi^2 s_W^2 M_W^2} = -\frac{c_W^2}{s_W^2}\Delta\rho. \tag{1.68}$$

Eventually we can write Δr as follows:

$$\Delta r = \Delta\alpha\left(M_Z^2\right) - \frac{c_W^2}{s_W^2}\Delta\rho + \Delta r_{rem}, \tag{1.69}$$

where Δr_{rem} includes the remaining higher-order corrections that we have not considered explicitly. Δr contains all high-order corrections to the muon decay excluding the QED corrections in the Fermi model, which are absorbed in the definition of G_μ. Then we can replace the definition of $\alpha(0)$ with the one derived from Eq. (1.62)

$$\alpha_{G_\mu} = \frac{\sqrt{2}G_\mu M_W^2 s_W^2}{\pi} = \alpha(0)(1 + \Delta r), \tag{1.70}$$

while the counterterm of the electric charge has to be modified as follows:

$$\delta Z_e \to \delta Z_e - \frac{1}{2}\Delta r = \delta Z_e^{G_\mu}, \tag{1.71}$$

in order to avoid double counting. In this way the quantity $\Delta\alpha\left(M_Z\right)$ that contains the hadronic contribution to the photon vacuum polarization is absorbed in the definition of α_{G_μ} and the dependence on the light quark masses is removed for all processes which do not involve external photons. Throughout this work we adopt the α_{G_μ} scheme if not stated otherwise.

1.5 Unstable particles and complex-mass scheme

In the discussion we have developed so far we have never mentioned that many of the SM particles, as W and Z bosons, the Higgs boson and the top quark, have a short lifetime τ and decay into other particles. In this section we briefly illustrate the issues related to the introduction of finite width effects in the calculations of S-matrix elements involving unstable particles and we introduce the complex mass-scheme [43, 51, 52], which has been used in the calculations presented in this work. If massive gauge bosons are treated as stable particles, the poles of the related propagators $1/\left(p^2 - M^2\right)$ give rise to divergences in S-matrix elements for processes involving gauge bosons as intermediate states. These divergences can be avoided by considering gauge bosons as unstable particles and, consequently, by introducing the finite widths in the propagators. From a perturbative point of view, particle widths arise naturally from the the Dyson resummation formula

$$
\begin{aligned}
\Delta^{VV}\left(p^2\right) &= \frac{i}{p^2 - M^2} + \frac{i}{p^2 - M^2}\left(\hat{\Sigma}_T^V\left(p^2\right)\right)\frac{i}{p^2 - M^2} + \cdots = \\
&= \frac{i}{p^2 - M^2}\sum_{n=0}^{\infty}\left(\frac{-\hat{\Sigma}_T^V\left(p^2\right)}{p^2 - M^2}\right)^n = \\
&= \frac{i}{p^2 - M^2 + \hat{\Sigma}_T^V\left(p^2\right)} = -\left(\hat{\Gamma}^{VV}\left(p, -p\right)\right)^{-1},
\end{aligned}
\tag{1.72}
$$

from which it follows that the width is related to the imaginary part of the gauge-boson self energy

$$
\Gamma_V\left(p^2\right) = \frac{\operatorname{Im}\hat{\Sigma}_T^V\left(p^2\right)}{M_V}.
\tag{1.73}
$$

It should be then evident that the width of a particle represents a higher-order effect and its inclusion in a fixed-order calculation entails a mixing between different perturbative orders. In particular, as pointed out in Ref. [53], the two most adopted schemes at LEP, the fixed-width scheme and the running-width scheme both violate gauge invariance. Different prescriptions have

been developed to overcome this issue and an overview on the possible solutions can be found in Ref. [54]. We just mention the pole expansion scheme, which had been widely used in the past for the calculation of radiative corrections in processes involving resonances [55, 56]. Whilst it provides gauge invariant results, the pole expansion can be used only in resonance regions. This scheme can be improved adopting an effective field theory approach in the threshold regions [57, 58]. In this work we adopt the complex-mass scheme, first introduced in Ref. [59] for lowest-order calculations and then generalized to one-loop calculations [43, 51, 52]. In this scheme the W and Z boson masses are promoted to be complex quantities, defined by the location of the poles of the related propagators

$$\mu_W^2 = \bar{M}_W^2 - i\bar{\Gamma}_W \bar{M}_W, \qquad \mu_Z^2 = \bar{M}_Z^2 - i\bar{\Gamma}_Z \bar{M}_Z, \qquad (1.74)$$

where the bars are used to distinguish pole masses and widths from the on-shell definitions. We remark, as pointed out in Ref. [60, 61], that the pole location is a S-matrix property, and consequently, it is a gauge invariant quantity. Since the weak boson masses and widths quoted on the Review of Particle Physics by the Particla Data Group [62] have been extracted at LEP adopting the on-shell scheme, the conversion formulae from LEP values to the pole-values (see Ref. [63]) read

$$\bar{M}_V = \frac{M_V^{\text{LEP}}}{\sqrt{1 - \left(\frac{\Gamma_V^{\text{LEP}}}{M_V^{\text{LEP}}}\right)^2}}, \qquad \bar{\Gamma}_V = \frac{\Gamma_V^{\text{LEP}}}{\sqrt{1 - \left(\frac{\Gamma_V^{\text{LEP}}}{M_V^{\text{LEP}}}\right)^2}}. \qquad (1.75)$$

From a formal point of view, the complex-mass scheme consists in an analytic continuation of the masses in the complex plane. Ward identities and Slavnon-Taylor identities, being algebraic relations, are still satisfied. Consequently, matrix element gauge invariance and unitarity hold order by order in perturbation theory. Let us stress that in order to preserve the gauge invariance of S-matrix elements, the complex masses have to be used everywhere in the Feynman rules. For instance, according to the relation

$$\cos^2 \theta_W = 1 - \sin^2 \theta_W = \frac{\mu_W^2}{\mu_Z^2}, \qquad (1.76)$$

the weak mixing angle becomes a complex quantity. In the one-loop generalization, proposed in Ref. [43], the complex masses are introduced at the Lagrangian level by splitting the real bare masses into complex renormalized masses and complex counterterms. Although we limit the discussion to weak gauge bosons, the complex-mass scheme applies to all unstable particles as top quark and Higgs boson. The on-shell renormalization conditions have to

be consistently generalized. Therefore, in addition to the counterterms for W and Z boson masses

$$M_{W,0}^2 = \mu_W^2 + \delta\mu_W^2, \tag{1.77a}$$

$$M_{Z,0}^2 = \mu_Z^2 + \delta\mu_Z^2, \tag{1.77b}$$

we perform the renormalization of the fields. The analogous splitting of the bare fields introduced in (1.48) reads

$$W_0^\pm = \left(1 + \frac{1}{2}\delta\mathcal{Z}_W\right)W^\pm, \tag{1.78a}$$

$$\begin{pmatrix} Z_0 \\ A_0 \end{pmatrix} = \begin{pmatrix} 1 + \frac{1}{2}\delta\mathcal{Z}_{ZZ} & \frac{1}{2}\delta\mathcal{Z}_{ZA} \\ \frac{1}{2}\delta\mathcal{Z}_{AZ} & 1 + \frac{1}{2}\delta\mathcal{Z}_{AA} \end{pmatrix} \begin{pmatrix} Z \\ A \end{pmatrix}. \tag{1.78b}$$

We note that renormalization constants and renormalized fields are complex. This means that the renormalized Lagrangian is not hermitian, while the total Lagrangian of course is. If we replace the masses and the counterterms in Eqs. (1.54a-1.54d) with their complex counterparts we can rewrite the expressions for the renormalized self-energies as follows:

$$\hat{\Sigma}_T^{WW}\left(k^2\right) = \Sigma_T^{WW}\left(k^2\right) + \left(k^2 - \mu_W^2\right)\delta\mathcal{Z}_W - \delta\mu_W^2, \tag{1.79a}$$

$$\hat{\Sigma}_T^{ZZ}\left(k^2\right) = \Sigma_T^{ZZ}\left(k^2\right) + \left(k^2 - \mu_Z^2\right)\delta\mathcal{Z}_{ZZ} - \delta\mu_Z^2, \tag{1.79b}$$

$$\hat{\Sigma}_T^{AZ}\left(k^2\right) = \Sigma_T^{AZ}\left(k^2\right) + \frac{1}{2}k^2\delta\mathcal{Z}_{AZ} + \frac{1}{2}\left(k^2 - \mu_Z^2\right)\delta\mathcal{Z}_{ZA}, \tag{1.79c}$$

$$\hat{\Sigma}_T^{AA}\left(k^2\right) = \Sigma_T^{AA}\left(k^2\right) + k^2\delta\mathcal{Z}_{AA}. \tag{1.79d}$$

$$\tag{1.79e}$$

Following the procedure outlined in Sec. 1.4, the renormalization conditions can be expressed in terms of renormalized self-energies as follows:

$$\hat{\Sigma}_T^{WW}\left(\mu_W^2\right) = 0, \qquad \left.\frac{\partial\hat{\Sigma}_T^{WW}\left(k^2\right)}{\partial k^2}\right|_{k^2=\mu_W^2} = 0, \tag{1.80a}$$

$$\hat{\Sigma}_T^{ZZ}\left(\mu_Z^2\right) = 0, \qquad \left.\frac{\partial\hat{\Sigma}_T^{ZZ}\left(k^2\right)}{\partial k^2}\right|_{k^2=\mu_Z^2} = 0, \tag{1.80b}$$

$$\left.\frac{\partial\hat{\Sigma}_T^{AA}\left(k^2\right)}{\partial k^2}\right|_{k^2=0} = 0, \tag{1.80c}$$

$$\hat{\Sigma}_T^{AZ}\left(\mu_Z^2\right) = 0, \tag{1.80d}$$

$$\hat{\Sigma}_T^{AZ}\left(0\right) = 0. \tag{1.80e}$$

The conditions on $\hat{\Sigma}_T^{WW}$ and $\hat{\Sigma}_T^{ZZ}$ fix the mass counterterms in such a way that the renormalized boson masses are equal to the location of the poles of the related propagators. The remaining conditions fix the counterterm for the fields. We remark that, unlike the on-shell conditions, in the complex-mass scheme the renormalization conditions are not limited to the real part of the self-energies.

The solutions of the renormalization conditions in Eqs. (1.80), expressed in terms of unrenormalized self-energies are

$$\delta\mu_W^2 = \Sigma_T^{WW}\left(\mu_W^2\right), \qquad\qquad \delta\mathcal{Z}_W = -\left.\frac{\partial\Sigma_T^{WW}\left(k^2\right)}{\partial k^2}\right|_{k^2=\mu_W^2}, \qquad (1.81a)$$

$$\delta\mu_Z^2 = \Sigma_T^{ZZ}\left(\mu_Z^2\right), \qquad\qquad \delta\mathcal{Z}_{ZZ} = -\left.\frac{\partial\Sigma_T^{ZZ}\left(k^2\right)}{\partial k^2}\right|_{k^2=\mu_Z^2}, \qquad (1.81b)$$

$$\delta\mathcal{Z}_{AA} = -\left.\frac{\partial\Sigma_T^{AA}\left(k^2\right)}{\partial k^2}\right|_{k^2=0}, \qquad (1.81c)$$

$$\delta\mathcal{Z}_{AZ} = -\frac{2\Sigma_T^{AZ}(\mu_Z^2)}{\mu_Z^2}, \qquad (1.81d)$$

$$\delta\mathcal{Z}_{ZA} = \frac{2\Sigma_T^{AZ}(0)}{\mu_Z^2}. \qquad (1.81e)$$

In order to avoid the mathematical difficulties relative to the analytic continuation of the two-point functions entering the self-energies in Eqs. (1.81), we can adopt an approximate treatment where self-energies on the complex pole in the momentum transfer k^2 are expressed as an expansion around real arguments,

$$\Sigma_T^{WW}\left(\mu_W^2\right) = \Sigma_T^{WW}\left(M_W^2\right) + \left(\mu_W^2 - M_W^2\right)\Sigma_T^{\prime\,WW}\left(M_W^2\right) + \mathcal{O}\left(\alpha^3\right), \quad (1.82a)$$

$$\Sigma_T^{ZZ}\left(\mu_Z^2\right) = \Sigma_T^{ZZ}\left(M_Z^2\right) + \left(\mu_Z^2 - M_Z^2\right)\Sigma_T^{\prime\,ZZ}\left(M_Z^2\right) + \mathcal{O}\left(\alpha^3\right), \quad (1.82b)$$

$$\frac{1}{\mu_Z^2}\Sigma_T^{AZ}\left(\mu_Z^2\right) = \frac{1}{\mu_Z^2}\Sigma_T^{AZ}\left(0\right) + \frac{1}{M_Z^2}\Sigma_T^{AZ}\left(M_Z^2\right) - \frac{1}{M_Z^2}\Sigma_T^{AZ}\left(0\right) + \mathcal{O}\left(\alpha^2\right),$$

$$(1.82c)$$

where the prime denotes differentiation with respect to the argument. The $\mathcal{O}\left(\alpha^2\right)$ and $\mathcal{O}\left(\alpha^3\right)$ contributions result from the products of self-energies Σ_T^{VV} and terms of the form $(\mu_V^2 = M_V^2)$, which are of $\mathcal{O}\left(\alpha\right)$ and are UV-finite at one-loop level. It is important to remark that the expansion described above must preserve the one-loop accuracy. It has been noted in Ref. [52] that the self-energy diagram with a virtual photon emitted and absorbed by a W boson leads to a contribution with a branch cut in $\Sigma_T^{WW}(\mu_W^2)$ which breaks

the validity of the expansion. In order to restore the one-loop accuracy Eq. (1.82a) has to be modified as follows:

$$\Sigma_T^{WW}\left(\mu_W^2\right) = \Sigma_T^{WW}\left(M_W^2\right) + \left(\mu_W^2 - M_W^2\right)\Sigma_T'^{WW}\left(M_W^2\right) + c_T^W + \mathcal{O}\left(\alpha^3\right),$$
(1.83)

with the constant

$$c_T^W = \frac{i\alpha}{\pi}M_W\Gamma_W = \frac{\alpha}{\pi}\left(M_W^2 - \mu_W^2\right).$$
(1.84)

By inserting the approximate expansions of the self-energies in the expressions of the renormalization counterterms, we obtain the following results:

$$\delta\mu_W^2 = \Sigma_T^{WW}\left(M_W^2\right) + \left(\mu_W^2 - M_W^2\right)\Sigma_T'^{WW}\left(M_W^2\right) + c_T^W,$$
(1.85a)

$$\delta\mu_Z^2 = \Sigma_T^{ZZ}\left(M_Z^2\right) + \left(\mu_Z^2 - M_Z^2\right)\Sigma_T'^{ZZ}\left(M_Z^2\right),$$
(1.85b)

$$\delta\mathcal{Z}_W = -\left.\frac{\partial\Sigma_T^{WW}\left(k^2\right)}{\partial k^2}\right|_{k^2=M_W^2},$$
(1.85c)

$$\delta\mathcal{Z}_{ZZ} = -\left.\frac{\partial\Sigma_T^{ZZ}\left(k^2\right)}{\partial k^2}\right|_{k^2=M_Z^2},$$
(1.85d)

$$\delta\mathcal{Z}_{ZA} = \frac{2\Sigma_T^{AZ}\left(0\right)}{\mu_Z^2},$$
(1.85e)

$$\delta\mathcal{Z}_{AZ} = -\frac{2\Sigma_T^{AZ}\left(M_Z\right)}{M_Z^2} + \left(\frac{\mu_Z^2}{M_Z^2} - 1\right)\delta\mathcal{Z}_{ZA}.$$
(1.85f)

(1.85g)

Then, by replacing the counterterms in (1.79) with their explicit expressions we finally get

$$\hat{\Sigma}_T^{WW}\left(k^2\right) = \Sigma_T^{WW}\left(k^2\right) + \left(k^2 - M_W^2\right)\delta Z_W - \delta M_W^2 - c_T^W,$$
(1.86a)

$$\hat{\Sigma}_T^{ZZ}\left(k^2\right) = \Sigma_T^{ZZ}\left(k^2\right) + \left(k^2 - M_Z^2\right)\delta Z_{ZZ} - \delta M_Z^2,$$
(1.86b)

$$\hat{\Sigma}_T^{AZ}\left(k^2\right) = \Sigma_T^{AZ}\left(k^2\right) + \frac{1}{2}k^2\delta Z_{AZ} + \frac{1}{2}\left(k^2 - M_Z^2\right)\delta Z_{ZA}.$$
(1.86c)

and the renormalization constants turn out to be

$$\delta M_W^2 = \Sigma_T^{WW} \left(M_W^2 \right), \tag{1.87a}$$

$$\delta M_Z^2 = \Sigma_T^{ZZ} \left(M_Z^2 \right), \tag{1.87b}$$

$$\delta Z_W = - \left. \frac{\partial \Sigma_T^{WW}}{\partial k^2} \right|_{k^2 = M_W^2}, \tag{1.87c}$$

$$\delta Z_{ZZ} = - \left. \frac{\partial \Sigma_T^{ZZ}}{\partial k^2} \right|_{k^2 = M_Z^2}, \tag{1.87d}$$

$$\delta Z_{AZ} = -2 \frac{\Sigma_T^{AZ} \left(M_Z^2 \right)}{M_Z^2}, \tag{1.87e}$$

$$\delta Z_{ZA} = 2 \frac{\Sigma_T^{AZ} \left(0 \right)}{M_Z^2}. \tag{1.87f}$$

All in all, the expressions for the counterterms in Eqs. (1.87) have the same form of the corresponding ones in the on-shell scheme, without taking the real part of the renormalized self-energies. In case of the charged particles, extra constants must be added to preserve the one-loop accuracy of the result.

Owing to the definition in (1.76), the renormalization of the complex angle reads

$$\frac{\delta s_W}{s_W} = -\frac{c_W^2}{s_W^2} \frac{\delta c_W}{c_W} = -\frac{c_W^2}{2 s_W^2} \left(\frac{\delta \mu_W^2}{\mu_W^2} - \frac{\delta \mu_Z^2}{\mu_Z^2} \right), \tag{1.88}$$

Finally, the electric charge is fixed, in complex-mass scheme, through the condition

$$\frac{\delta e}{e} = \frac{1}{2} \left. \frac{\partial \Sigma^{AA} \left(k^2 \right)}{\partial k^2} \right|_{k^2 = 0} - \frac{s_W}{c_W} \frac{\Sigma^{AZ} \left(0 \right)}{\mu_Z^2}. \tag{1.89}$$

Therefore, also the charge renormalization constant and the renormalized charge become complex. Since the imaginary part of the bare charge vanishes, the imaginary part of the charge renormalization constant is directly fixed by the imaginary part of self-energies. In one-loop calculations, the imaginary part of the renormalized charge drops out in the corrections to the absolute square of the matrix element, because the charge factorizes from the lowest-order matrix element. Starting from the two-loop level, the imaginary part has to be taken into account.

In conclusion, the complex-mass scheme represents a consistent scheme for the inclusion of finite widths effects in the calculation of cross sections and decay widths. Gauge invariance and unitarity are preserved order by order in the perturbative expansion. Furthermore, it is rather easy to be implemented in the calculations and it is applicable in the full phase space, not being restricted to the resonant regions. For this reason, in the calculations presented in this work, the complex-mass scheme has been adopted.

Chapter 2

Infrared divergences and the Parton Shower algorithm

In the previous chapter we have introduced the problem of UV divergences in the calculation of radiative corrections to a generic EW process. In particular, we have seen that UV singularities originate from infinite loop momenta and are removed by a renormalization procedure. This chapter deals with another kind of divergences, arising in the calculation of higher-order corrections when massless particles are involved. In Sec. 2.1 the problem of infrared (IR) singularities in QED, occurring when the energy of a virtual photon goes to zero in the loop, is introduced. In a general framework, *i.e.* without the need to specify the underlying leading order process, we will show that the calculation of real corrections develops the same IR divergences when the energy of the emitted photon goes to zero. We will demonstrate that IR divergences cancel in the sum of virtual and real corrections. We will also show that photon emission is particularly enhanced in the collinear region, namely close to the direction of the emitting particle. The large corrections coming from collinear photons can be summed to all orders in a process independent way. To this end the collinear factorization is introduced in Sec. 2.2. In Sec. 2.3 the QED Altarelli-Parisi (AP) equations are derived. Finally in Sec. 2.4 we introduce the Parton Shower (PS) algorithm, which provides an exact numerical solution of the Altarelli-Parisi equation in QED and allows for a detailed description of multiphoton final states.

2.1   Infrared singularities in QED

In the introduction we have anticipated that IR divergences occurring in virtual and real higher-order corrections cancel out in physical observables. In this section we will show how IR singularities arise in real and virtual corrections for the QED case. The results can be easily generalized to QCD. We derive the main results of the general treatment of IR singularities given by Yennie, Frautschi and Suura [64], following the discussion developed in Refs. [63, 65] avoiding technical details and highlighting the cancellation between real and virtual divergent contributions.

Let us start by considering a process involving i initial and f final state particles that in principle can be of any type. In order to isolate an outgoing fermion labeled by the index l, the matrix element $\mathcal{M}^{i \to f}$ can be written, without any loss of generality, as

$$\mathcal{M}^{i \to f}(p_l, p) = \bar{u}(p_l) A(p_l, p). \tag{2.1}$$

If we consider the case where the fermion l emits a photon with momentum k and Lorentz index μ, the matrix element becomes

$$\mathcal{M}^{i \to f\gamma} = \mathcal{M}^{i \to f\gamma}_{\mu}(k, p_l, p)\varepsilon^{\mu *}(k, h), \tag{2.2}$$

where $\varepsilon^{\mu}(k, h)$ is the polarization vector of the emitted photon with momentum k and helicity h, while the remaining part of the amplitude is collected in $\mathcal{M}^{i \to f\gamma}_{\mu}$, whose explicit expression reads

$$\mathcal{M}^{i \to f\gamma}_{\mu}(k, p_l, p) = \bar{u}(p_l)\left[-ieQ\gamma_{\mu}\right]\left[\frac{i\left(\slashed{p}_l + \slashed{k} + m\right)}{(p_l + k)^2 - m^2 + i\epsilon}\right]A(p_l + k, p). \tag{2.3}$$

In the soft-photon approximation, obtained by taking the limit $k \to 0$, Eq. (2.3) becomes

$$\mathcal{M}^{i \to f\gamma}_{\mu}(k, p_l, p) \sim \bar{u}_l(p)\frac{2eQp_{l,\mu}}{2p_l \cdot k + i\epsilon}A(p_l, p) = \frac{2eQp_{l,\mu}}{2p_l \cdot k + i\epsilon}\mathcal{M}^{i \to f}(p_l, p), \tag{2.4}$$

where we have made use of the relation

$$\bar{u}(p_l)\gamma_{\mu}\left(\slashed{p}_l + m\right) = \bar{u}(p_l)\left[2p_{l,\mu} - \left(\slashed{p}_l - m\right)\gamma_{\mu}\right] = \bar{u}(p_l) 2p_{l,\mu}. \tag{2.5}$$

From Eq. (2.3) it appears that the amplitude is divergent in the infrared limit. The factorization formula for photon emission from an incoming fermion differs from Eq. (2.3) only for a $(-)$ sign and holds also when the fermion is

replaced with another particle, *e.g.* a W boson. Summing over all external particles we obtain the amplitude for the emission of an additional soft photon in the $i \rightarrow f$ process,

$$\mathcal{M}_{\mu}^{i \rightarrow f \gamma}(k, p_l, p) \sim \mathcal{M}^{i \rightarrow f}(p) \sum_{l=1}^{i+f} \frac{2 e Q_l p_{l,\mu}}{2 \eta_l p_l \cdot k + i\epsilon}, \tag{2.6}$$

where $\eta_l = +1$ ($\eta_l = -1$) for an outgoing (incoming) particle. This expression can be further generalized for the emission of n soft photons. The final result reads

$$\mathcal{M}_{\mu_1 \cdots \mu_n}^{i \rightarrow f, \gamma_1 \cdots \gamma_n}(p, k) \sim \mathcal{M}^{i \rightarrow f}(p) \prod_{m=1}^{n} \left\{ \sum_{l=1}^{i+f} \frac{2 e Q_l \, p_{l,\mu_m}}{2 \eta_l p_l \cdot k_m + i\epsilon} \right\}. \tag{2.7}$$

The last equation is the starting point for the calculation of virtual and real corrections in soft-photon approximation.

The virtual amplitude can be derived by taking, for an even number of photons, the diagrams contributing to Eq. (2.7) and joining two photon lines in all possible ways. Then, according to Feynman rules, for each virtual photon we must multiply the amplitude by a photon propagator $-i g_{\mu\nu}/ (k^2 + i\epsilon)$. Finally, we have to perform the loop integrals, which correspond to the integration over the photon momenta k. The formula for the virtual amplitude is

$$\mathcal{M}_{V,n}^{i \rightarrow f}(p) = \frac{1}{n!} \left(\frac{1}{2} \sum_{l,m} e^2 Q_l Q_m \mathcal{J}_{lm} \left(p_l, p_m \right) \right)^n \mathcal{M}^{i \rightarrow f}(p), \tag{2.8}$$

where $\mathcal{J}_{lm} \left(p_l, p_m \right)$ is the loop integral

$$\mathcal{J}_{lm} \left(p_l, p_m \right) = -i \int \frac{d^4 k}{2\pi^4} \frac{4 p_l p_m}{(k^2 + i\epsilon) \left(2 \eta_l p_l k + i\epsilon \right) \left(-2 \eta_m p_m k + i\epsilon \right)}. \tag{2.9}$$

The overall factor $1/n!$ in Eq. (2.8) is required in order to get rid of the equivalent terms obtained by a permutation of the integrals $\mathcal{J}$ (*e.g.* $\mathcal{J}_{12}\mathcal{J}_{34} = \mathcal{J}_{34}\mathcal{J}_{12}$), while the factor $1/2$ within the brackets cancels the equivalent terms with the end point of the photon lines exchanged (e.g $\mathcal{J}_{12} = \mathcal{J}_{21}$). Eq. (2.8) takes into account also the case where the photon is emitted and reabsorbed by the same particle. These terms originate from wave-function renormalization of external particles, entering the calculation of a given S-matrix element through the LSZ reduction formula and, according to the adopted renormalization scheme, through the counterterms of the external fields.

The integral in Eq. (2.9) is divergent in both UV and IR regime. The IR singularities can be regularized introducing an unphysical lower energy cutoff k_{min} in the integrals. We introduce also an upper cutoff k_{max} which can be arbitrarily chosen. The integral can be evaluated with standard techniques (see Ref. [63]) and the final result, for the case $l \neq m$, is

$$\mathrm{Re}\,\mathcal{J}_{lm}^{IR}\left(p_l, p_m\right) = \frac{\eta_l \eta_m}{8\pi^2} \left[\frac{1}{\beta_{lm}} \log \frac{1 - \beta_{lm}}{1 + \beta_{lm}}\right] \log \frac{k_{max}}{k_{min}}, \qquad (2.10)$$

where we have taken just the real part of the integral because the IR divergent imaginary part drops out by squaring the matrix element and therefore is irrelevant. The integral depends on the external momenta through β_{lm}, which is the relative velocity of the particles l and m in the rest frame of the lm system

$$\beta_{lm} = \sqrt{1 - \frac{m_l^2 m_m^2}{\left(p_l \cdot p_m\right)^2}}. \qquad (2.11)$$

The IR part of the loop integral for $l = m$ can be derived from Eq. (2.10) by putting $\eta_l \eta_m = 1$ and taking the limit $\beta_{lm} \to 0$. It follows that

$$\mathcal{J}_{ll} = \frac{1}{8\pi^2} \log \frac{k_{max}}{k_{min}}. \qquad (2.12)$$

We remark that while the IR singularities arise in Eqs. (2.10) and (2.12) by taking the limit $k_{min} \to 0$, the expression in Eq. (2.10) is divergent also in the limit $\beta_{lm} \to 1$, which corresponds to $m_l = m_m = 0$. Therefore, although $\log\left(\frac{1 - \beta_{lm}}{1 + \beta_{lm}}\right)$ becomes large for high energies ($E \gg m$) the fermion masses prevent this logarithmic term to diverge.

In order to remove the IR singularities arising in the calculation of the virtual corrections we have to consider the emission of n additional photons in the $i \to f$ process. Since there is no possibility to detect a photon with vanishing energy, a process with a fixed number of final state particles is experimentally indistinguishable from the corresponding one where a generic number of additional soft photons are emitted. For this reason the calculation of the cross section for a given process beyond leading order must include real contributions due to the emission of an arbitrary number of unresolved photons. In the soft-photon approximation the S-matrix element can be derived by contracting the Lorentz indexes $\mu_1 \cdots \mu_n$ in Eq. (2.7) with n photon polarization vectors, leading to

$$\mathcal{M}^{i \to f, \gamma_1 \cdots \gamma_n}\left(p, k\right) = \mathcal{M}^{i \to f}\left(p\right) \prod_{m=1}^{n} \left\{\sum_{l=1}^{i+f} \frac{eQ_l p_{l,\mu} \varepsilon^{\mu\,*}(k_m, h_m)}{\eta_l p_l k_m}\right\}, \qquad (2.13)$$

where h_i denotes the helicities of photons with momenta k_i. The cross section for the emission of n soft photons in the $i \to f$ process is obtained by squaring the matrix element in Eq. (2.13), and since we are inclusive on the soft radiation, we have to integrate over the (n)-body phase space and sum over photon polarizations. In the sum we use the formula

$$\sum_{\lambda=1}^{2} \varepsilon_\mu^* (k, \lambda) \, \varepsilon_\nu (k, \lambda) = -g_{\mu\nu} - \frac{k_\mu k_\nu}{k^2} + \frac{n_\mu k_\nu + n_\nu k_\mu}{kn}, \qquad (2.14)$$

where n is a generic light-like four vector. Since from the electric charge conservation follows that $\sum_l \eta_l Q_l = 0$, only the first term survives in the sum. The cross section formula for soft-photon emission reads

$$d\sigma^{i \to f, \gamma_1 \cdots \gamma_n}(p) = \sigma^{i \to f}(p) \frac{1}{n!} \prod_{i=1}^{n} \left\{ \sum_{l,m} e^2 Q_l Q_m \mathcal{I}_{lm}^i (p_l, p_m) \right\}, \qquad (2.15)$$

where $\mathcal{I}_{lm}^i$ is the integral over the photon phase space

$$\mathcal{I}_{lm}^i (p_l, p_m) = -\frac{1}{(2\pi)^3} \int \frac{d^3 \mathbf{k}_i}{2E_i} \eta_l \eta_m \frac{p_l p_m}{(p_l \cdot k_i)(p_m \cdot k_i)}. \qquad (2.16)$$

Therefore, in the soft-photon approximation the part accounting for additional photon emission is factorized from the underlying leading order process. In particular, the terms $\mathcal{I}_{lm}^i$ originate from the interference of the subprocesses with the photon i emitted respectively from the external legs l and m, while the terms $\mathcal{I}_{ll}$ arise by squaring the matrix elements with the photon i attached to the external leg l. As in the virtual case we work out the integral in Eq. (2.16) by introducing an infrared regulator k_{min} and an upper limit ΔE for the energy of the photon. The final result reads:

$$\mathcal{I}_{lm} (p_l, p_m) = -\frac{\eta_l \eta_m}{8\pi^2} \left[\frac{1}{\beta_{lm}} \log \frac{1 + \beta_{lm}}{1 - \beta_{lm}} \right] \log \frac{\Delta E}{k_{min}}. \qquad (2.17)$$

The factor within square brackets arises from the integration over the angular degrees of freedom, while the term $\log(\Delta E / k_{min})$ follows from the integration over the photon energy. As in Eq. (2.10) the fermion mass prevents the angular integral to diverge in phase-space regions in which the photon becomes collinear to one of the fermions.

It is easy to note that the dependence on the IR regulator k_{min} drops out in the sum, which turns out to be finite. Since there is no upper bound to the number of soft photons emitted by initial and final state particles, we

can take the limit $n \to \infty$ in the sum of the virtual and real contributions to the cross section. Eventually we get

$$d\sigma_{soft}^{i\to f}(p) = d\sigma^{i\to f}(p) \exp\left\{\sum_{l,m} e^2 Q_l Q_m \left[\text{Re } \mathcal{J}_{lm}\left(p_l, p_m\right) + \mathcal{I}_{lm}\left(p_l, p_m\right)\right]\right\}.$$
$$(2.18)$$

Then, by replacing $\mathcal{J}_{lm}\left(p_l, p_m\right)$ and $\mathcal{I}_{lm}\left(p_l, p_m\right)$ with their expressions we get

$$d\sigma_{soft}^{i\to f}(p) = d\sigma^{i\to f}(p) \left(\frac{\Delta E}{k_{max}}\right)^{\alpha \mathcal{B}^{i\to f}}, \qquad (2.19)$$

where

$$\mathcal{B}^{i\to f} = -\frac{1}{2\pi} \sum_{l,m} Q_l Q_m \eta_l \eta_m \frac{1}{\beta_{lm}} \log \frac{1 + \beta_{lm}}{1 - \beta_{lm}}. \qquad (2.20)$$

In Eq. (2.19) ΔE plays the rôle of energy separation between the soft regime, where the final state photons cannot be resolved by the experimental setup, and the hard regime where the photon energy is greater than the threshold of the detector and it can be experimentally isolated. Finally, k_{max} can be thought as the maximum energy that photons can reach and can be put equal to the energy scale of the process.

Few important remarks follow from the analysis of cross section formula in Eq. (2.19). First of all we should note that the classical result which states that a moving charged particle is always accompanied by electromagnetic radiation is recovered in the QED framework by the vanishing of the cross section of Eq. (2.19) in the limit $\Delta E \to 0$, whose physical meaning is that in a given process an arbitrary number of soft photons is always produced. By contrast, the r.h.s. becomes equal to the Born cross section by putting $\Delta E = k_{max}$. This means that a leading order result is completely inclusive on the additional emission of photons. The cancellation of IR divergences in QED with finite fermion masses was proven by the Bloch-Nordsiek (BN) theorem [66]. This result can be extended also to non-Abelian theories as QCD, where quarks are usually treated as massless particles and consequently also collinear divergences arise in virtual and real contributions. The Kinoshita-Lee-Nauenberg (KLN) theorem [67, 68] gives the formal proof that in the sum over all degenerate states infrared and collinear singularities drop out.

2.2   Collinear factorization

In the previous section we have considered the cancellation of IR divergences arising in higher-order corrections. In particular, working in the soft-photon

approximation, we have seen that the fermion mass prevents the angular integral to diverge. However, when the energy scale of a given scattering processes is much larger than light-fermions mass scales, the emission of collinear photons may lead to a large logarithmic enhancement. For instance, if we consider a process with a single charged particle in the initial and final state, Eq. (2.20) becomes

$$
\lim_{\beta \to 1} \mathcal{B}(p, p') = \lim_{\beta \to 1} \frac{Q}{2\pi} \left[\frac{2}{\beta} \log \frac{1+\beta}{1-\beta} - 4 \right] = \frac{Q}{2\pi} \left[\log \frac{(p'-p)^2}{m^2} - 1 \right], \quad (2.21)
$$

where p and p' are respectively the momenta of initial and final state particles. The inclusion of these large collinear contributions in the cross section leads to the so-called leading-logarithmic (LL) accuracy. Then, in the remaining part of this chapter we describe a strategy for the inclusion of collinear contributions to all orders in perturbation theory.

In this section we show that the factorization of photon emission in the S-matrix calculations holds also in the collinear limit, *i.e.* when only the transverse component of the photon momentum goes to zero ($k_T \to 0$). Let us start by considering an initial state electron emitting a collinear photon. In the reference frame in which the momentum of the emitting particle lies in the z-direction, the photon momentum can be written as

$$
k = (1-z)\, p + k_T + \xi \eta, \quad (2.22)
$$

where η is a light-like 4-vector and $k \cdot \eta \neq 0$. From the on-shell condition we derive the relations

$$
\xi = \frac{|k_T^2|}{2\,(p \cdot \eta)\,(1-z)}, \qquad (p-k)^2 = -\frac{|k_T^2|}{1-z}. \quad (2.23)
$$

Then, the S-matrix element for the process $i \to f + \gamma$, with the photon emitted by the initial state electron l is

$$
\mathcal{M}^{i \to f\gamma}(p, p_l, k) = \left[-ie \frac{i\left(\slashed{p}_l - \slashed{k}\right)}{(p_l - k)^2} \gamma_\mu u(p_l)\, \varepsilon^{\mu*}(k, \lambda) \right] \mathcal{M}^{i \to f}(p, p_l - k),
$$
$$
(2.24)
$$

and using the relations in eqs. (2.22) and (2.23) we get

$$
\mathcal{M}^{i \to f\gamma}(p, p_l, k) = \left[-e \frac{\left(\slashed{p}_l - \slashed{k}\right)}{|k_T^2|/(1-z)} \gamma_\mu u(p_l)\, \varepsilon^{\mu*}(k, \lambda) \right] \mathcal{M}^{i \to f}(p, p_l - k).
$$
$$
(2.25)
$$

Working out the Dirac algebra and using the relations $\not{p}_l u(p_l) = 0$ and $k^\mu \varepsilon^*_\mu = 0$ the matrix element is reduced to

$$\mathcal{M}^{i \to f\gamma}(p, p_l, k) = \left[e \frac{2z k_{T,\mu} + (1-z)\not{k}_T \gamma_\mu}{|k_T^2|} u(p_l) \, \varepsilon^{\mu *}(k, \lambda) \right] \mathcal{M}^{i \to f}(p, p_l - k) \,. \tag{2.26}$$

Eventually, in order to calculate the cross section, we have to take the square of the matrix element in Eq. (2.26), average over the spin of the initial states particles, sum over the spin of the final state particles and integrate over the phase space. In particular, with the change of variables in the phase space of the photon:

$$\frac{d^3 k}{2k^0 (2\pi)^3} = \frac{d^2 k_T}{2(2\pi)^3} \frac{dz}{1-z}, \tag{2.27}$$

we can write the cross section for the radiative process in the following factorized form:

$$d\sigma^{i \to f\gamma}_{coll}(p, p_l, k_T, z) = \left[\frac{\alpha}{2\pi} \frac{1+z^2}{1-z} \frac{d|k_T^2|}{|k_T^2|} dz \right] \sigma^{i \to f}(p, zp_l) \,, \tag{2.28}$$

or, equivalently,

$$d\sigma^{i \to f\gamma}_{coll}(p, p_l, q_l, z) = \left[\frac{\alpha}{2\pi} \frac{1+z^2}{1-z} \frac{dq_l^2}{q_l^2} dz \right] \sigma^{i \to f}(p, zp_l) \,, \tag{2.29}$$

where $q_l^2 = (p_l - k)^2$ is the change of virtuality of the electron after the photon emission. In Eq. (2.23) we have used the change of variable $dq_l^2/q_l^2 = d|k_T|^2/|k_T|^2$. The same factorization formula holds also in the case of photon emission by an outgoing electron, provided that we replace $\sigma^{i \to f}(p, zp_l)$ with $\sigma^{i \to f}(p, p_l)$ on the r.h.s of Eqs. (2.28) and (2.29).

From the factorized cross section formula we can derive the following physical interpretation: the probability that the virtuality of the incoming electron l evolves from q_l^2 to $q_l^2 + dq_l^2$ with the emission of a collinear photon, carrying a fraction $(1-z)$ of its energy, does not depend on the underlying hard process and is given by the expression

$$\frac{\alpha}{2\pi} \frac{dq_l^2}{q_l^2} P_{ee}(z), \tag{2.30}$$

where

$$P_{ee}(z) = \frac{1+z^2}{1-z} \tag{2.31}$$

is the Altarelli-Parisi splitting vertex which represents the energy distribution of the emitted photon energy. The singularity arising for $z \to 1$ corresponds

to the infrared divergence. In the previous section we have seen that the
BN theorem states that only the sum of virtual and real contributions is
IR finite. A nice feature of collinear factorization is that we can derive the
leading logarithmic virtual contributions using probabilistic arguments and
avoiding explicit loop calculations. In fact, an electron can evolve from a
virtuality q^2 to $q^2 + dq^2$ in two ways: with or without emitting a photon.
The probability for the first case is given by Eq. (2.30). In order to preserve
the unitarity, the probability of evolving without photon emission, which
includes Born and virtual corrections can be written as follows:

$$P_0 = 1 - \frac{\alpha}{2\pi} \frac{dq_l^2}{q_l^2} \int_0^1 P_{ee}(z)\, dz. \tag{2.32}$$

The divergence for $z \to 1$ corresponds to the IR singularity arising in the
evaluation of the loop integral that we have encountered in the previous
section. Accordingly to the BN theorem, in order to have a IR finite cross
section we have to the take the sum of real and virtual contributions. The
final result reads

$$
d\sigma_{coll}^{i \to f(\gamma)}(p, p_l, q_l, z) = \left\{ \left[1 - \frac{\alpha}{2\pi} \frac{dq_l^2}{q_l^2} \int_0^1 P_{ee}(x)\, dx \right] \delta(1-z) + \right.
$$
$$
\left. \frac{\alpha}{2\pi} \frac{dq_l^2}{q_l^2} P_{ee}(z) \right\} \sigma^{i \to f}(p, z p_l), \tag{2.33}
$$

which is equivalent to

$$d\sigma_{coll}^{i \to f(\gamma)}(p, p_l, q_l, z) = \delta(1-z)\sigma^{i \to f}(p) + \frac{\alpha}{2\pi} \frac{dq_l^2}{q_l^2} P_{ee}^+(z)\sigma^{i \to f}(p, z p_l), \tag{2.34}$$

where in the last equation we have introduced the regularized Altarelli-Parisi
vertex

$$P_{ee}^+(z) = P_{ee}(z) - \delta(1-z) \int_0^1 P_{ee}(x) dx. \tag{2.35}$$

2.3 The Altarelli-Parisi equation in QED

In Sec. 2.1 we have pointed out that the classical emission of electromagnetic
radiation by a moving charged particle is reproduced in QED in terms of
soft-photon emission. In particular, we have seen that the cross section goes
to zero if we take the limit $\Delta E \to 0$ in Eq. (2.19). Therefore, in a scattering

process, an initial state charged electron evolves from the original on-shell condition emitting soft and/or collinear radiation and acquiring a negative virtuality which is bounded by the scale of the hard process. By contrast, for final state particles the evolution starts from the scale of the hard process up to the particle mass. This leads us to introduce the electron-electron splitting function $f_{ee}(x, s)$, *i.e.* the probability density to find an electron, at the scale s, with a fraction x of its original energy, and whose s evolution is ruled by the related Altarelli-Parisi (AP) equation.

To derive the AP equation for the electron-electron splitting function we use the probabilistic arguments introduced in the last section. The density function $f_{ee}(x, s + ds)$ is given by the formula

$$
\begin{aligned}
f_{ee}(x, s + ds) = f_{ee}(x, s) \left[1 - \frac{\alpha}{2\pi} \frac{ds}{s} \int_0^1 dx P_{ee}(x) \right] \\
+ \frac{\alpha}{2\pi} \frac{ds}{s} \int_x^1 dy \int_0^1 dz P_{ee}(z) f_{ee}(y, s) \delta(zy - x),
\end{aligned}
\tag{2.36}
$$

where the first term corresponds to the probability for the electron to change its virtuality from s to $s + ds$ without emitting a photon, while the second term accounts for the probability to emit a photon, remaining with a fraction $x = zy$ of its initial energy (y is the fraction of the initial energy carried by the electron before the emission of the photon). From Eq. (2.36) it is straightforward to derive the AP equation

$$
\begin{aligned}
s\frac{\partial}{\partial s} f_{ee}(x, s) = -\frac{\alpha}{2\pi} \int_0^1 dz P_{ee}(z) \\
+ \frac{\alpha}{2\pi} \int_0^1 \frac{dz}{z} P(z) f_{ee}(\frac{x}{z}, s) \vartheta\left(\frac{x}{z} - x\right) \vartheta\left(1 - \frac{x}{z}\right),
\end{aligned}
\tag{2.37}
$$

which can be modified by introducing the regularized vertex defined in Eq. (2.35) and using the identity

$$
f_{ee}(x, s) = \left[\frac{1}{z} f_{ee}\left(\frac{x}{z}, s\right) \vartheta\left(\frac{x}{z} - x\right) \vartheta\left(1 - \frac{x}{z}\right) \right]_{z=1}.
\tag{2.38}
$$

We finally get

$$
s\frac{\partial}{\partial s} f_{ee}(x, s) = \frac{\alpha}{2\pi} \int_x^1 \frac{dz}{z} P_{ee}^+(z) f_{ee}\left(\frac{x}{z}, s\right).
\tag{2.39}
$$

Throughout this section and the previous one we have focused our attention only on the emission of photon by electrons and we have derived the

AP equation for the electron-electron splitting function $f_{ee}(x, s)$. The same arguments can be used to derive the evolution equations for other splitting functions, as $f_{e\gamma}(x, s)$, which gives the probability to find, at scale s, a photon inside an electron with a fraction energy x of the original electron, or $f_{\gamma\gamma}(x, s)$, $f_{\gamma e}(x, s)$, and $f_{\gamma\bar{e}}(x, s)$ which are the density functions for the photon. The discussion on collinear emission can be also extended to QCD and the AP equation for parton distribution functions can be derived with analogous arguments. For the details we refer to the original papers [69, 70, 71].

2.4 The Parton Shower algorithm in QED

In literature several analytic and numerical solutions of the AP equations are available (for a complete discussion the reader can refer to [72] and the references therein). In this section we describe the QED Parton Shower (PS) algorithm, which provides a Monte Carlo solution of the AP equation for the electron. This method has the important feature of giving access to the kinematics of the emitted photons, allowing for a detailed description of the final states.

The kernel of the PS algorithm is the Sudakov form factor $\Pi(s_f, s_i)$, which is defined as the probability for an electron to evolve from the virtuality s_i to the virtuality s_f without emitting radiation above a given fraction ε of the initial electron energy. According to the definition of the Altarelli-Parisi splitting function $P_{ee}(z)$ we can write

$$\Pi(s_f + ds_f, s_i) = \Pi(s_f, s_i) \left[1 - \frac{\alpha}{2\pi} \frac{ds_f}{s_f} \int_0^{1-\varepsilon} P(z)dz \right]. \qquad (2.40)$$

From this definition we can write the differential equation for the Sudakov form factor as follows:

$$\frac{d\Pi(s_f', s_i)}{\Pi(s_f', s_i)} = -\frac{\alpha}{2\pi} \frac{ds_f'}{s_f'} I^+(\varepsilon), \qquad (2.41)$$

where

$$I^+(\varepsilon) = \int_0^{1-\varepsilon} P(z)dz = -2\log\varepsilon - \frac{1}{2}(1-\varepsilon)^2 - 1 + \varepsilon. \qquad (2.42)$$

The solution of Eq. (2.41) is

$$\Pi(s_f, s_i) = \exp\left\{ -\frac{\alpha}{2\pi} \log\frac{s_f}{s_i} I^+(\varepsilon) \right\}. \qquad (2.43)$$

It should be noted that Eq. (2.43) represents an alternative way to realize the exponentiation of the soft and virtual corrections with respect to Eq. (2.18) and ϵ represents the infrared separator between the soft and the hard photon emission. In order to define the PS algorithm, we have to derive an iterative solution of the AP equation for the electron. Using the definition of the regularized AP vertex given in Eq. (2.35), we rewrite the AP equation (2.39) as

$$
\begin{aligned}
s\frac{\partial}{\partial s}f_{ee}(x,s) &= \frac{\alpha}{2\pi}\int_x^1 \frac{P_{ee}(z)}{z}f_{ee}\left(\frac{x}{z},s\right)dz - \left[\frac{\alpha}{2\pi}\int_0^1 P_{ee}(t)dt\right]f_{ee}(x,s) \\
&= \frac{\alpha}{2\pi}\left\{\int_x^{x^+}\frac{P_{ee}(z)}{z}f_{ee}\left(\frac{x}{z},s\right)dz \right.\\
&\quad \left. -\left[f_{ee}(x,s)\int_0^1 P_{ee}(t)dt - \int_{x^+}^1\frac{P_{ee}(z)}{z}f_{ee}\left(\frac{x}{z},s\right)dz\right]\right\} \\
&\simeq \frac{\alpha}{2\pi}\left\{\int_x^{x^+}\frac{P_{ee}(z)}{z}f_{ee}\left(\frac{x}{z},s\right)dz - I^+(\varepsilon)f_{ee}(x,s)\right\},
\end{aligned}
$$
(2.44)

with $x^+ = 1 - \varepsilon$. The last approximate equality follows by taking the limit $z \to 1$ in the third integral, and consequently by taking $f_{ee}(x,s)$ out from it. Using Eq. (2.41) we replace $I^+(\varepsilon)$, obtaining the following equation:

$$
d\left[f_{ee}(x,s')\Pi(s,s')\right] = \frac{\alpha}{2\pi}\Pi(s,s')\frac{ds'}{s'}\int_x^{x^+}\frac{P_{ee}(z)}{z}f_{ee}\left(\frac{x}{z},s'\right),
$$
(2.45)

whose solution reads

$$
f_{ee}(x,s) = \Pi\left(s,m^2\right)\delta\left(1-x\right) + \frac{\alpha}{2\pi}\int_{m^2}^s\frac{ds'}{s'}\Pi(s,s')\int_x^{x+}\frac{dz}{z}P_{ee}(z)f_{ee}(\frac{x}{z},s'),
$$
(2.46)

where we have used the initial condition $f_{ee}(x,m^2) = \delta\left(1-x\right)$. Reminding the definition of $f_{ee}(x,s)$, Eq. (2.46) states that the probability to find, at the scale s, the electron with a fraction x of its original energy, is the sum of two contributions: the first term of (2.46) accounts for the evolution from the initial scale m^2 to scale s without photon emissions above the energy threshold ε, while the second represents the probability of a photon emission at scale s'. The evolution from the initial scale m^2 to the branching scale s' is absorbed in the term $f_{ee}(\frac{x}{z},s')$, Therefore Eq. (2.46) is an implicit solution of the AP equation, which can be solved iteratively. The complete solution

is an infinite sum of terms, where $\Pi\left(s, m^2\right)\delta\left(1-x\right)$ is the first term, while the $(n+1)$-th term is

$$\left(\frac{\alpha}{2\pi}\right)^n \int_{m^2}^{s} \frac{ds_1}{s_1} \int_{m^2}^{s_1} \frac{ds_2}{s_2} \cdots \int_{m^2}^{s_{n-1}} \frac{ds_n}{s_n} \Pi\left(s, s_1\right)\Pi\left(s_1, s_2\right)\cdots\Pi\left(s_n, m^2\right) \times$$

$$\times \int_{0}^{x^+} dx_1 \int_{0}^{x^+} dx_2 \cdots \int_{0}^{x^+} dx_n P_{ee}\left(x_1\right) P_{ee}\left(x_2\right)\cdots P_{ee}\left(x_n\right)\delta\left(x - x_1 x_2 \cdots x_n\right)$$

$$(2.47)$$

From the discussion we have developed so far it should be easily understood that the branching evolution, described by the iterative solution of the AP equation, is a Markov process, in the sense that what happens at a given stage of the evolution does not depend on the sequence of the preceding events. It follows that Monte Carlo methods are particularly suitable to simulate the emission of additional photons in a generic hard scattering. In particular, the Parton Shower algorithm is based on the implicit expression of the AP equation in (2.45) and it provides an exact numerical solution of the AP equation, in the sense that, for a given virtuality s, it generates x according to $f_{ee}(x, s)$. The steps of the algorithm for an initial state electron are the following:

1. set the initial virtuality $s' = m^2$;

2. generate a random number ξ;

3. solve the equation $\Pi(s'', s') = \xi$ for s'';

4. if $s'' \leq s$ no photon emission occurred and the algorithm stops;

5. if $s'' > s$ a photon emission has occurred. Then the energy fraction z carried by the electron after photon emission has to be generated according to the AP vertex $P_{ee}(z)$.

6. update the virtuality $s' = s''$. Go back to step 2.

At this point some critical comments on the PS algorithm are in order. First of all we remark that, according to the probabilistic interpretation of the AP equation, the PS algorithm preserves the unitarity. This crucial property can be easily understood from a close analysis of the $(n+1)$-th term of $f_{ee}(x, s)$ in (2.47). In fact from the rule of composite probability follows that

$$\Pi(s, s_1)\Pi(s_1, s_2)\cdots\Pi(s_n, m^2) = \Pi(s, m^2), \qquad (2.48)$$

so that performing the integral over x we get

$$\int_0^1 dx f_{ee}(x, s) = \Pi\left(s, m^2\right) \sum_{n=0}^{\infty} \frac{1}{n!} \left(\frac{\alpha}{2\pi} I^+ \log \frac{s}{m^2}\right)^n =$$
$$= \Pi(s, m^2)\Pi^{-1}(s, m^2) = 1. \tag{2.49}$$

The unitarity has an important consequence: the PS algorithm does not change the total cross section calculated at the Leading Order accuracy, whereas it allows to separate the contributions coming from different photon multiplicities. From Eq. (2.49) we can read out the probability that n photons are emitted in the final states, given by

$$\mathcal{P}(n) = \Pi\left(s, m^2\right) \frac{1}{n!} \left(\frac{\alpha}{2\pi} I^+ \log \frac{s}{m^2}\right)^n . \tag{2.50}$$

Moreover, we must stress that the PS provides the reconstruction of the kinematics during the shower evolutions, allowing a detailed description of the final state. We limit to mention that there is more than one prescription for the reconstructions of the momenta of the final state particles, starting from the energy fractions and the virtualities generated by the PS at each branching. A critical discussion on this delicate argument is given in Ref. [73], which the reader can refer to for further details.

A comment has to be done on the sign of the virtualities generated by the PS algorithm. In particular, moving towards the hard scattering, an initial state particle produces a photon cascade (the so called space-like shower), evolving from the mass shell condition decreasing its virtuality down to a maximum negative value. On the contrary, if we consider a final state particle the PS starts at a maximum positive virtuality fixed by the scale of the hard process and it runs out when the mass shell condition is achieved.

We conclude this chapter with a final remark. In the PS framework each external charged particle produces its own photon shower independently from the other ones. It follows that quantum effects, coming from the interference between contributions in which the same photons are emitted by different external particles, are not taken into account. In Chapter 4 we will introduce an improved PS algorithm which is able to simulate collinear emissions including interference effects.

State of the art in Higgs physics

To better understand how the work presented in this dissertation lies in the current Higgs physics program at the LHC, we present a brief overview on Higgs physics. In Sec. 3.1 we summarize the status of experimental and theoretical constraints on Higgs boson mass before LHC started collecting data. In Sec. 3.2 we describe the relevant Higgs production and decay modes, providing, for the various channels, an overview on the status of theoretical calculations and the available numerical tools. In Sec. 3.3 we recap the main aspects of the historical discovery, by ATLAS and CMS, of a new boson compatible with the SM Higgs boson. Finally, in Sec. 3.4 we review the current knowledge of the Higgs boson properties, as the mass, the CP nature and the couplings to the other SM particles.

3.1   Introduction

In Chapter 1 we have seen that gauge bosons and fermions acquire mass through the EWSB mechanism: the spontaneous breaking of the $SU(2)_L \otimes U(1)_Y$ gauge symmetry is realized by a complex scalar doublet which acquires a non-vanishing vacuum expectation value. Three degrees of freedom are absorbed in the longitudinal components of weak bosons, while the remaining one corresponds to the Higgs particle, a scalar boson with $J^{\mathrm{CP}} = 0^{++}$ quantum numbers under charge and parity conjugation.

The Higgs boson mass is a free parameter of the SM. Nevertheless, before entering the LHC era, there were both experimental and theoretical arguments suggesting the mass range where the Higgs boson was expected to be found. Direct Higgs searches at LEP2 allowed to put a lower limit on the Higgs mass $M_H \gtrsim 114$ GeV at 95 % confidence level (CL) [75]. Further-
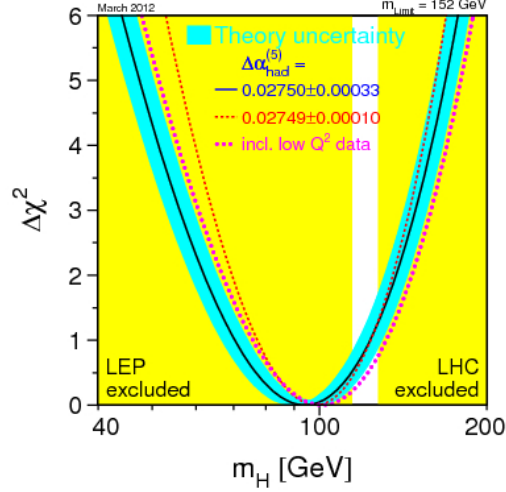
Figure 3.1:   The $\Delta\chi^2$ of the fit to the electroweak precision data as a function of M_H. The solid line results when all data are included and the blue/shaded band is the estimated theoretical error from unknown higher-order corrections. The effects of including the low Q^2 data and the use of a different value for $\Delta\alpha_{had}$ are also shown. [74].

more, the global fit of the electroweak precision data, to which the Higgs boson contributes through higher-order corrections, yields the best fit value $M_H = 92^{+34}_{-26}$ GeV, corresponding to an upper value of $M_H \lesssim 160$ GeV (see Fig. 3.1 taken from [74]).

After the shutdown of the LEP collider in 2000, the direct searches for the Higgs boson continued at Fermilab's Tevatron $p\bar{p}$ collider. The combined results from approximately 10 fb^{-1} recorded by the CDF and D0 experiments [76] excluded two ranges in M_H: between 90 GeV and 109 GeV, and between 149 GeV and 182 GeV. In addition, a broad excess was seen in the mass range $115\,\text{GeV} < M_H < 140\,\text{GeV}$ with a local significance of 3σ at $M_H = 125$ GeV.

Besides direct searches of the Higgs particle and theoretical constraints based on the analysis of available data, lower and upper limits on the Higgs boson mass can be derived by pure theoretical arguments. First of all, the Higgs boson mass has a crucial impact on the unitarity of the SM. It is known that, at very high energies, the cross section of a process with external gauge bosons is dominated by the longitudinal contribution of the gauge bosons themselves. The Electroweak Equivalence Theorem [77, 78, 19] states that in these circumstances external gauge bosons can be replaced by the relative

Goldstone bosons. It follows that for scattering processes involving external vector bosons, such as $WW \rightarrow WW$ scattering, the cross section grows up with the energy, leading, at some stage, to unitarity violation, so that an upper bound $M_H \lesssim 700$ GeV has been derived by imposing unitarity in high energy scatterings [79].

Other important hints on the Higgs boson mass come from the running of the Higgs self-coupling λ_H, whose variation with the energy scale Q^2 is ruled by the Renormalization Group Equations (RGE). For a large value of the Higgs mass, $\lambda_H(Q^2)$ is a monotonically increasing function of the energy and it could become, at some stage, infinite. On the other side, for small values of λ_H, higher-order corrections would drive the self-coupling to negative values, leading to an unstable vacuum. These arguments have been used to derive theoretical constraints on the quartic Higgs coupling and hence on the Higgs boson mass. We skip the details, for which we refer to Ref. [80] and references therein. We limit ourselves to report the lower and upper limits on the Higgs boson mass for the case in which the validity of the SM is extended up to the Planck scale $M_P \sim 10^{18}$ GeV. In this conservative scenario the Higgs mass lies in the range $130\,\text{GeV} \lesssim M_H \lesssim 180\,\text{GeV}$ (see Ref. [81]).

From this point of view, the discovery of the Higgs boson with a mass of 125 GeV represents a triumph of the SM and it confirms its validity in the description of high energy processes. The averaged mass value measured by ATLAS and CMS collaborations, $M_H = 125.1 \pm 0.24$ GeV [29] is remarkably close to the best-fit value extracted from the analysis of LEP2 precision data, confirming the predictive power of the SM. Furthermore, the condition for the absolute stability of the electroweak vacuum $\lambda(M_P) > 0$ has been recently derived [82]. The analysis takes into account all available higher-order contributions and it gives the lower bound $M_H \gtrsim 129$ GeV for the present value of top quark mass and the strong coupling constant, $m_t = 173.2 \pm 0.9$ GeV and $\alpha_S(M_Z) = 0.1184 \pm 0.0007$ [62]. Allowing for a 2σ variation of the top mass one obtains $M_H \geq 125.6$, a value that is close to the mass of the new particle discovered at the LHC.

3.2 Higgs production and decay channels

A Higgs particle with a mass of 125 GeV has the nice feature to be produced in several channels at the LHC and to be detected in a variety of decay modes, allowing a detailed study of the Higgs properties. In order to understand the relative importance of the various channels, we illustrate the salient features of the main production and decay modes. This overview will be also useful to review the state of the art of theoretical calculations and the relative
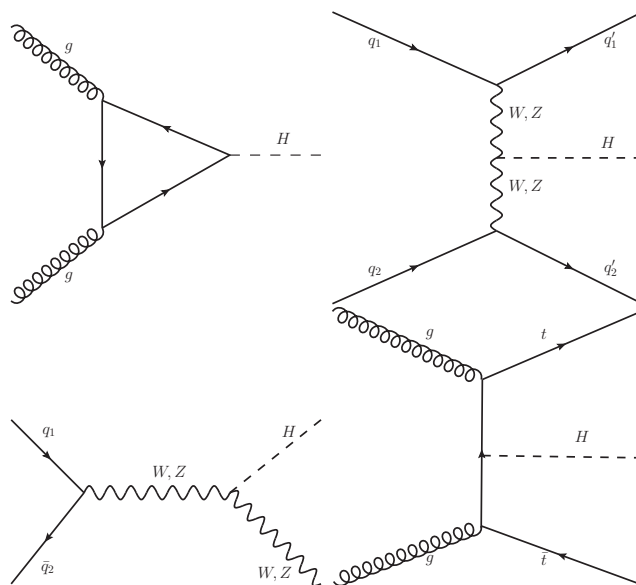
Figure 3.2: LO diagrams for the main Higgs production modes: gluon-gluon fusion (top-left diagram), vector boson fusion (top-right diagram), VH associated production (bottom-left diagram) and $t\bar{t}H$ associated production (bottom right diagram).

uncertainties. A detailed description of technical aspects is beyond the scope of this review. The reader may refer to the three CERN reports by the LHC Higgs Cross Section Working Group [25, 26, 27] and to the references therein and to the upcoming CERN Yellow Report 4 which will be published soon **??**.

3.2.1 Production modes

The main production mechanisms at the LHC are gluon-gluon fusion, vector boson fusion (VBF), associated production with a gauge boson (VH) and associated production with top quarks. Some illustrative examples of lowest order Feynman diagrams are depicted in Fig. 3.2.

Gluon-gluon fusion

Gluon-gluon fusion through a heavy-quark loop [83] is the main production channel of the Higgs boson at hadron colliders (see Figs. 3.3 and 3.4). The inclusive cross section for a Higgs boson mass of 125 GeV (≈ 20 pb at $\sqrt{s} = 7 - 8$ TeV and ≈ 50 pb at $\sqrt{s} = 13$ TeV) is roughly one order of magnitude larger than the vector boson fusion cross section. The impact of QCD
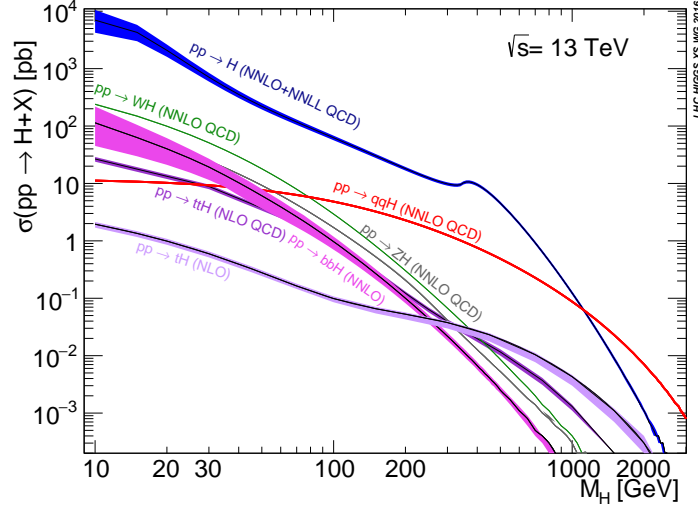
Figure 3.3: Inclusive Higgs boson cross section as a function of the Higgs boson mass in the mass range [10, 2000] GeV for a center-of-mass energy of 13 TeV in proton-proton (*pp*) collisions (taken from [28]).
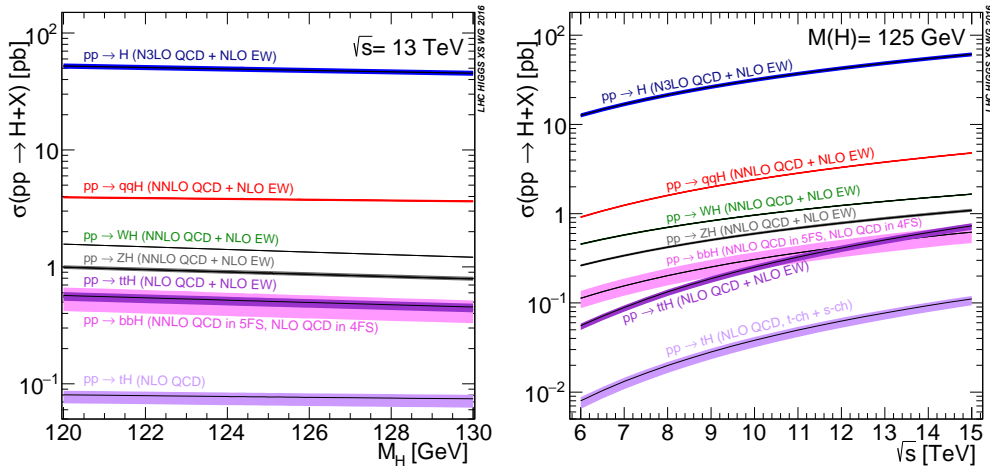

Figure 3.4: Left plot: Inclusive cross section for the main Higgs production modes as a function of the Higgs boson mass for a center-of-mass energy of 13 TeV in *pp* collisions. Right plot: Higgs boson cross section for $M_H = 125$ Gev of the hadronic center-of-mass energy (taken from [28]).

corrections is very large and many efforts have been devoted in recent years to reduce the theoretical uncertainties. Since the limit $m_t \to \infty$ provides a very good approximation for the evaluation of the main top-quark contributions, QCD corrections are usually evaluated from an effective Lagrangian containing a local operator $H G^a_{\mu\nu} G^{a\,\mu\nu}$, where $G_{\mu\nu}$ is the field-strength tensor of the gluon field. In this framework NLO [84, 85, 86] and next-to-next-to-leading order (NNLO) [87, 88, 89] QCD corrections have been calculated for cross section and distributions, showing a slowly convergent perturbative QCD expansion. With respect to the LO prediction, NLO QCD corrections increase the cross section by approximately 80%, while NNLO corrections lead to a further enhancement of 20%. Finally, N^3LO QCD corrections to the inclusive cross section have been recently computed in the heavy top-quark approximation [90]. The up-to-date master formula for the calculation of the inclusive gluon-gluon fusion cross section is taken from Ref. [91] and it reads

$$\hat{\sigma} \simeq R_{LO} \left(\hat{\sigma}_{EFT} + \delta_t \hat{\sigma}^{NNLO}_{EFT} + \delta \hat{\sigma}_{EW} \right) + \delta \hat{\sigma}^{LO}_{m.e.} + \delta \hat{\sigma}^{NLO}_{m.e.}. \qquad (3.1)$$

In this formula all the available higher-order corrections are included. QCD corrections up to N^3LO accuracy and calculated in the EFT framework are absorbed in $\hat{\sigma}_{EFT}$. The rescaling factor

$$R_{LO} = \frac{\sigma^{LO}_{ex.}}{\sigma^{LO}_{EFT}}, \qquad (3.2)$$

improves the validity of the EFT approximation, with $\sigma^{LO}_{ex.}$ denoting the exact (hadronic) LO cross section in the SM, with a massive top quark and 5 massless quarks. The effect of top, bottom and charm masses at LO and NLO are included through the terms $\delta \hat{\sigma}^{LO}_{m.e.}$ and $\delta \hat{\sigma}^{NLO}_{m.e.}$. Beyond NLO, only EFT results are available. However, subleading corrections at NNLO calculated in the effective theory as an expansion in the inverse top mass (see Refs. [92, 93, 94, 95]) are included in Eq. (3.1) through the term $\delta_t \hat{\sigma}^{NNLO}_{EFT}$. Finally, $\mathcal{O}(\alpha)$ electroweak corrections [96, 97, 98] and mixed QCD-EW corrections of $\mathcal{O}(\alpha \alpha^3_S)$ [99] are included through the term $\delta \hat{\sigma}_{EW}$. Using the master formula in Eq. (3.1) the best-prediction for the inclusive gluon-gluon cross section for a center-of-mass energy $s = 13$ TeV is

$$\sigma = 48.58 \, \text{pb}^{+2.22\,\text{pb}\,(+4.56\%)}_{-3.27\,\text{pb}\,(-6.72\%)} \, (\text{theory}) \pm 1.56 \, \text{pb} \, (3.20\%) \, (\text{PDF} + \alpha_S). \quad (3.3)$$

The impact of N^3LO QCD corrections on the inclusive cross section with respect to the sum of all other contributions detailed above is of the order of 3%. Regarding the uncertainties quoted in (3.3), the PDF and α_s uncertainties are computed following the recommendation of the PDF4LHC working

group [100]. The remaining theoretical uncertainties in (3.3) are obtained by adding linearly various sources of theoretical uncertainty affecting the different contributions to the inclusive cross section. We limit ourselves to remark that the inclusion of N³LO QCD corrections stabilizes the effect of varying the factorization and renormalization scales in the interval $[M_H/4, M_H]$, reducing it by a factor of five compared to NNLO.

Fixed-order calculations can be further improved by resumming the soft-gluon contributions at all orders. In this context, the best available prediction for the total cross section is given by the formula

$$\sigma_{N^3LO+N^3LL} = \sigma_{N^3LO} + \Delta_3\sigma_{N^3LL}, \tag{3.4}$$

where the term $\Delta_3\sigma_{N^3LL}$ contains the all-orders resummation of enhanced collinear contributions at N³LL accuracy minus its expansion at N³LO [101].

Besides the improvements in the calculation of the inclusive cross section, accurate theoretical predictions of differential distributions are of great importance in order to probe the properties of the Higgs boson. To improve the signal to background ratio experimental cuts are implemented in the analysis. Furthermore, in many analysis, the events are separated according to the jet multiplicity. This separation is very useful to improve the signal to background ratio. For instance, $t\bar{t}$ pair production is a dominant background for the Higgs searches in the WW decay channel and it is removed by requiring zero jets in the final state. An accurate description of differential distributions is therefore necessary for a meaningful comparison between experimental data and theoretical predictions computed with Monte Carlo event generators. Several parton level codes for the computation of differential distributions in gluon-gluon fusion production are available [102, 103, 104, 105, 106, 107]. Regarding hadron level generators, three codes are used in experimental analysis: `Gosam+Sherpa` [108, 109], `MG5_aMC@NLO` [110] and `POWHEG NNLOPS` [111].

Vector boson fusion

The Higgs boson production in association with two hard jets is an essential process for the Higgs boson searches at the LHC and it receives contributions from different processes. The Higgs production via vector boson fusion (VBF) proceeds via the $t-$ or $u-$channel scattering of two quarks, mediated by a W or Z boson, with the Higgs boson radiated off the weak boson propagator. The two jets have a strong tendency to be emitted in the forward and backward directions with a large rapidity gap in between. In fact, the gluon emission in the central rapidity region is suppressed by the color-singlet nature of the weak-gauge boson exchange [112, 113]. This peculiarity drives the choice of selection cuts in order to increase the VBF signal with respect

to background processes, such as loop-induced gluon-gluon fusion $H + 2$ jets production and Higgs production in association with a W, Z bosons which decays into a $q\bar{q}$ pair. From the theoretical side, several Monte Carlo programs are available:

- `HAWK` is a parton level event generator for Higgs production in VBF and VH channels. Regarding $H + 2$ jets channel `HAWK` provides the complete NLO QCD and EW corrections for all vector boson fusion and quark-antiquark annihilation diagrams, *i.e.* the s-channel Higgs production in association with a weak boson decaying hadronically. Higgs off-shell effects can be taken into account in the calculation. For further details we refer to [114, 115];

- `VBFNLO` is a parton level event generator for the simulation of various processes with weak bosons at NLO QCD accuracy [116, 117, 118]. For VBF Higgs production $\mathcal{O}(\alpha)$ EW corrections are included. Moreover, running options for the inclusion of anomalous couplings are available;

- VBF-induced Higgs production has been implemented in the `POWHEG BOX` [119] allowing the matching of NLO QCD corrections with a Parton Shower event generator according to the `POWHEG` method [120]. More recently, the implementation of Higgs production in association with three jets via VBF, based on the NLO QCD calculation described in Ref. [121], has also become available;

- Higgs production through VBF, possibly in association with extra jets, can be generated automatically in `MadGraph5_aMC@NLO`, allowing phenomenological studies at NLOPS accuracy [122, 123];

- LO, NLO and NNLO QCD corrections to VBF Higgs production approach are included in the `VBF@NNLO` program [124, 125]. The higher-order corrections are calculated in the structure function approach, *i.e.* by treating the quark lines independently.

WH and ZH associated production

The Higgs productions in association with a W or a Z boson, also known as Higgs-strahlung processes, are important channels at the LHC, mostly because they provide a relatively clean environment for the search of Higgs boson decay into bottom quarks. At NLO, QCD corrections to VH associated productions are similar to the NLO QCD corrections to Drell-Yan process [126] and can be written in a factorized form. By contrast, NLO EW

corrections cannot be factorized and have been calculated in Ref. [127, 128]. At NNLO, Drell-Yan corrections [129] constitute a subset of VH associated production. In addition, loop induced contributions which are sensitive to the Yukawa couplings have to be taken into account in the calculations (see Refs. [130, 131, 132]). Also for VH production different tools are available:

- as already mentioned, the parton level event generator `HAWK` calculates full NLO QCD and EW corrections to the VH associated production in the channels $pp \to WH \to \nu_l l H$ and $pp \to ZH \to llH/\nu\nu H$ [128]. As for VBF production, Higgs boson off-shell effects can be taken into account;

- NLO QCD accuracy for Higgs associated production with additional jets can be obtained at NLO QCD accuracy with `MadGraph5_aMC@NLO` using the `FxFx` merging technique [133];

- the complete NNLO QCD corrections are available in `MCFM` [134], including the decays of the unstable Higgs and vector bosons;

- `VHNNLO` is a parton level program for the calculation of fully differential cross sections for $pp \to WH$ and $pp \to ZH$ including up to second order QCD corrections. The decays of the weak bosons into leptons and the Higgs decay a $b\bar{b}$ pair are taken into account [135].

- `VH@NNLO` is a numerical program for the VH associated production, and it includes NNLO QCD as well as NLO EW corrections [136].

Higgs production in association with a $t\bar{t}$ pair

Higgs boson production in association with a top-quark pair can provide important information on the the top-Higgs Yukawa coupling. The LO cross section for this production channel was computed in Refs. [137, 138, 139, 140]. Later, the NLO QCD corrections were evaluated [141, 142, 143, 144, 145] yielding a moderate increase of the total cross section of about 20%, but reducing significantly the scale dependence of the inclusive cross section. The total theoretical errors, estimated by combining the uncertainties from factorization and renormalization scales, the value of α_S, and parton distributions, amount to $10 - 15\%$ of the corresponding inclusive cross section. Fixed order QCD calculations of $t\bar{t}H$ production have been interfaced with parton-shower using `MC@NLO` and `POWHEG` methods and several tools are nowadays available (see for instance Refs. [146, 147, 148, 149, 150]). Quite recently, $\mathcal{O}(\alpha)$ EW corrections have been calculated in Refs. [151, 152, 153]. Although their effect on total rates is usually suppressed with respect to NLO QCD corrections
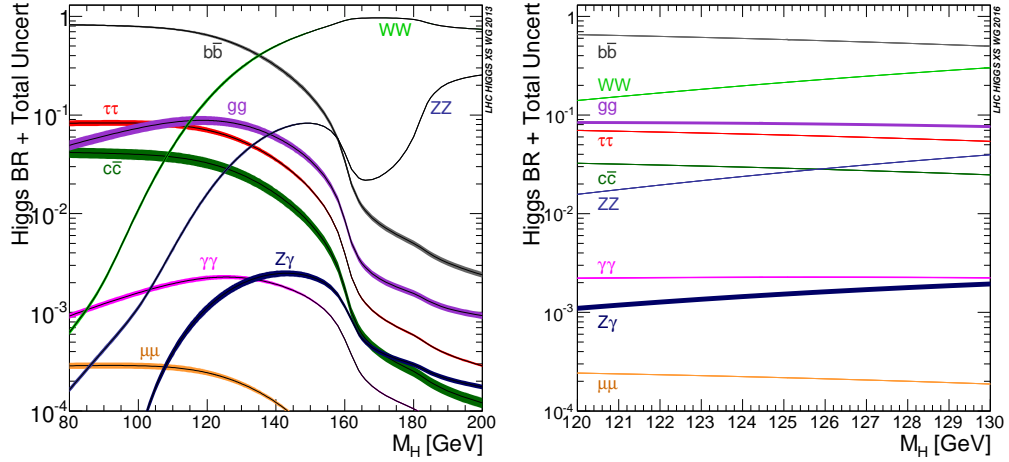
Figure 3.5: Standard Model Higgs boson decay branching ratios as a function of the Higgs boson mass. In the left plot the mass range [80, 200] GeV is considered, while in the right plot a zoom in the tight mass window [120, 130] GeV is shown (taken from [28]).

by a factor of order α/α_S, they can be enhanced by electroweak Sudakov logarithms [154] in the high energy limit.

3.2.2 Higgs boson decay: branching ratios and total width

For a detailed study of the Higgs boson properties, precision calculations of all relevant Higgs partial decay widths are mandatory. A Higgs boson mass of 125 GeV provides the opportunity to access to several decay channels and consequently to explore the couplings of the Higgs boson to many SM particles. In Fig. 3.5 the contributions of different decay channels to the total Higgs width are shown. The dominant decay modes are $H \to b\bar{b}$ and $H \to WW^*$, followed by $H \to gg$, $H \to c\bar{c}$ and $H \to ZZ^*$. The decays of unstable weak bosons into quarks or leptons have to be taken into account, considering leptonic, semileptonic and hadronic final states. Finally, with smaller rates, the decays $H \to \gamma\gamma$, $H \to Z\gamma$ and $H \to \mu^-\mu^+$ follow. Let us remark that loop-induced channels as Higgs decay into gluons, photons and $Z\gamma$ can provide indirect access to the coupling of the Higgs to heavy quarks, W and Z bosons and even to the Higgs self-coupling [155]. The Higgs total width is given by the sum of all partial contributions. For the evaluation of the theoretical uncertainties to the partial and total width we limit to mention that there are two sources of uncertainties: the first ones

arise from the uncertainties of the input parameters, while the second ones are due to the missing higher-order corrections. For further details we refer to Ref. [156].

HDECAY [157, 158] and Prophecy4f [39, 40, 41, 42] are the reference tools for the calculations of branching ratios and total Higgs width. In particular, for a given value of the Higgs mass, HDECAY calculates the partial decay widths for all kinematically accessible channels. The decays $H \to b\bar{b}$ and $H \to c\bar{c}$ are computed including the complete massless QCD corrections up to N^{4}LO accuracy [159], with a corresponding scale dependence of about 0.2%. The complete EW NLO corrections have been recently implemented. The corresponding accuracy is of the order of 0.5% for $M_H < 135$ GeV. The same applies to the EW corrections to $H \to \tau^+\tau^-$. For Higgs decays into top quarks HDECAY includes the complete NLO QCD corrections [160, 161, 162, 163, 164, 165] interpolated to the large-Higgs-mass results at N^{4}LO far above the threshold [159]. The scale dependence is below 5%. Regarding the EW corrections, only the contributions due to the self-interaction of the Higgs boson are included. The contribution of the neglected EW corrections amounts to about 0.5% for $M_H < 500$ GeV. For the loop induced $H \to gg$ decay, the related QCD corrections are calculated up to N^{3}LO [166] accuracy. The uncertainty from scale dependence is about 3%. NLO EW corrections are also included [98]. The impact of missing higher orders is estimated to be below 1%. For $H \to \gamma\gamma$ channel, HDECAY includes the full NLO QCD and EW corrections [96, 97, 98, 167, 168, 169]. Also for this process the uncertainty due to missing higher-orders is about 1%. The partial decay width $H \to Z\gamma$ is included in HDECAY at LO including the virtual W, top, bottom and τ loop contributions. The QCD corrections are small in the intermediate Higgs mass range [170] and can thus safely be neglected. The associated theoretical uncertainty is about 1%. The electroweak corrections to this decay mode are unknown and the consequent theoretical uncertainty is about 5% in the intermediate Higgs mass range.

On the other hand, Prophecy4f is a Monte Carlo event generator for $H \to W^*W^*/Z^*Z^* \to 4f$ decay channels. Leptonic, semi-leptonic, and hadronic final states are considered. The code calculates the partial width for any possible 4-fermion final state, including complete NLO QCD and EW corrections. The dominant two-loop contributions in the heavy-Higgs-mass limit proportional to $G_F^2 M_H^4$ are included according to Refs. [171, 172]. Since the calculations are performed in the complex-mass scheme (see Sec. 1.5 and Refs. [43, 51]), on-shell approximations are not necessary and the results are valid above, near, and below the gauge-boson pair thresholds. Eventually, the master formula for the calculation of the Higgs total width reads
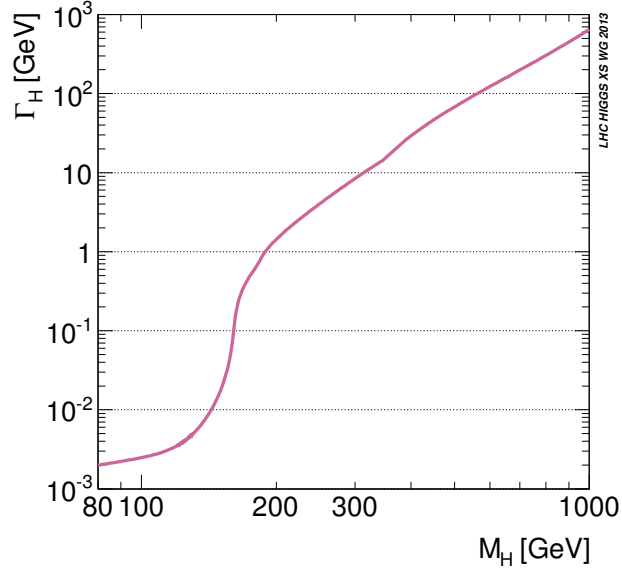
Figure 3.6: Total Higgs width as a function of the Higgs mass (taken from [28]).

$$\Gamma_H = \Gamma^{\text{HD}} - \Gamma_{ZZ}^{\text{HD}} - \Gamma_{WW}^{\text{HD}} + \Gamma_{4f}^{\text{Proph.}}, \tag{3.5}$$

where Γ^{HD} is the total Higgs width calculated with `HDECAY`, while $\Gamma_{4f}^{\text{Proph.}}$ includes the decay width into four fermions at NLO QCD and EW accuracy, calculated with `Prophecy4f`. This term can be split into WW, ZZ and interference contributions:

$$\Gamma_{4f}^{\text{Proph.}} = \Gamma_{H \to W^*W^* \to 4f} + \Gamma_{H \to Z^*Z^* \to 4f} + \Gamma_{H \to W^*W^*/Z^*Z^* - \text{int}}. \tag{3.6}$$

The terms Γ_{ZZ}^{HD} and Γ_{WW}^{HD} in Eq. (3.5) stand for the `HDECAY` partial widths for the Higgs decay into a pair of on-shell W and Z bosons and they have to be subtracted in order to avoid double counting.

For $M_H = 125$ GeV the total Higgs width is about 4 MeV (see Fig. 3.6), too small to be resolved experimentally. Nevertheless, a method for constraining the Higgs width has been proposed in recent years. This method is based on the substantial Higgs off-shell contribution to $pp \to H \to VV$ cross section [173] and it has allowed ATLAS [174] and CMS [175] to put the upper limits $\Gamma_H < 7.5\,\Gamma_H^{\text{SM}}$ and $\Gamma_H < 5.4\,\Gamma_H^{\text{SM}}$ at 95% CL, respectively.
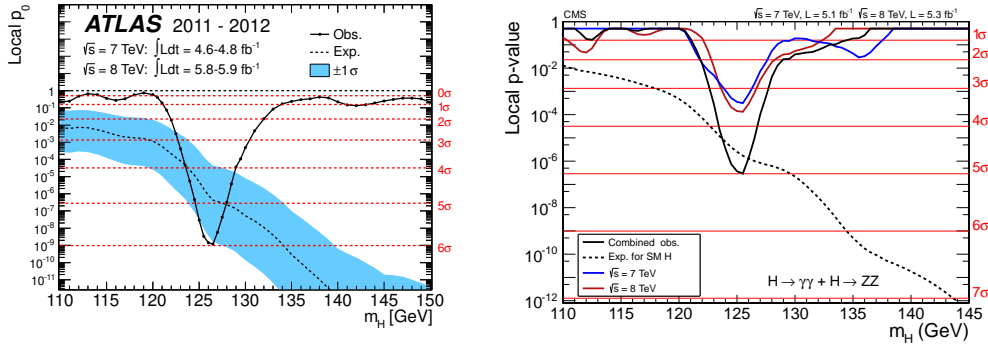
Figure 3.7: Left panel: observed local significance (solid line) p_0 for the combination of the data collected by ATLAS at 7 TeV and 8 TeV in the $H \to \gamma\gamma$ and $H \to 4\ell$ channels. The dashed curve shows the expected local p_0 under the hypothesis of a SM Higgs boson signal at that mass with its 1σ (from Ref. [23]). Right panel: The observed local p-value for 7 TeV and 8 TeV data collected by CMS, and their combination as a function of the SM Higgs boson mass. The dashed line shows the expected local p-values for a SM Higgs boson with a mass M_H (from Ref. [24]).

3.3 The discovery of the Higgs boson

In Sec. 3.1 we have summarized the state of the art in Higgs searches before LHC started collecting data. On July 4th, 2012, ATLAS [23] and CMS [24] collaboration announced the observation of a new narrow resonance with a mass of about 125 GeV. The analyzed data by ATLAS corresponded to an accumulated luminosity of 4.8 fb^{-1} at $\sqrt{s} = 7$ TeV in 2011 and 5.8 fb^{-1} at $\sqrt{s} = 8$ TeV in 2012, while for CMS the corresponding values of integrated luminosity are 5.1 fb^{-1} at $\sqrt{s} = 7$ TeV and 5.3 fb^{-1} at $\sqrt{s} = 8$ TeV. The evidence was that the new particle decays into $\gamma\gamma$ and ZZ^* with rates compatible with the Higgs hypothesis. Since the discovery of the new particle, ATLAS and CMS continued collecting data and all the subsequent analysis have consolidated the hypothesis that the new particle is the Higgs boson. In 2013, at the end of LHC Run-1, both ATLAS and CMS had reached an integrated luminosity of about 20 fb^{-1}, without finding any evidence of departures from the SM hypothesis.

For a Higgs boson mass of 125 GeV the five decay channels which could play a relevant rôle at the LHC are the Higgs decay into a pair of bottom quarks, the Higgs decay into a $\tau\bar{\tau}$ pair, the four fermions decays $H \to WW, ZZ \to 4f$ and the Higgs decay into two isolated photons. Despite their relative small branching ratio, the two main decay channels involved in the new boson discovery are the $H \to \gamma\gamma$ and $H \to Z^*Z^* \to 4l$ channels.

In fact the sensitivity to a specific channel depends on a certain number of factors: the production cross section, the branching ratio of the decay channel, the mass resolution of the detector and the level of the background of the final state. The excellent mass resolution (of the order of 1-2%) and the relative clean environment have made these two channels of crucial importance for the discovery of the Higgs boson and for the determination of its properties. In the $H \to \gamma\gamma$ channel a search is performed for a narrow peak over a smoothly falling background in the invariant mass distribution of two high p_T photons. The background in this channel stems from prompt $\gamma\gamma$, $\gamma+$ jet and dijet processes. On the other side, the search of the Higgs boson in the channel $H \to Z^*Z^* \to \ell^+\ell^-\ell'^+\ell'^-$, with $\ell = e, \mu$, is performed by looking for a narrow mass peak over a small continuous background dominated by the $t-$ and $u-$channel $q\bar{q}$ annihilation into a pair of Z bosons and the gluon-gluon fusion into two Z bosons mediated by a quark box. The excess of events in these channels were confirmed by the high sensitivity channel $H \to W^*W^* \to 2\ell2\nu$, despite its low mass resolution (about 20%). When the discovery of the new boson was announced, ATLAS observed the largest excess with a local significance of 5.9σ at a mass $M_H = 126.5$ GeV, while CMS observed maximum significance of 4.9σ at a mass of $M_H = 125.5$ GeV, as shown in Fig. 3.7.

3.4   Properties of the discovered Higgs boson

As already mentioned, after the discovery of the new boson, ATLAS and CMS continued collecting data in order to study its properties and to confirm that the new particle is the SM Higgs boson. To this end, a strong effort has been made to investigate the properties of the new boson using the entire Run-1 data. An essential ingredient for a direct study of the EWSB sector is the precise measurement of the Higgs boson mass. As we have seen in the previous section, the two decays channels with the best mass resolution are $H \to \gamma\gamma$ and $H \to Z^*Z^* \to 2\ell2\ell'$ with $\ell, \ell' = e, \mu$. The Higgs mass measurements are performed independently in these two channel. The results are then combined to increase the total accuracy. In Fig. 3.8 the summary of the mass measurement performed by ATLAS and CMS for the two photons and four leptons channels and for a combined analysis is reported. The most accurate measurement of the Higgs mass is provided by the combined analysis of ATLAS and CMS data [29] and it gives the result:

$$M_H = 125.09 \pm 0.21 \, \text{stat.} \pm 0.11 \, \text{syst. GeV} \qquad (3.7)$$
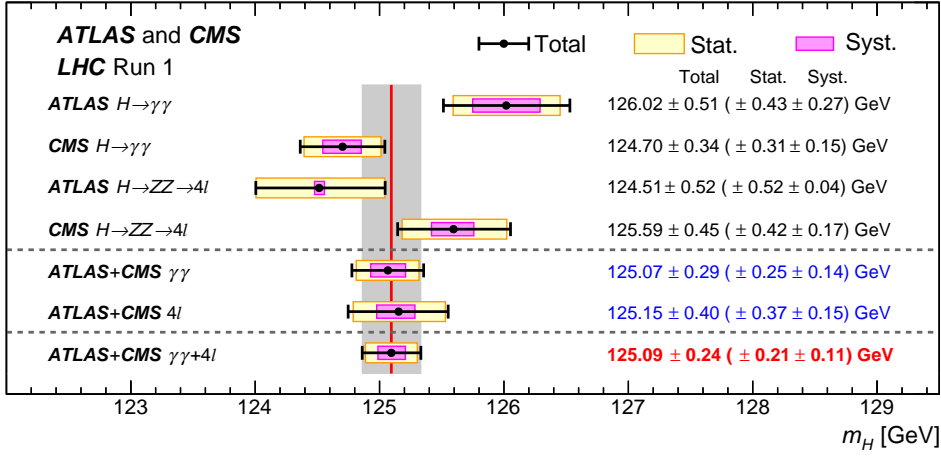
Figure 3.8: Summary of Higgs boson mass measurements from the individual analyses of 7 and 8 TeV data by ATLAS and CMS and from the combined analysis (from Ref. [29])

The extremely high precision measurement (the total uncertainty is about 0.2%) is dominated by statistical uncertainty and will be further improved by the analysis of present and future data collected at the LHC.

The compatibility of data with the SM hypothesis is foremost investigated by measuring the signal strength μ in the relevant decay modes. μ measures the departure from the theoretical SM prediction for a specific Higgs production mode times the decay branching fraction $H \to XX$ and it is given by the equation

$$\mu_{XX} = \frac{\sigma_{exp.}(pp \to H \to XX)}{\sigma_{SM}(pp \to H \to XX)} = \frac{\sigma_{exp.}(pp \to H) \times \mathrm{BR}_{exp.}(H \to XX)}{\sigma_{SM}(pp \to H) \times \mathrm{BR}_{SM}(H \to XX)}.$$
(3.8)

According to this equation, the rates are measured separately for the main Higgs production modes. As for the Higgs mass measurement, ATLAS and CMS data have been combined to increase the level of accuracy [32]. Fig. 3.9 shows the measured signal strength for the main production and decay modes. The compatibility between data and SM predictions is about 24% and 75% for production and decay strengths, respectively. The combined signal strength

$$\mu = 1.09 \pm 0.07 \text{ (stat.)} \pm 0.04 \text{ (syst.)} \pm 0.03 \text{ (th.)}$$
(3.9)

is in good agreement with the SM hypothesis. The Higgs boson production via gluon fusion and the Higgs boson decays into gauge bosons have been
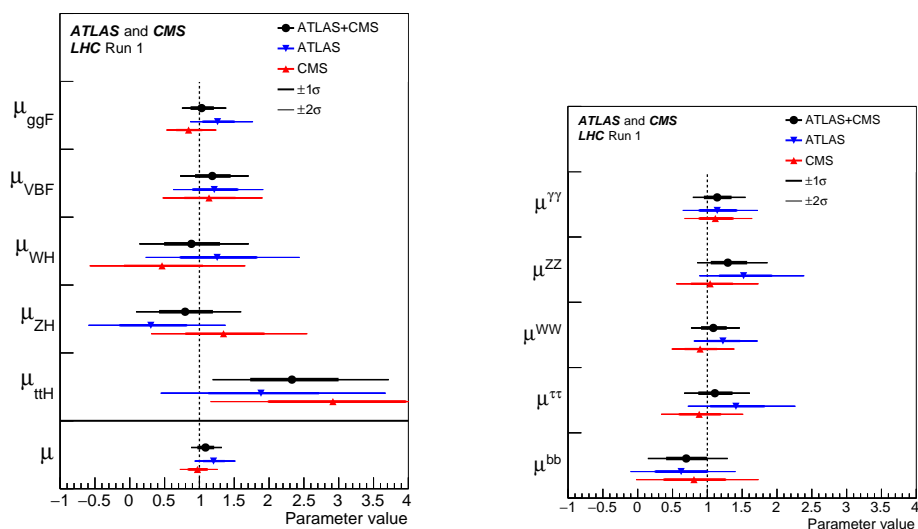
Figure 3.9: The measured production (left) and decay (right) signal strengths μ relative to the SM prediction for the combination of ATLAS and CMS data. Also shown are the results from each experiment [32].

observed with high significance independently by the two experiments. The combination of ATLAS and CMS data leads in addition to the clear observation of VBF production and $H \to \tau^+\tau^-$ decays with signal significance of 5.4σ and 5.5σ, respectively. The significance for the VH prodcution is above 3σ. The combined significance for the $t\bar{t}H$ production is 4.4σ , whereas only 2.2σ is expected, corresponding to a measured excess of events of 2.3σ with respect to the SM prediction. The signal strengths measured in each individual channel can be expressed in terms of the Higgs boson couplings relative to the SM prediction. The ratios of coupling stregths are measured in a model-independent way with a precision of 10%-20%, showing a good agreement with the SM predictions. The potential presence of physics beyond the SM is also probed using specific assumptions on the presence of new particles in gluon-gluon fusion production and $\gamma\gamma$ decay loops, or in direct Higgs boson decays. Under the assumption that there are no new particles appearing in the loops or in direct decays, the p-value of the compatibility between the data and the SM predictions is about 74%.

Besides detailed analysis of the Higgs boson to SM particles, the study of spin-parity properties represents a fundamental test in order to unveil the real nature of the new particle. To this end, extensive tests of various spin-parity J^{CP} hypothesis have been performed. These tests are based on the analysis of kinematic and angular correlation of the Higgs decay products.

All the alternative scenarios have been excluded at more than 99.9% confidence level in favor of the SM hypothesis of a spin 0^{++} particle [30, 31]. Possible small admixture of non SM CP states are still allowed and are now probed by measuring the tensor structure of the Higgs couplings to weak bosons. Moreover, the distribution in the azimuthal angle between the two jets produced in association with the Higgs in the VBF channel discriminates a CP–even from a CP–odd state [176]. Therefore, the VBF channel with the Higgs decaying into a $\tau^+\tau^-$ pair improves the sensitivity to the CP nature of the Higgs boson [177]. There is currently no sensitivity to set limits at 95% confidence level, but the limits obtained at 68% confidence level are about a factor of ten stronger than the corresponding results from $H \rightarrow VV^{(*)}$ decays.

Higgs boson decay into four charged leptons

The LHC Run-2 started in the spring of 2015, with centre-of-mass energy of 13 TeV and with a consequent increment of the Higgs total cross section by a factor of 2 with respect to the Run-1. At the end of Run-2, in 2017, it is foreseen that 100 fb^{-1} of collision data will have been collected, arriving at 300 fb^{-1} in 2021 at the end of Run-3. Then, the accelerator will be subject an important upgrade to significantly increase the luminosity. Indeed, the next phase is known as High Luminosity LHC (HL-LHC) [33, 34, 35]. The hope is to reach an integrated luminosity of about 3 ab^{-1} within 2030-35.

With these expected values of integrated luminosity there are many measurements that could be significantly improved. With an integrated luminosity of about 100 fb^{-1} the mass of the Higgs boson will be determined with a total uncertainty lower than 100 MeV, as opposed to the current 300 MeV. This measurement, combined with increasingly more precise measurements of W boson and top quark masses, will enable a very stringent verification of the theory. It will be also possible to measure Higgs couplings with a precision enhanced by 10% (limited by the theoretical uncertainty on the cross section). These couplings are particularly sensitive to the phenomena of new physics, especially when they are generated by quantum loops, as in the case of Higgs production via gluon-gluon fusion or in the $\gamma\gamma$ and $Z\gamma$ decay. Finally, important and still unexplored ingredients of the EWSB sector are the Higgs trilinear and quartic self couplings. The small expected rates, the mild dependence of the cross section on the trilinear coupling and the difficulty of selecting signal from background, make the determination of the Higgs self-coupling through the measurement of Higgs pair production total cross section a very challenging task [178, 179, 180]. An alternative and

potentially competitive method, based on the indirect effects of anomalous trilinear Higgs self-coupling on single Higgs production at the LHC, has been recently proposed in Ref. [155].

From this brief introduction it should appear that, in order to compare the SM predictions with very precise data, the reduction of theoretical uncertainties is mandatory. This motivates our work on the Higgs decay into four charged leptons. As already stressed in the previous chapter, this decay channel plays a particularly relevant rôle, as it provides the cleanest experimental signature, given by a peak in the four lepton mass spectrum on top of a flat and small background. Actually, the $H \to 4\ell$ decay mode allows to derive a precise mass measurement in the different combinations of leptonic final states, to assess the spin-parity quantum numbers using sensitive angular distributions and to perform precision tests of the SM at the level of differential cross sections [181]. In this chapter we describe the main features of the calculation of the full $\mathcal{O}(\alpha)$ EW corrections to the $H \to Z^{(*)}Z^{(*)} \to 4\ell$ decay channel and the matching procedure for the consistent inclusion of a QED PS algorithm, in order to simulate the multiple photon emission exclusively. The calculation is available in an event generator, Hto4l[1], providing a new tool for the simulation of the Higgs boson decay into four charged leptons at NLOPS accuracy. This chapter is organized as follows: in Sec. 4.1 we introduce the notations and the conventions adopted in the calculation. In Sec. 4.2 and in Sec. 4.3 we describe the main features of the calculation of $\mathcal{O}(\alpha)$ EW corrections. Finally, in Sec. 4.4 we introduce the matching scheme adopted for the inclusion of a QED PS algorithm on top of the NLO calculation and we detail how this scheme has been implemented in our calculation.

4.1 Conventions and notations

Throughout this work we adopt the conventions defined in Ref. [48]. The couplings entering the tree-level amplitudes are

$$C_{HZZ} = \frac{\mu_W}{c_W^2 s_W} \qquad g_{Z\ell\ell}^+ = -\frac{s_W}{c_W} Q_\ell \qquad g_{Z\ell\ell}^- = -\frac{s_W}{c_W} Q_\ell + \frac{I_{W,\ell}^3}{s_W c_W}. \qquad (4.1)$$

Q_ℓ is the relative charge of the particle with respect to the proton electric charge, *i.e.* for leptons $Q_\ell = -1$, while $I_{W,\ell}^3$ is the third component of the weak isospin of the left-handed part of the lepton field, and since we limit our calculations to Higgs decay into charged leptons, $I_{W,\ell}^3 = -1/2$. We remark
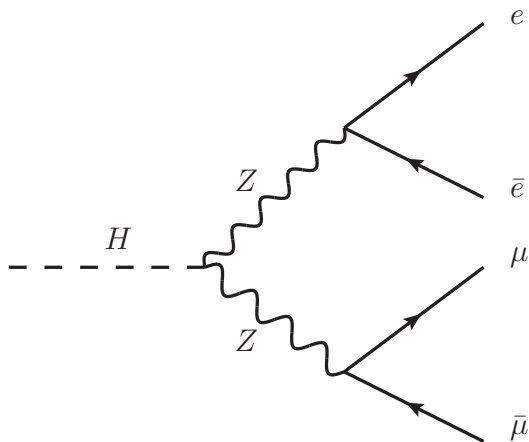
---

[1]The reference web page is http:/www.pv.infn.it/hepcomplex/hto4l.html

Figure 4.1: LO Feynman diagram for the $H \to 2e2\mu$. In the case of identical particles ($H \to 4e, 4\mu$) an additional diagrams, obtained by switching two identical particles, contributes to the LO decay width.

that according to the complex-mass scheme, detailed in Sec. 1.5 and adopted in this calculation, the masses of gauge bosons are complex quantities given by the expressions

$$\mu_V = M_V - i\Gamma_V M_V \qquad V = W, Z. \tag{4.2}$$

Consequently, the Feynman rules for the vertexes and the propagators have to be written in terms of complex masses. In particular, the weak mixing angle is given by the relation

$$c_W^2 = 1 - s_W^2 = \frac{\mu_W^2}{\mu_Z^2}. \tag{4.3}$$

4.2 Leading Order calculation

In the tree-level approximation, there is only one diagram contributing to the Higgs decay into two pairs of different flavor leptons, $H \to 2e2\mu$, as depicted in Fig. 4.1. For the sake of clearness, in the following we will always deal with the case of different flavor leptons pairs. It is understood that for the decay channels $H \to 4e$ and $H \to 4\mu$, a second tree-level diagram, obtained by exchanging two identical particles, has to be taken into account in the calculations.

The tree-level matrix element for the process $H \to Z^{(*)}Z^{(*)} \to 2e2\mu$ reads

$$\mathcal{M}_0 = iC_{HZZ}\, g_{\mu\nu} \left\{ \frac{-ig^{\mu\lambda}}{(p_1+p_2)^2 - \mu_Z^2} \bar{u}_e^{s_1}(p_1) \left[ie\gamma_\lambda \left(g_Z^+ \omega_+ + g_Z^- \omega_- \right) \right] v_e^{s_2}(p_2) \right\}$$
$$\left\{ \frac{-ig^{\nu\rho}}{(p_3+p_4)^2 - \mu_Z^2} \bar{u}_\mu^{s_3}(p_3) \left[ie\gamma_\rho \left(g_Z^+ \omega_+ + g_Z^- \omega_- \right) \right] v_\mu^{s_4}(p_4) \right\},$$

$$(4.4)$$

with

$$\omega_\pm = \frac{1}{2}(1 \pm \gamma_5). \qquad (4.5)$$

The LO partial decay width is given by squaring the matrix element in Eq. (4.4), summing over the spin configurations and integrating over the four-body phase space. Eventually we get the following expression

$$\Gamma^{\text{LO}}\left(H \to 2e2\mu\right) = \frac{1}{2M_H} \int |\mathcal{M}_0(H \to 2e2\mu)|^2\, d\Phi_4, \qquad (4.6)$$

where $d\Phi_4$ is the four-body phase-space

$$d\Phi_4 = \left(\sum_{i=1}^{4} \frac{d^3 p_i}{(2\pi)^3\, 2E_i} \right) (2\pi)^4\, \delta^{(4)} \left(P_H - \sum_{i=1}^{4} p_i \right). \qquad (4.7)$$

4.3 Next-to-Leading Order corrections

The decay width for the Higgs decay into four charged leptons is given, at NLO electroweak accuracy, by the master formula

$$\Gamma^{\text{NLO}}\left(H \to 4l\right) = \int d\,\Gamma^{\text{LO}} + \frac{1}{2M_H} \left\{ \int d\,\Gamma^{virt.} + \int d\,\Gamma^{real} \right\}. \qquad (4.8)$$

The $\mathcal{O}\left(\alpha\right)$ corrections consist of QED and purely weak contributions. Since the $H \to 4\ell$ decay is a neutral-current process, these two subsets are separately gauge invariant and can be computed independently from each other. As a consequence, the virtual part of NLO corrections can be written as

$$\frac{1}{2M_H} \int d\,\Gamma^{virt.} = \frac{1}{2M_H} \left\{ \int 2\text{Re}\left[\mathcal{M}_V^{\text{QED}}\left(\mathcal{M}_0\right)^* \right] d\Phi_4 + \right.$$
$$\left. + \int 2\text{Re}\left[\mathcal{M}_V^{weak}\left(\mathcal{M}_0\right)^* \right] d\Phi_4 \right\}, \qquad (4.9)$$

Both QED and pure weak corrections develop UV singularities have to be removed according to a given renormalization scheme. On the other hand,

QED virtual diagrams are also IR divergent. In Sec. 2.1 we have seen that, according to KLN theorem, IR divergences arising in virtual and real QED corrections cancel in the sum, leading to infrared safe observables.

Whereas the IR divergences are regulated by introducing a fictitious photon mass, finite lepton masses act as a natural cutoff for the singularities associated to collinear photon emission. For this reason, the kinematics of the radiative process is calculated including exactly the contribution of lepton masses. In order to allow the cancellation of soft IR singularities, also the tree-level kinematics is calculated by taking lepton masses into account. This gives automatically the correct phase space integration boundaries for the virtual contributions where a virtual photon is connected to an external lepton pair. Although the kinematics is treated exactly, the non-IR $\mathcal{O}(\alpha)$ virtual amplitudes are calculated in the approximation of neglecting finite fermion mass effects (with the exception of the quark Yukawa couplings, *e.g.* in the fermion-loop Higgs vertex corrections). These contributions are neglected in our calculation as they are irrelevant in view of a target accuracy of the order of 0.1% and their inclusion would make the numerical computation more time consuming.

Before entering into the details of the calculation an important remark is in order. The tree-level amplitude, as well as the amplitude for the real radiation process, contains poles in the phase space, corresponding to the points where the momenta of the $\ell^+\ell^-$ and $\ell^+\ell^-\gamma$ systems cross the zero of the inverse propagators, *i.e.* when $(p_{\ell^+} + p_{\ell^-})^2 = M_Z^2$ or $(p_{\ell^+} + p_{\ell^-} + p_\gamma)^2 = M_Z^2$. These poles are avoided considering the Z boson as an unstable particle, *i.e.* by inserting the finite Z-width in the propagators. This, however, would spoil the IR cancellation between real and virtual corrections unless the QED virtual corrections in Eq. (4.9) are calculated with unstable Z bosons. For these reasons, as anticipated, we adopt the complex-mass scheme [43, 51], which allows a consistent treatment of finite width effects, avoiding gauge invariance and unitarity violations, and whose general features are described in Sec. 1.5: weak gauge-bosons masses become complex quantities identified by the location of the related propagators in the complex plane (see Eq. 1.74). For consistency, complex masses have to be used everywhere in the calculations, in the propagators, as wells as in the Feynman rules for the vertexes. Furthermore, in order to evaluate loop diagrams with internal top quarks, complex top mass has been introduced as well.

4.3.1 Real corrections

For the real part of $\mathcal{O}(\alpha)$ QED corrections we have to consider the inculsive emission of a photon. The related Feynman diagrams are obtained by at-
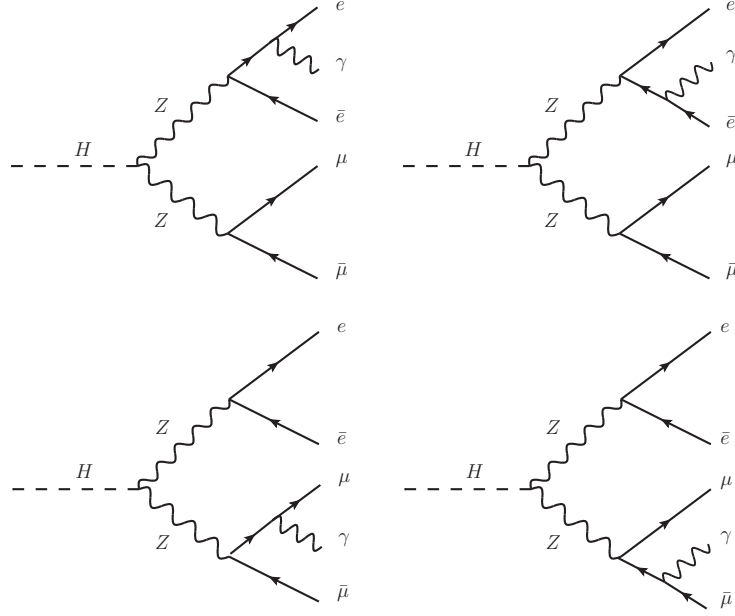
Figure 4.2: Feynman diagrams for real corrections.

taching a real photon to each lepton leg. The matrix element for the emission of an additional real photon in the $H \to 2e2\mu$ channel is given by the sum of the four diagrams represented in Fig. (4.2) and it reads explicitly

$$\mathcal{M}\left(H \to 2e2\mu + \gamma\right) = \mathcal{M}_1 + \mathcal{M}_2 + \mathcal{M}_3 + \mathcal{M}_4 \tag{4.10}$$

with

$$\mathcal{M}_1 = iC_{HZZ}\, g_{\mu\nu} \times$$
$$\left\{ \frac{-ig^{\mu\lambda}}{(p_1 + p_2 + k)^2 - \mu_Z^2} \left[(-ie)\,\gamma_\sigma \epsilon^\sigma \frac{i\left(\slashed{p}_1 + \slashed{k} + m_e\right)}{2p_1 \cdot k} \right] \times \right.$$
$$\left. \times\, \bar{u}_e^{s_1}\left(p_1\right) \left[ie\gamma_\lambda \left(g_Z^+ \omega_+ + g_Z^- \omega_- \right) \right] v_e^{s_2}(p_2) \right\}$$
$$\left\{ \frac{-ig^{\nu\rho}}{(p_3 + p_4)^2 - \mu_Z^2} \bar{u}_\mu^{s_3}\left(p_3\right) \left[ie\gamma_\rho \left(g_Z^+ \omega_+ + g_Z^- \omega_- \right) \right] v_\mu^{s_4}(p_4) \right\}, \tag{4.11}$$

$$\mathcal{M}_2 = iC_{HZZ}\,g_{\mu\nu}\times$$

$$\left\{ \frac{-ig^{\mu\lambda}}{(p_1+p_2+k)^2-\mu_Z^2} \left[(-ie)\,\gamma_\sigma \epsilon^\sigma \frac{i\left(-\not{p_2}-\not{k}+m_e\right)}{2p_2\cdot k} \right] \times \right.$$

$$\left. \times\, \bar{u}_e^{s_1}\,(p_1)\left[ie\gamma_\lambda\left(g_Z^+\omega_+ + g_Z^-\omega_-\right)\right]v_e^{s_2}(p_2) \right\}$$

$$\left\{ \frac{-ig^{\nu\rho}}{(p_3+p_4)^2-\mu_Z^2}\bar{u}_\mu^{s_3}\,(p_3)\left[ie\gamma_\rho\left(g_Z^+\omega_+ + g_Z^-\omega_-\right)\right]v_\mu^{s_4}(p_4) \right\}, \tag{4.12}$$

$$\mathcal{M}_3 = iC_{HZZ}\,g_{\mu\nu}\times$$

$$\left\{ \frac{-ig^{\mu\lambda}}{(p_1+p_2)^2-\mu_Z^2}\bar{u}_e^{s_1}\,(p_1)\left[ie\gamma_\lambda\left(g_Z^+\omega_+ + g_Z^-\omega_-\right)\right]v_e^{s_2}(p_2) \right\}$$

$$\left\{ \frac{-ig^{\nu\rho}}{(p_3+p_4+k)^2-\mu_Z^2} \left[(-ie)\,\gamma_\sigma \epsilon^\sigma \frac{i\left(\not{p_3}+\not{k}+m_\mu\right)}{2p_3\cdot k} \right] \times \right.$$

$$\left. \times\, \bar{u}_\mu^{s_3}\,(p_3)\left[ie\gamma_\rho\left(g_Z^+\omega_+ + g_Z^-\omega_-\right)\right]v_\mu^{s_4}(p_4) \right\}, \tag{4.13}$$

$$\mathcal{M}_4 = iC_{HZZ}\,g_{\mu\nu}\times$$

$$\left\{ \frac{-ig^{\mu\lambda}}{(p_1+p_2)^2-\mu_Z^2}\bar{u}_e^{s_1}\,(p_1)\left[ie\gamma_\lambda\left(g_Z^+\omega_+ + g_Z^-\omega_-\right)\right]v_e^{s_2}(p_2) \right\}$$

$$\left\{ \frac{-ig^{\nu\rho}}{(p_3+p_4+k)^2-\mu_Z^2} \left[(-ie)\,\gamma_\sigma \epsilon^\sigma \frac{i\left(-\not{p_4}-\not{k}+m_\mu\right)}{2p_4\cdot k} \right] \times \right.$$

$$\left. \times\, \bar{u}_\mu^{s_3}\,(p_3)\left[ie\gamma_\rho\left(g_Z^+\omega_+ + g_Z^-\omega_-\right)\right]v_\mu^{s_4}(p_4) \right\}, \tag{4.14}$$

The IR singularities are treated according to the standard procedure of assigning a small fictitious mass λ to the photon in the computation. The integral over the phase-space of the photon is then split in two parts

$$\frac{1}{2M_H}\int d\Gamma_{\text{real}} = \frac{1}{2M_H}\int d\Phi_4 \left\{ |\mathcal{M}_0|^2 \times e^2 \sum_{i,j=1}^{4} Q_iQ_j \mathcal{I}_{ij}\left(p_i,p_j,k,\lambda,\epsilon\right) \right\}$$

$$+ \frac{1}{2M_H}\int_\epsilon^{E_{\text{max}}} d\Phi_5\,|\mathcal{M}(H\to 4\ell+\gamma)|^2, \tag{4.15}$$

where M_H is the Higgs mass, ϵ is a soft-hard energy separator ($\epsilon \ll M_H$), $\mathcal{M}_0$ is the amplitude of the lowest-order (LO) process $H\to 4\ell$ and $\mathcal{M}(H\to 4\ell+\gamma)$ is the matrix element of the radiative process $H\to 4\ell+\gamma$, $d\Phi_5$ being the 4 leptons plus 1 photon phase space element. On the r.h.s. of Eq. (4.15) the first term has been written according to the the soft-photon

factorization formula (2.17) derived in Sec. 2.1, where $\mathcal{I}_{ij}\left(p_i, p_j, k, \lambda, \epsilon\right)$ stands for

$$\mathcal{I}_{ij}\left(p_i, p_j, k, \lambda, \epsilon\right) = -\frac{1}{(2\pi)^3} \int_\lambda^\epsilon \frac{\mathrm{d}k_0}{2k_0} \int \mathrm{d}\Omega_k \eta_i \eta_j \frac{p_i \cdot p_j}{(p_i \cdot k)(p_j \cdot k)}. \tag{4.16}$$

The integral over the soft-photon phase space has been evaluated analytically in [182] (see also [48]) and it reads

$$\mathcal{I}_{ij}\left(p_i, p_j, k, \lambda, \epsilon\right) = 4\pi \frac{\xi p_i p_j}{(\xi p_i)^2 - p_j^2} \left\{ \frac{1}{2} \log \frac{(\xi p_i)^2}{p_j^2} \log \frac{4\epsilon^2}{\lambda^2} \right.$$
$$\left. \left[\frac{1}{4} \log^2 \frac{u_0 - |\mathbf{u}|}{u_0 + |\mathbf{u}|} + \mathrm{Li}_2\left(1 - \frac{u_0 + |\mathbf{u}|}{v}\right) + \mathrm{Li}_2\left(1 - \frac{u_0 - |\mathbf{u}|}{v}\right) \right]_{u=p_j}^{u=\alpha p_i} \right\}, \tag{4.17}$$

where ξ is the positive solution of the equation

$$\xi^2 p_i^2 - 2\xi p_i \cdot p_j + p_j^2 = 0, \tag{4.18}$$

while

$$v = \frac{(\xi p_i)^2 - p_j^2}{2\left(\xi p_{i0} - p_{j0}\right)}. \tag{4.19}$$

For $\mathbf{p}_i = \mathbf{p}_j = \mathbf{p}$, Eq. (4.17) can be written as

$$\mathcal{I}_{ij} = 2\pi \frac{p \cdot q}{(p_0 + q_0)|\mathbf{p}|} \left\{ \frac{1}{2} \log \frac{p_0 + \mathbf{p}}{p_0 - \mathbf{p}} \log \frac{4\epsilon^2}{\lambda^2} - \mathrm{Li}_2\left(\frac{2|\mathbf{p}|}{p_0 + \mathbf{p}}\right) - \frac{1}{4} \log^2 \frac{p_0 + \mathbf{p}}{p_0 - \mathbf{p}} \right.$$
$$\left. \frac{1}{2} \log \frac{q_0 + \mathbf{p}}{q_0 - \mathbf{p}} \log \frac{4\epsilon^2}{\lambda^2} - \mathrm{Li}_2\left(\frac{2|\mathbf{p}|}{q_0 + \mathbf{p}}\right) - \frac{1}{4} \log^2 \frac{q_0 + \mathbf{p}}{q_0 - \mathbf{p}} \right\}. \tag{4.20}$$

For diagonal contributions, namely when $p_i = p_j$, Eq. (4.20) takes the simplified form

$$\mathcal{I}_{ii} = 2\pi \left\{ \log \frac{4\epsilon^2}{\lambda^2} + \frac{p_0}{|\mathbf{p}|} \log \frac{p_0 - |\mathbf{p}|}{p_0 + |\mathbf{p}|} \right\}. \tag{4.21}$$

The hard-emission part of the bremsstrahlung corrections is calculated by squaring the matrix element in Eq. (4.10). The Dirac algebra has been carried out by means of symbolic manipulation program `FORM` [183] and the integral has been evaluated using standard MC techniques with importance sampling.

In order to achieve the cancellation of IR divergences, the photon mass λ has to be introduced in the evaluation of the QED virtual amplitudes as well.

Then the IR cancellation follows by taking, in the numerical limit $\lambda \to 0$, the sum of Eq. (4.10) and the QED contribution to Eq. (4.9). As a cross-check of the calculation, we tested that the inclusive NLO QED correction coincides with $2 \cdot 3/4 \, (\alpha/\pi)$, which is correctly twice the inclusive final-state $\mathcal{O}(\alpha)$ electromagnetic correction to the $Z \to \ell^+ \ell^-$ decay [184].
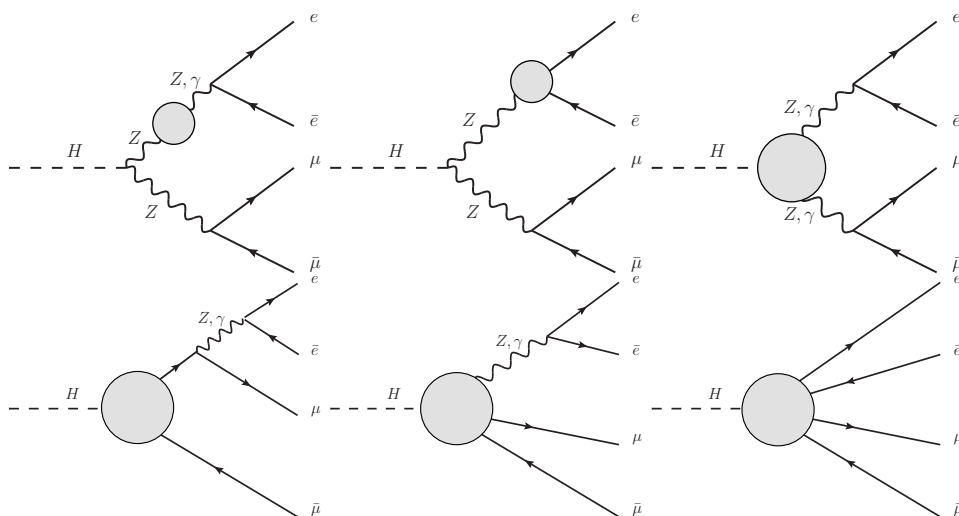
4.3.2 Survey of virtual corrections and renormalization

Figure 4.3: Generic virtual diagrams contributing to $\mathcal{O}(\alpha)$ corrections. On the first line the three UV divergent subsets of virtual contributions are represented: self-energy corrections (left diagram); $Z\ell\ell$ vertex corrections (center diagram); HVV corrections (right diagram). On the second line the remaining three UV finite subset of virtual contributions are depicted: rank-3 virtual corrections in which a $\ell\bar{\ell}$ arises from a loop-induced decay of the Higgs boson, while the missing lepton-antilepton pair is produced by the decay of an intermediate photon or Z boson, emitted by one of the two external lepton (left diagram); box corrections (center diagram); pentagons corrections (right diagram). Pentagons corrections and $Z\ell\ell$ vertex corrections, contain both QED and pure weak corrections, while the remaining four subset are present only when full EW corrections are considered.

We start this section by describing the general aspects underlying the computation of the complete $\mathcal{O}(\alpha)$ virtual corrections. Since we work in the 't Hooft-Feynman gauge, all the particles present in the spectrum of the SM, including the Fadeev-Popov and Higgs-Kibble ghosts, are involved in the calculation. As already mentioned, the virtual amplitudes are calculated in the approximation of neglecting fermion masses, except in the fermionic corrections to the Higgs vertex. The matrix elements $\mathcal{M}_V^{QED}$ and $\mathcal{M}_V^{weak}$ in Eq. (4.9) can be split in two contributions, the first containing all the

virtual diagrams contributing to QED and pure weak corrections, whereas the second contains the sum of the counterterms associated to a each vertex and to each propagator according to the on-sell renormalization scheme. The Feynman rules for the counterterms are taken from Ref. [48], as well as the expressions of the unrenormalized self-energies. Since we adopt the α_{G_μ} scheme, introduced in Sec. 1.4.2, the counterterm of the electric charge must be rescaled according to Eq. (1.71).

The virtual diagrams can be classified according to the topology as in Fig. (4.3). In particular, one-loop corrections receive contributions from self-energy, vertex, box, and pentagons corrections. The related ultraviolet divergences are regularized by means of dimensional regularization. The reduction of the tensor n-point functions is carried out by means of the symbolic manipulation program FORM [183]. The necessary scalar form factors with complex masses are evaluated using Looptools v2.10 [185, 186], which implements the evaluation of the reduction of tensor five-point integrals according to Refs. [187, 188], as well as according to Passarino-Veltman reduction techniques [189]. The form factors are calculated with complex masses and real external squared momenta. This is sufficient for the implementation of the complex-mass scheme, introduced in Refs. [43, 51] (see Sec. 1.5). In the remaining part we describe the main feature of the various subset of virtual diagrams.

Self-energy corrections

Self-energy corrections appear in the pure weak part of the calculation. Since we are considering a process mediated, at tree level, by Z bosons, we must consider $Z - A$ transitions arising at one-loop level. The matrix-elements for self energy corrections read

$$\mathcal{M}_{self} = \mathcal{M}_e + \mathcal{M}_\mu = \mathcal{M}_e^{ZZ} + \mathcal{M}_e^{ZA} + \mathcal{M}_\mu^{ZZ} + \mathcal{M}_\mu^{ZA}, \qquad (4.22)$$

where e and μ distinguish the self energy corrections of the two intermediate Z bosons, while in the second equality we have explicitly separated the diagonal transitions $(Z - Z)$ from the non-diagonal ones $(Z - A)$. Each part of the amplitude contains the unrenormalized self-energy and the related counterterm. After having introduced the shorthand notation $D_V = k^2 - M_V^2$ we can write explicitly:
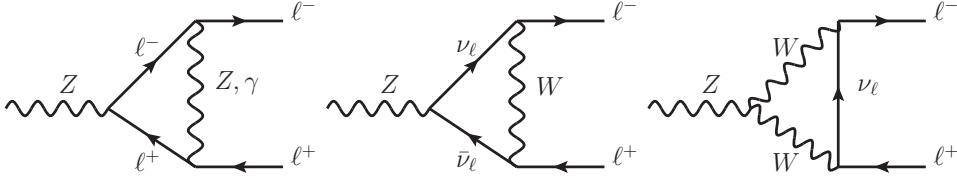
Figure 4.4: One-loop diagrams contributing to $Z\ell^+\ell^-$ vertex.

$$\mathcal{M}_e^{ZZ} = iC_{HZZ}\, g_{\mu\nu}$$
$$\left\{ \frac{(-ig^{\mu\sigma})\left[\Sigma_T^{ZZ}(k^2) - \left(C_1^{ZZ}k^2 - C_2^{ZZ}\right)\right](-ig^{\sigma\lambda})}{D_Z\left(k^2\right)D_Z\left(k^2\right)} \times \right.$$
$$\left. \times \bar{u}_e^{s_1}\left(p_1\right)\left[ie\gamma_\lambda\left(g_Z^+\omega_+ + g_Z^-\omega_-\right)\right]v_e^{s_2}(p_2) \right\}$$
$$\left\{ \frac{-ig^{\nu\rho}}{(p_3+p_4)^2 - \mu_Z^2}\bar{u}_\mu^{s_3}\left(p_3\right)\left[ie\gamma_\rho\left(g_Z^+\omega_+ + g_Z^-\omega_-\right)\right]v_\mu^{s_4}(p_4) \right\}, \tag{4.23}$$

$$\mathcal{M}_e^{ZA} = iC_{HZZ}\, g_{\mu\nu}$$
$$\left\{ \frac{(-ig^{\mu\sigma})\left[\Sigma_T^{ZZ}(k^2) - i\left(C_1^{ZA}k^2 - C_2^{ZA}\right)\right](-ig^{\sigma\lambda})}{D_Z\left(k^2\right)D_A\left(k^2\right)}\bar{u}_e^{s_1}\left(p_1\right)\left[-ie\gamma_\lambda\right]v_e^{s_2}(p_2) \right\}$$
$$\left\{ \frac{-ig^{\nu\rho}}{(p_3+p_4)^2 - \mu_Z^2}\bar{u}_\mu^{s_3}\left(p_3\right)\left[ie\gamma_\rho\left(g_Z^+\omega_+ + g_Z^-\omega_-\right)\right]v_\mu^{s_4}(p_4) \right\}, \tag{4.24}$$

where $k = p_1 + p_2$. The remaining amplitudes $\mathcal{M}_\mu^{ZZ} + \mathcal{M}_\mu^{ZA}$ can be derived by switching the lepton currents, while the explicit expressions for the self energies $\Sigma_T^{ZZ}(k^2)$ and $\Sigma_T^{AZ}(k^2)$ can be found in Appendix B of [48]. The expressions for the counterterms are

$$C_1^{ZZ} = \delta Z_{ZZ} \qquad\qquad C_2^{ZZ} = M_Z^2\delta Z_{ZZ} + \delta M_Z^2 \tag{4.25}$$

$$C_1^{AZ} = \frac{1}{2}\delta Z_{AZ} + \frac{1}{2}\delta Z_{ZA} \qquad C_2^{AZ} = M_Z^2\delta Z_{ZA}. \tag{4.26}$$

$Z\ell^+\ell^-$ vertex corrections

The $\mathcal{O}\left(\alpha\right)$ EW corrections on the $Z\ell^+\ell^-$ vertex can be split in two gauge invariant subset. On one side, QED corrections are given by the exchange of a virtual photon between two leptons attached to the same Z propagator. On

the other side there are tree types of pure weak corrections: the first type can be easily obtained by replacing the virtual photon with a virtual Z boson, while the remaining two contributions are characterized by the presence of W bosons and neutrinos (see Fig 4.4). We remark that one-loop contributions containing Higgs bosons and Higgs-Kibble fields have not to be considered in the limit of vanishing lepton masses. The matrix element for the insertion of one-loop corrections to $Z\ell^+\ell^-$ vertex can be written in the following concise form

$$\mathcal{M}_{Z\ell^+\ell^-} = \mathcal{M}_{Ze^+e^-} + \mathcal{M}_{Z\mu^+\mu^-}, \tag{4.27}$$

with

$$\mathcal{M}_{Ze^+e^-} = iC_{HZZ}\, g_{\mu\nu} \times$$
$$\left\{ \frac{-ig^{\mu\lambda}}{(p_1 + p_2)^2 - \mu_Z^2} \bar{u}_e^{s_1}(p_1) \left[ieV_\lambda^e(p_1, p_2) \right] v_e^{s_2}(p_2) \right\}$$
$$\left\{ \frac{-ig^{\nu\rho}}{(p_3 + p_4)^2 - \mu_Z^2} \bar{u}_\mu^{s_3}(p_3) \left[ie\gamma_\rho \left(g_Z^+\omega_+ + g_Z^-\omega_- \right) \right] v_\mu^{s_4}(p_4) \right\}, \tag{4.28}$$

$$\mathcal{M}_{Z\mu^+\mu^-} = iC_{HZZ}\, g_{\mu\nu} \times$$
$$\left\{ \frac{-ig^{\mu\lambda}}{(p_1 + p_2)^2 - \mu_Z^2} \bar{u}_e^{s_1}(p_1) \left[ie\gamma_\lambda \left(g_Z^+\omega_+ + g_Z^-\omega_- \right) \right] v_e^{s_2}(p_2) \right\}$$
$$\left\{ \frac{-ig^{\nu\rho}}{(p_3 + p_4)^2 - \mu_Z^2} \bar{u}_\mu^{s_3}(p_3) \left[ieV_\rho^\mu(p_3, p_4) \right] v_\mu^{s_4}(p_4) \right\}, \tag{4.29}$$

The form factors $V_\lambda^e(p_1, p_2)$ and $V_\rho^\mu(p_3, p_4)$ contain the integrals arising from the one-loop diagrams depicted in Fig. 4.4

$$V_\lambda^\ell(p_i, p_j) = V_\lambda^{\gamma\ell\ell}(p_i, p_j) + V_\lambda^{Z\ell\ell}(p_i, p_j) +$$
$$V_\lambda^{W\nu_\ell\nu_\ell}(p_i, p_j) + V_\lambda^{WW\nu_\ell}(p_i, p_j) \tag{4.30}$$

The explicit expression of the generic QED one loop integrals reads

$$V_\lambda^{\gamma\ell\ell}(p_i, p_j) = e^2 \int \frac{d^D q}{(2\pi)^D} \frac{g^{\sigma\tau}\gamma_\sigma \left(\slashed{q} + \slashed{p}_i \right) \gamma_\lambda \left(g_Z^+\omega_+ + g_Z^-\omega_- \right) \gamma_\tau \left(\slashed{q} - \slashed{p}_j \right)}{(q^2 - \lambda^2) \left[(q + p_i)^2 - m_\ell^2 \right] \left[(q - p_j)^2 - m_\ell^2 \right]}. \tag{4.31}$$

We remark that in the last integral a photon fictitious mass λ has been introduced to regularize the correspondent soft divergence in the integral. We omit to write the explicit expression for the other form factors in Eq. (4.30) which follow from a straightforward application of the Feynman rules. The UV divergences are canceled by the following substitutions

$$g_{Z\ell\ell}^+ \rightarrow g_{Z\ell\ell}^+ \left[1 + \frac{\delta g_{Z\ell\ell}^+}{g_{Z\ell\ell}^+} + \frac{1}{2}\left(\delta Z_{ZZ} + \delta Z_\ell^R + \delta Z_\ell^{R,\dagger}\right)\right] - Q_\ell \frac{1}{2}\delta Z_{AZ}, \quad (4.32)$$

$$g_{Z\ell\ell}^- \rightarrow g_{Z\ell\ell}^- \left[1 + \frac{\delta g_{Z\ell\ell}^-}{g_{Z\ell\ell}^-} + \frac{1}{2}\left(\delta Z_{ZZ} + \delta Z_\ell^L + \delta Z_\ell^{L,\dagger}\right)\right] - Q_\ell \frac{1}{2}\delta Z_{AZ}, \quad (4.33)$$

where

$$\delta g_{Z\ell\ell}^+ = -\frac{s_W}{c_W}Q_\ell \left[\delta Z_e + \frac{1}{c_W^2}\frac{\delta s}{s}\right], \quad (4.34)$$

$$\delta g_{Z\ell\ell}^- = -\frac{I_{W\ell}^3}{s_W c_W}\left[\delta Z_e + \frac{s_W^2 - c_W^2}{c_W^2}\frac{\delta s}{s}\right] + \delta g_{Z\ell\ell}^+. \quad (4.35)$$

It is important to note that the QED counterterms are included in $\delta Z_\ell^{L(\dagger)}$ and $\delta Z_\ell^{R(\dagger)}$. Thus, to calculate the QED part of the $\mathcal{O}(\alpha)$ EW corrections it is sufficient to isolate the QED part in the evaluation of the fermionic self-energies (see Eqs. (1.55k) and (1.55l)). These contributions are also IR divergent and are the virtual counterparts of the IR singularities in Eq. (4.21).

HVV vertex corrections

While at LO the $H \rightarrow 4\ell$ decay channel proceeds through the Higgs decay into two intermediate Z bosons, at NLO $Z\gamma$ and $\gamma\gamma$ loop-induced contributions have to be taken into account, so that we have to consider the following four $\mathcal{O}(\alpha)$ contributions:

$$\begin{aligned}
\mathcal{M}_1^{HZZ} = i \left[V_{\mu\nu}^{HZZ}(k_{12}, k_{34}) + \delta C^{HZZ}(k_{12}, k_{34})g_{\mu\nu}\right] \\
\left\{\frac{-ig^{\mu\lambda}}{k_{12}^2 - \mu_Z^2}\bar{u}_e^{s_1}(p_1)\left[ie\gamma_\lambda\left(g_Z^+\omega_+ + g_Z^-\omega_-\right)\right]v_e^{s_2}(p_2)\right\} \\
\left\{\frac{-ig^{\nu\rho}}{k_{34}^2 - \mu_Z^2}\bar{u}_\mu^{s_3}(p_3)\left[ie\gamma_\rho\left(g_Z^+\omega_+ + g_Z^-\omega_-\right)\right]v_\mu^{s_4}(p_4)\right\},
\end{aligned} \quad (4.36)$$

$$\begin{aligned}
\mathcal{M}_1^{H\gamma Z} = i \left[V_{\mu\nu}^{H\gamma Z}(k_{12}, k_{34}) + \delta C^{H\gamma Z}(k_{12}, k_{34})g_{\mu\nu}\right] \\
\left\{\frac{-ig^{\mu\lambda}}{k_{12}^2}\bar{u}_e^{s_1}(p_1)\left[-ie\gamma_\lambda\right]v_e^{s_2}(p_2)\right\} \\
\left\{\frac{-ig^{\nu\rho}}{k_{34}^2 - \mu_Z^2}\bar{u}_\mu^{s_3}(p_3)\left[ie\gamma_\rho\left(g_Z^+\omega_+ + g_Z^-\omega_-\right)\right]v_\mu^{s_4}(p_4)\right\},
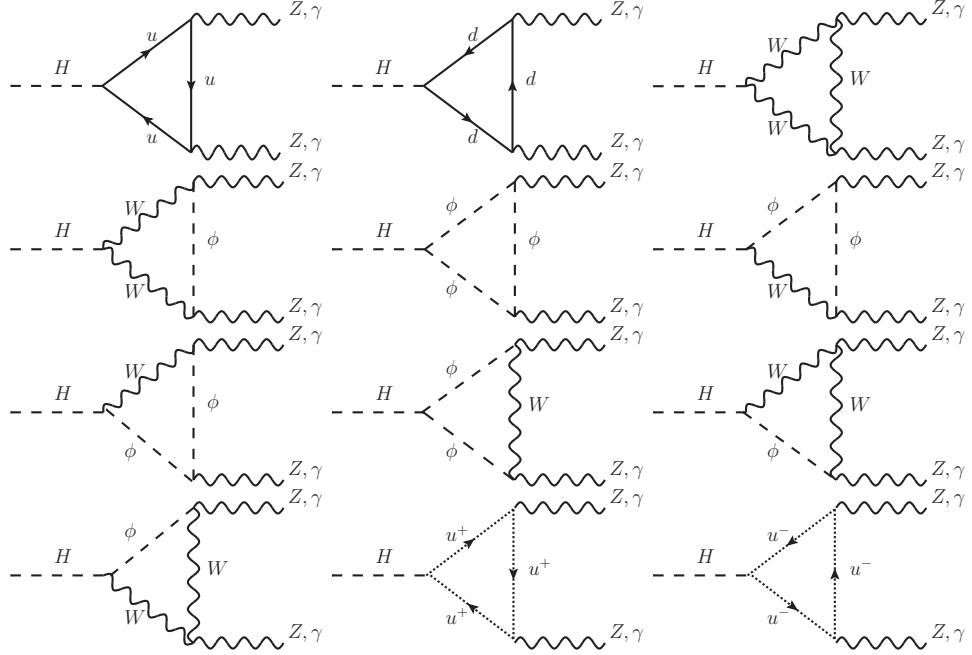\end{aligned} \quad (4.37)$$

Figure 4.5: Charged Rank-3 one-loop contributions to HVV vertex. According to Feynman rules, the intermediate Z bosons can be replaced by photons.
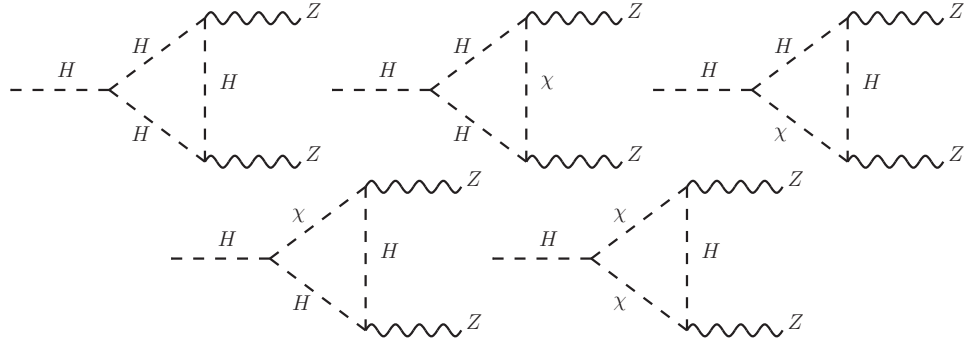

Figure 4.6: Neutral Rank-3 one-loop contributions to HVV vertex. This subset of virtual diagrams does not give rise to loop-induced $HZ\gamma$ and $H\gamma\gamma$ vertexes.

$$\mathcal{M}_1^{HZ\gamma} = i \left[V_{\mu\nu}^{HZ\gamma}(k_{12}, k_{34}) + \delta C^{HZ\gamma}(k_{12}, k_{34}) g_{\mu\nu} \right]$$
$$\left\{ \frac{-ig^{\mu\lambda}}{k_{12}^2 - \mu_Z^2} \bar{u}_e^{s_1}(p_1) \left[ie\gamma_\lambda \left(g_Z^+ \omega_+ + g_Z^- \omega_- \right) \right] v_e^{s_2}(p_2) \right\} \quad (4.38)$$
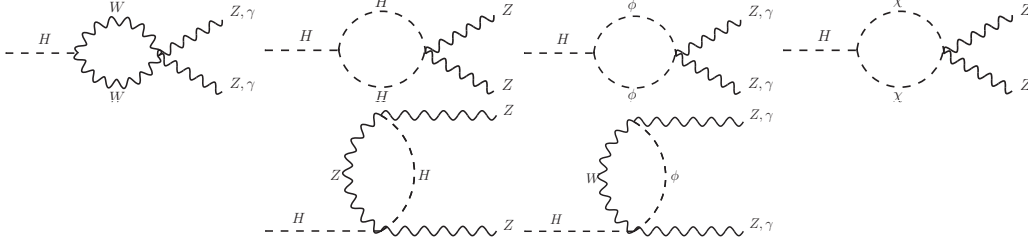$$\left\{ \frac{-ig^{\nu\rho}}{k_{34}^2} \bar{u}_\mu^{s_3}(p_3) \left[-ie\gamma_\rho \right] v_\mu^{s_4}(p_4) \right\},$$

Figure 4.7: Charged and neutral rank-2 one-loop contributions to HVV vertex.

$$\mathcal{M}_1^{H\gamma\gamma} = i \left[V_{\mu\nu}^{H\gamma\gamma}(k_{12}, k_{34}) \right]$$
$$\left\{ \frac{-ig^{\mu\lambda}}{k_{12}^2} \bar{u}_e^{s_1}(p_1) \left[-ie\gamma_\lambda \right] v_e^{s_2}(p_2) \right\}$$
$$\left\{ \frac{-ig^{\nu\rho}}{k_{34}^2} \bar{u}_\mu^{s_3}(p_3) \left[-ie\gamma_\rho \right] v_\mu^{s_4}(p_4) \right\},$$
(4.39)

with $k_{12} = p_1 + p_2$ and $k_{34} = p_3 + p_4$. The form factors $V_{\mu\nu}^{HV_1V_2}$ absorb all rank-2 and rank-3 contributions to HVV vertex listed Figs. 4.5, 4.6 and 4.7. It is interesting to note that loop induced $HZ\gamma$, $H\gamma Z$ and $H\gamma\gamma$ contributions arise only from loop contributions with internal charged particles.

In the evaluation of fermionic loop contributions all lepton and quarks have been taken into account. The values for fermion masses are listed in the next chapter. According to the complex-mass scheme, we evaluate the loop contributions with internal top-quarks with a complex mass $\mu_t = \sqrt{m_t - im_t\Gamma_t}$, where Γ_t is set to

$$\Gamma_t = \frac{G_\mu (m_t^2 - M_W^2)^2 (m_t^2 + 2M_W^2)}{8\sqrt{2}\pi m_t^3}$$
(4.40)

Finally, the expressions for δC^{HZZ} and $\delta C^{HZ\gamma}$ are:

$$\delta C^{HZZ} = M_W^2 \frac{1}{s_W c_W^2} \left[\delta Z_e + \frac{2s_W^2 - c_W^2}{c_W^2} \frac{\delta s_W}{s_W} + \frac{1}{2}\frac{\delta M_W^2}{M_W^2} + \frac{1}{2}\delta Z_H + \delta Z_{ZZ} \right],$$
(4.41)

$$\delta C^{HZ\gamma} = M_W^2 \frac{1}{2s_W c_W^2} \delta Z_{ZA}.$$
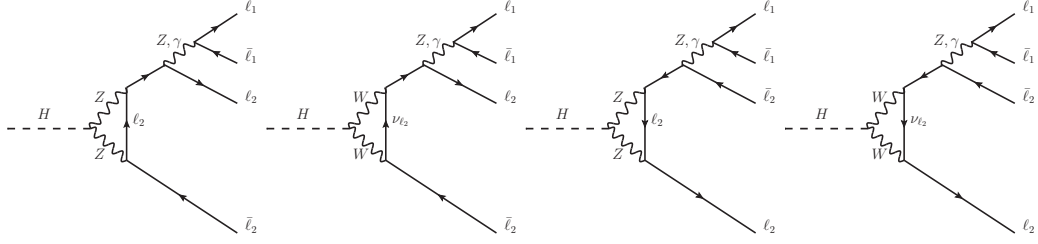(4.42)

Figure 4.8: One-loop diagrams in which the Higgs boson decays in the $\ell_1\bar{\ell}_1$ pair, with one of the two leptons emitting a neutral gauge boson which decays in the missing $\ell_2\bar{\ell}_2$ pair. Four analogous diagrams obtained by switching the two lepton currents are included in the calculation.

Additional vertex corrections

The contributions owing to this subset of UV finite one-loop corrections arise from those diagrams where the Higgs boson decays, through a neutral or charged loop, into a $\ell\bar{\ell}$ pair. Then, one of the external leptons emits a photon or a Z boson which decays in the missing $\ell\bar{\ell}$ pair. The virtual diagrams contributing to this subset of one-loop corrections are depicted in Fig. 4.8. The correspondent matrix elements can be written in the following compact way:

$$
\begin{aligned}
\mathcal{M}_{ee}^{Z} = {}& \bar{u}_e^{s_1}(p_1)\left[iV_\nu(p_1+p_3+p_4,p_2)+iV_\nu(p_1,p_2+p_3+p_4)\right]v_e^{s_2}(p_2)\\
& \left\{\frac{-ig^{\nu\rho}}{(p_3+p_4)^2-\mu_Z^2}\bar{u}_\mu^{s_3}(p_3)\left[ie\gamma_\rho\left(g_Z^+\omega_++g_Z^-\omega_-\right)\right]v_\mu^{s_4}(p_4)\right\},
\end{aligned}
\tag{4.43}
$$

$$
\begin{aligned}
\mathcal{M}_{ee}^{\gamma} = {}& \bar{u}_e^{s_1}(p_1)\left[iV_\nu(p_1+p_3+p_4,p_2)+iV_\nu(p_1,p_2+p_3+p_4)\right]v_e^{s_2}(p_2)\\
& \left\{\frac{-ig^{\nu\rho}}{(p_3+p_4)^2}\bar{u}_\mu^{s_3}(p_3)\left[-ie\gamma_\rho\right]v_\mu^{s_4}(p_4)\right\}.
\end{aligned}
\tag{4.44}
$$

The analogous contributions $\mathcal{M}_{\mu\mu}^{Z}$ and $\mathcal{M}_{\mu\mu}^{\gamma}$ can be obtained just by switching the lepton currents in Eqs. (4.43) and (4.44). The form factors $V_\nu(p_ip_j)$ include charged and neutral loop contributions, and the dependence on the external momenta needs to distinguish which of the initial external leptons have emitted the Z boson or the photons which then decays in the missing lepton-antilepton pair.
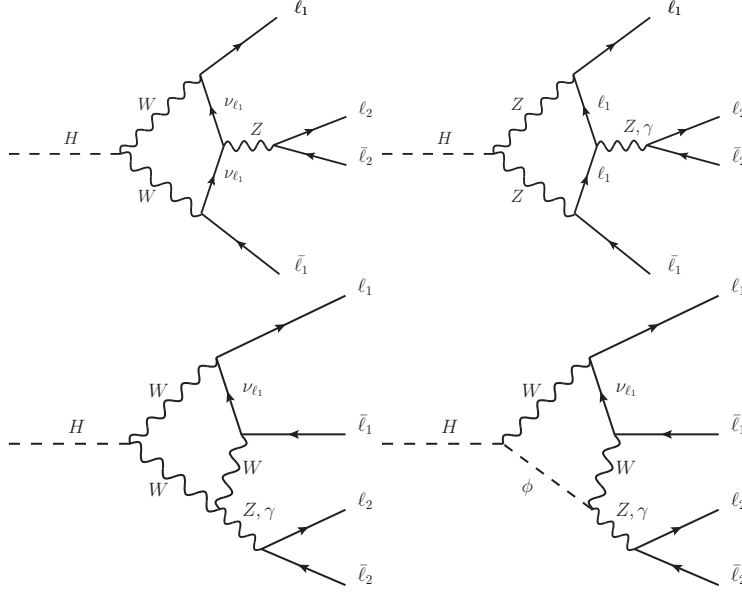
Figure 4.9: Box diagrams in which the Higgs boson decays in the $\ell_1\bar{\ell}_1$ pair, with one of the intermediate particles in the loop emitting a neutral gauge boson which decays in the missing $\ell_2\bar{\ell}_2$ pair. Four analogous diagrams obtained by switching the two lepton currents are taken into account in the calculation.

Box corrections

The UV finite corrections owing to this subset arise from the loop induced Higgs boson decay into a $\ell\bar{\ell}$ pair. The missing lepton-antilepton pair is produced by the decay of a photon or a Z boson, emitted by one of the internal legs, as shown in Fig. 4.9. As in the previous case, both neutral and charged box corrections contribute to the virtual $\mathcal{O}(\alpha)$ corrections. In the case of neutral box corrections the additional gauge boson can be emitted only by the virtual lepton, while in the case of charged loop, the possibility of emission by one of the virtual W bosons has to be taken into account. The correspondent virtual amplitudes can be written as follows:

$$
\begin{aligned}
\mathcal{M}_{ee}^Z = \bar{u}_e^{s_1}(p_1) &\left[iB_\nu^Z(p_1, p_2, p_3 + p_4) \right] v_e^{s_2}(p_2) \\
&\left\{ \frac{-ig^{\nu\rho}}{(p_3 + p_4)^2 - \mu_Z^2} \bar{u}_\mu^{s_3}(p_3) \left[ie\gamma_\rho \left(g_Z^+ \omega_+ + g_Z^- \omega_- \right) \right] v_\mu^{s_4}(p_4) \right\},
\end{aligned}
\tag{4.45}
$$
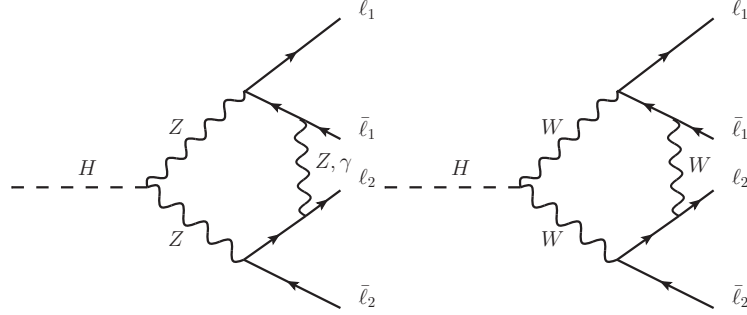
Figure 4.10: 5-point contributions to $H \to 4\ell$ decay channel. Analogous diagrams obtained by considering all the possible combinations are taken into account in the calculation.

$$\mathcal{M}_{ee}^{Z} = \bar{u}_{e}^{s_1}\left(p_1\right)\left[iB_{\nu}^{\gamma}(p_1, p_2, p_3 + p_4)\right]v_{e}^{s_2}(p_2)$$
$$\left\{\frac{-ig^{\nu\rho}}{(p_3 + p_4)^2 - \mu_Z^2}\bar{u}_{\mu}^{s_3}\left(p_3\right)\left[ie\gamma_{\rho}\left(g_Z^{+}\omega_{+} + g_Z^{-}\omega_{-}\right)\right]v_{\mu}^{s_4}(p_4)\right\}, \qquad (4.46)$$

where the form factors B_{ν}^{γ} and B_{ν}^{Z} include the virtual contribution depicted in Fig. 4.9.

Pentagon corrections

The last subset of virtual corrections which have to be taken into account are the so-called pentagons corrections, which can be easily obtained by connecting two leptons coming from the decay of different gauge bosons with a virtual boson, as depicted in Fig. 4.10. The general form of the virtual amplitudes reads

$$\mathcal{M}_{ee}^{Z} = \Big[E_{13}(p_1, p_2, p_3, p_4) + E_{14}(p_1, p_2, p_3, p_4)+$$
$$E_{23}(p_1, p_2, p_3, p_4) + E_{24}(p_1, p_2, p_3, p_4)\Big]\times \qquad (4.47)$$
$$\Big[\bar{u}_{e}^{s_1}\left(p_1\right)v_{e}^{s_2}(p_2)\Big]\Big[\bar{u}_{\mu}^{s_3}\left(p_3\right)v_{\mu}^{s_4}(p_4)\Big],$$

where the form factors E_{ij} include the three contributions depicted in Fig. 4.10 with the additional internal leg connected to leptons i and j. Pentagons corrections can be split in QED contributions, where the virtual boson which closes the loop is a photon, and weak contributions, when the additional

virtual particle is a Z or a W boson. These contributions are UV finite. However, QED pentagons are IR-divergent. The IR regulator λ has to be used as fictitious mass of the photon in the evaluations of five-point integrals. The dependence on λ is then removed in the sum of the virtual and real parts.

4.4 Matching NLO electroweak corrections to QED Parton Shower

The $\mathcal{O}(\alpha)$ QED corrections are expected a priori to provide the dominant contribution to Higgs decay into four charged leptons. In fact, from a close inspection of NLO corrections, it appears that large logarithms of the form $\alpha \log\left(m_l^2/Q^2\right)$ arise in the sum of virtual and real QED corrections. These large logarithmic enhancements arise in phase-space regions in which the photon is emitted at small angle with respect to one of the final state leptons. The same collinear logarithms arise also after the integration of the hard photon contribution in Eq. (4.15). In Chapter 2 we have seen that collinear contributions can be factorized from the underlying LO matrix elements. Since collinear emissions of photons are always produced by moving charged leptons, we have introduced the electron structure function $f_{ee}(x, s)$, which provides the probability to find, at a given scale s, the electron with a fraction x of its original energy. The evolution of the structure functions from an initial scale s_i to a final scale s_f is ruled by the Altarelli-Parisi (AP) equations. Finally, in Chapter 2, we have introduced the Parton Shower (PS) algorithm, which provides a numerical solution of the AP equations and it allows a detailed description of the multiphoton final states. From the discussion we have developed so far, the PS algorithm may seem an alternative approach to fixed-order computations: instead of calculating all the virtual and real contributions at a given order in the perturbative expansion, the PS provides the resummation of the dominant contributions to all orders. However, there are cases in which the comparison between theoretical predictions and experimental data requires a level of accuracy such that NLO corrections have to be combined with multiple photon emission effects provided by the PS. The matching of the two contributions is a highly non-trivial task. Since part of the fixed-order corrections are included in the PS, a consistent matching scheme must avoid double counting of LL contributions at $\mathcal{O}(\alpha)$. In this section we present the scheme adopted for the matching of the complete $\mathcal{O}(\alpha)$ EW corrections to Higgs decay into four charged leptons with a PS algorithm. This scheme has been developed for the matching of NLO

corrections to PS for QED processes at low energy [190, 191] and then successfully applied to Drell-Yan W/Z production at hadron colliders [192, 193]. For the sake of clarity the matching scheme is first introduced for a toy model and then applied to the Higgs decay into four leptons.

4.4.1 The matching scheme

In order to write compact formulae we illustrate the matching scheme for an unphysical process with only one charged external particle emitting photons. Working in PS approximation, a general expression for the cross section with the emission of an arbitrary number of photons can be written as

$$d\sigma_\infty = \Pi(Q^2, \epsilon) \sum_{n=0}^{\infty} \frac{1}{n!} \left| \mathcal{M}_n^{\text{PS}} \right|^2 d\Phi_n \qquad (4.48)$$

The Sudakov form factor $\Pi\left(Q^2, \epsilon\right)$ accounts for virtual and soft-photon emissions (up to ϵ) at the hard scale Q^2 and it can be expressed by the formula

$$\Pi\left(Q^2, \epsilon\right) = \exp\left(-\frac{\alpha}{2\pi} I^+ \log \frac{Q^2}{m^2}\right), \qquad I^+ = \int_0^{1-\epsilon} dz P\left(z\right), \qquad (4.49)$$

where $P(z)$ is the AP splitting function (see Sec. 2.2). $d\Phi_n$ is the exact phase-space element of the process, with n photons in the final state, divided by the incoming flux factor. Finally, $\left|\mathcal{M}_n^{\text{PS}}\right|^2$ describes, in collinear approximation, the process with the emission of n hard photons, with energy larger than ϵ in units of the radiating particle energy. As we have seen in Sec. 2.2, the collinear approximation allows to factorize the photon emission from the underlying Born matrix element. The squared amplitude for one-photon emission reads

$$\left| \mathcal{M}_1^{\text{PS}} \right|^2 = \frac{\alpha}{2\pi} I\left(k\right) \frac{8\pi^2}{E^2 z(1-z)} \left| \mathcal{M}_0 \right|^2. \qquad (4.50)$$

$I(k)$ is a function describing the angular spectrum of the photon. Then, from the integral over the angular part we get

$$\int d\Omega_k \, I(k) = \log \frac{Q^2}{m^2}, \qquad (4.51)$$

allowing the cancellation of infrared singularities in Eq. (4.48). The matching scheme consists, roughly speaking, in the inclusion of the missing $\mathcal{O}\left(\alpha\right)$ contributions in Eq. (4.48). The procedure can be better understood by comparing the exact $\mathcal{O}\left(\alpha\right)$ cross section with the $\mathcal{O}\left(\alpha\right)$ expansion of Eq. (4.48): According to the separation of the bremsstrahlung correction into a soft and

a hard part through an infrared regulator, the exact $\mathcal{O}\left(\alpha\right)$ cross section can be written as

$$\mathrm{d}\sigma_\alpha = \left(1 + C_\alpha\right)\left|\mathcal{M}_0\right|^2 \mathrm{d}\Phi_0 + \left|\mathcal{M}_1\right|^2 \mathrm{d}\Phi_1, \tag{4.52}$$

where the coefficient C_α contains the real matrix elements for soft-photon emission and the interference between the Born amplitude and the virtual ones. On the other hand the collinear approximation of this formula is given by

$$\begin{aligned}
\mathrm{d}\sigma_\alpha^{\mathrm{PS}} &= \left[1 - \frac{\alpha}{2\pi}I^+ \log\frac{Q^2}{m^2}\right]\left|\mathcal{M}_0\right|^2 \mathrm{d}\Phi_0 + \left|\mathcal{M}_1^{\mathrm{PS}}\right|^2 \mathrm{d}\Phi_1 \\
&= \left(1 + C_\alpha^{\mathrm{PS}}\right)\left|\mathcal{M}_0\right|^2 \mathrm{d}\Phi_0 + \left|\mathcal{M}_1^{\mathrm{PS}}\right|^2 \mathrm{d}\Phi_1
\end{aligned} \tag{4.53}$$

Then, by introducing the coefficients

$$F_{SV} = 1 + \left(C_\alpha - C_\alpha^{\mathrm{PS}}\right), \qquad F_H = 1 + \frac{\left|\mathcal{M}_1\right|^2 - \left|\mathcal{M}_1^{\mathrm{PS}}\right|^2}{\left|\mathcal{M}_1^{\mathrm{PS}}\right|^2}, \tag{4.54}$$

the formula for the exact NLO cross section ca be rewritten, up to terms of $\mathcal{O}\left(\alpha^2\right)$ as

$$\mathrm{d}\sigma_\alpha = F_{SV}\left(1 + C_\alpha^{\mathrm{PS}}\right)\left|\mathcal{M}_0\right|^2 \mathrm{d}\Phi_0 + F_H\left|\mathcal{M}_1^{\mathrm{PS}}\right|^2 \mathrm{d}\Phi_0. \tag{4.55}$$

Driven by this equation we can write the master formula for the resummed cross section at NLOPS accuracy

$$\mathrm{d}d_{\mathrm{mathced}}^\infty = F_{SV}\Pi(Q^2, \epsilon)\sum_{n=0}^\infty \frac{1}{n!}\left(\prod_{i=1}^n F_{H,i}\right)\left|\mathcal{M}_n^{\mathrm{PS}}\right|^2 \mathrm{d}\Phi_n \tag{4.56}$$

Since the $\mathcal{O}\left(\alpha\right)$ expansion of this formula coincides with the cross section in Eq. (4.52) the NLO accuracy is achieved, while the LL contributions are the same of Eq. (4.48). It is worth noticing that the coefficients F_{SV} and F_H are infrared safe and free of collinear logarithms. Therefore, this matching scheme allows to include infrared safe radiative corrections in the PS algorithm. In the next section we will see the application of this scheme to the realistic case of the Higgs boson decay into four charged leptons.

4.4.2 Higgs decay into four charged leptons at NLOPS accuracy

Let us start by detailing the PS algorithm that we have adopted in our calculation. At the end of Chapter 2 we have remarked that the simple PS

algorithm described in Sec. 2.4 has the drawback to neglect the interference of diagrams where the photon is emitted by different particles. Here we present an improved version of the algorithm, where the interferences are taken into account properly. The master formula for the partial decay width corrected for the emission of an arbitrary number of photons in a PS framework can be written as

$$\mathrm{d}\Gamma_\infty^{PS} = \frac{1}{2M_H}\Pi(\{p\},\epsilon)\sum_{n=0}^{\infty}\frac{1}{n!}\left|\mathcal{M}_n^{PS}(\{p\},\{k\})\right|^2 \mathrm{d}\Phi_n(\{p\},\{k\}) \quad (4.57)$$

where $\{p,k\}$ stands for the set of the final state lepton and photon momenta $p_1\cdots p_4, k_1,\cdots,k_n$, $|\mathcal{M}_n^{PS}|^2$ (of order α^n) is the PS approximation to the squared amplitude for the decay $H \rightarrow 4\ell + n\gamma$, $\mathrm{d}\Phi_n$ is the exact phase space for the decay, while $\Pi(\{p\},\epsilon)$ is the Sudakov form factor accounting for unresolved emission, *i.e.* soft (up to a cut-off energy ϵ) and virtual corrections in the PS approximation. The $(4+n)$-body phase space $\mathrm{d}\Phi_n$ reads explicitly

$$\mathrm{d}\Phi_n = \frac{1}{(2\pi)^{3n+8}}\delta^{(4)}\left(P_H - \sum_{j=1}^{4}p_j - \sum_{i=1}^{n}k_i\right)\prod_{j=1}^{4}\frac{\mathrm{d}^3\vec{p}_j}{2p_j^0}\prod_{i=1}^{n}\frac{\mathrm{d}^3\vec{k}_i}{2k_i^0} \quad (4.58)$$

It is understood that the integral over the phase space has a lower limit for the photon energies set to ϵ, to ensure the cancellation of the IR divergencies. The integral is performed after choosing a convenient set of independent variables and using multi-channel MC importance sampling techniques to improve the integration convergence and follow the peaking structure of the partial decay width of Eq. (4.57) to help event generation. The fully exclusive information on final state particles momenta is kept. Details of the implementation are given in Appendix A. The Sudakov form factor $\Pi(\{p\},\epsilon)$ can be written as follows:

$$\Pi(\{p\},\varepsilon) = \exp\left[-\frac{\alpha}{2\pi}LI_\epsilon\right] \qquad L \equiv \int \mathrm{d}\Omega_k(k^0)^2\sum_{i,j=1}^{4}\eta_i\eta_j\frac{p_i\cdot p_j}{(p_i\cdot k)(p_j\cdot k)},$$
$$(4.59)$$

where L generates the soft/virtual collinear logarithms, including also interferences effects of radiation coming from different charged legs, and I_ϵ, the integral of the Altarelli-Parisi vertex for the branching $\ell \rightarrow \ell + \gamma$, generates the infrared logarithms. It is explicitly given by:

$$I_\epsilon \equiv \int_0^{1-\epsilon} dz\,\frac{1+z^2}{1-z} = -2\ln\epsilon - \frac{3}{2} + 2\epsilon - \frac{1}{2}\epsilon^2. \quad (4.60)$$

In the definition of L, the integral is performed over the angular variables of k, and η_i equals 1 if i is an anti-fermion or -1 if it is a fermion.

Before discussing the inclusion of NLO corrections into Eq. (4.57), it is interesting to point out that the squared amplitudes with photon emissions are enhanced in regions of the phase space where the photons are soft and/or collinear or where the Z propagators are resonating. From this perspective, a good approximation to the exact matrix element can be written in the form:

$$
\mathcal{M}_n^{\text{soft}}(\{p\}, \{k\}, \{\sigma\}, \{\tau\}) =
$$
$$
C_{HZZ} \sum_{\{\mathcal{P}\}} \frac{J_{12}^\rho}{(p_1 + p_2 + Q_\mathcal{P})^2 - \mu_Z^2} \frac{J_{34,\rho}}{(p_3 + p_4 + R_\mathcal{P})^2 - \mu_Z^2} \times
$$
$$
\prod_{i=1}^n \frac{\eta_{\mathcal{P}_i} p_{\mathcal{P}_i} \cdot \varepsilon_{\tau_i}(k_i)}{p_{\mathcal{P}_i} \cdot k_i}, \tag{4.61}
$$

where for the sake of simplicity, we consider the decay $H \to 2e2\mu + n\gamma$, the generalization to $4e$ or 4μ being straightforward. In the previous equation, $\{\sigma, \tau\}$ label fermion and photon helicities, while $J_{ij}^\mu \equiv \bar{u}_{\sigma_i}(p_i) \gamma^\mu u_{\sigma_j}(p_j)$. $\mathcal{P}$ is a n-dimensional vector whose i^{th} component is the index of the fermion to which the ith photon is attached and the sum over $\mathcal{P}$ denotes all possible ways to share n photons among the four fermions. Finally, $Q_\mathcal{P}$ is the sum of the momenta of the photons, for a given $\mathcal{P}$, attached to the electron current ($R_\mathcal{P}$ to the muon current).

Equation (4.61) is derived from the amplitude for the emission of photons in the soft limit but keeping the dependence on the photon momenta in the Z propagators. The sum over the helicities of the squared amplitudes of Eq. (4.61) gives an approximation of the exact squared matrix elements, coherently including also interferences among diagrams. The final step to obtain $|\mathcal{M}_n^{PS}|^2$ of Eq. (4.57) from Eq. (4.61) is to replace the photon energy spectrum with the Altarelli-Parisi distribution for a better treatment of hard collinear radiation.

Finally, the matching scheme introduced in the previous section can be applied to Eq. (4.57), with the building blocks described above, getting the master formula:

$$
d\Gamma_\infty^{\text{matched}} = \frac{1}{2M_H} F_{SV} \, \Pi(\{p\}, \epsilon) \sum_{n=0}^\infty \frac{1}{n!} \left(\prod_{i=1}^n F_{H,i} \right) |\mathcal{M}_n^{PS}(\{p\}, \{k\})|^2 d\Phi_n \tag{4.62}
$$

where the coefficient F_{SV} and $F_{H,i}$ are

$$F_{SV} = 1 + \frac{d\Gamma_{SV}^{NLO} - d\Gamma_{SV}^{PS,\alpha}}{d\Gamma^{LO}} \qquad F_{H,i} = 1 + \frac{|\mathcal{M}_1^{NLO}(k_i)|^2 - |\mathcal{M}_1^{PS,\alpha}(k_i)|^2}{|\mathcal{M}_1^{PS,\alpha}(k_i)|^2}.$$

$$(4.63)$$

The correction factors F_{SV} and $F_{H,i}$ carry the information of the exact NLO calculation: $d\Gamma_{SV}^{NLO}$ is the sum of the virtual corrections of Eq. (4.9) and soft real correction given by the first line of Eq. (4.15), $d\Gamma_{SV}^{PS,\alpha}$ is its PS approximation, *i.e.* the $\mathcal{O}(\alpha)$ term without any real hard photon of Eq. (4.57), $\mathcal{M}_1^{NLO}(k_i)$ is the exact one-photon bremsstrahlung amplitude and $\mathcal{M}_1^{PS,\alpha}(k_i)$ is its PS approximation. Let us stress that F_{SV} and $F_{H,i}$ are by construction free of collinear and/or infrared logarithms and that the $\mathcal{O}(\alpha)$ expansion of Eq. (4.62) exactly coincides with the NLO calculation, without any double counting. Furthermore, Eq. (4.62) is still fully differential in the final state momenta and can be conveniently implemented in a MC event generator. Finally, we remark that the NLO virtual and real corrections used in F_{SV} and $F_{H,i}$ are strictly defined only for 0 or 1 photon, while in Eq. (4.62) they are used also when there are additional photons: this requires a mapping of the n-photons phase space to 0 or 1 photon phase space. The mapping is implemented in close analogy to the one adopted in Ref. [190].

Chapter 5

Numerical results

In the previous Chapter we have detailed the calculation of $\mathcal{O}\left(\alpha\right)$ EW corrections to the Higgs decay into four charged leptons and the matching between the fixed-order NLO calculation with a PS algorithm. Our calculations have been implemented in `Hto4l`, a Monte Carlo program which allows for the generation of unweighted events in the channels $H \to \ell^+\ell^-\ell'^+\ell'^-$ (with $\ell, \ell' = e, \mu$), up to NLOPS accuracy. In this section we show and discuss the numerical results provided by our calculation, as obtained with `Hto4l`. In Sec. 5.1 we show some tuned comparisons with the predictions of the reference code `Prophecy4f` at the level of NLO electroweak corrections. Then, in Sec. 5.2 we present our best predictions for various observables at NLOPS electroweak accuracy, as well as for Higgs production and decay in the presence of NLO QCD and electroweak corrections matched to PS. Finally, since `Hto4l` is supplied with an interface which allows to use our code in association with any event generator for the Higgs production, in Sec. 5.3 we show and discuss some distributions obtained by interfacing `Hto4l` with `POWHEG` in the channel $gg \to H \to 2e2\mu$.

5.1 Comparison with `Prophecy4f`

5.1.1 Input parameters

In the comparisons between `Hto4l` and `Prophecy4f v2.0`.[1] as well as in all the results presented in this chapter, we use the set of input parameters reported in Table (5.1)

The $M_{Z,W}$ and $\Gamma_{Z,W}$ are the running-width PDG values which have to be

---

[1]Available at `https://prophecy4f.hepforge.org/`

87

$\alpha(0) = 1/137.03599911$	$G_\mu = 1.16637\ 10^{-5}\ \text{GeV}^{-2}$	$M_Z = 91.1876\ \text{GeV}$
$M_W = 80.398\ \text{GeV}$	$\Gamma_W = 2.141\ \text{GeV}$	$\Gamma_Z = 2.4952\ \text{GeV}$
$m_e = 510.99892\ \text{KeV}$	$m_\mu = 105.658369\ \text{MeV}$	$m_\tau = 1.77684\ \text{GeV}$
$m_u = 190\ \text{MeV}$	$m_c = 1.4\ \text{GeV}$	$m_{\text{top}} = 172.5\ \text{GeV}$
$m_d = 190\ \text{MeV}$	$m_s = 190\ \text{MeV}$	$m_b = 4.75\ \text{GeV}$

Table 5.1: Values of the input parameters used in the numerical calculations.

converted to the fixed-width scheme described in Sec. 1.5. As we work in the G_μ scheme, for the electromagnetic coupling constant we use the expression

$$\alpha_{G_\mu} = \frac{\sqrt{2}\,G_\mu\,M_W^2\,\sin^2\theta_W}{\pi} \tag{5.1}$$

with $\sin^2\theta_W = 1 - M_W^2/M_Z^2$, in the calculation of the LO width and NLO weak corrections, while we use $\alpha(0)$ for the coupling of the photon to the external charged particles.[2] The top-quark width is set to the LO prediction in the SM, and a fixed width is employed in all the resonant propagators in the framework of the complex-mass scheme.

5.1.2 $\mathcal{O}\left(\alpha\right)$ corrections: comparisons to `Prophecy4f`

A sample of the `Prophecy4f` vs. `Hto4l` comparisons at NLO electroweak accuracy is shown in Tab. 5.2 and in Figs. 5.1-5.3, in order to check the technical accuracy of our predictions in its different aspects sketched in Sect. 4.3. Generally speaking, we observe very good agreement between our predictions and the independent results of `Prophecy4f`.

In Fig. 5.1 we show the comparison for the NLO width in the leptonic decay channels $H \to 2e2\mu$ and $H \to 4\mu$,[3] as a function of the Higgs mass in the range [125, 400] GeV, together with the relative contribution due to the NLO electroweak corrections where the effect of mass thresholds present in the loop computation is particularly visible. As can be seen, the two calculations perfectly agree. For the sake of clarity and completeness, we quote in Tab. 5.2 the predictions of the two codes for the decay channels $H \to 2e2\mu$ and $H \to 4\mu$ for three specific values of the Higgs mass: the level of agreement is within the statistical numerical uncertainty which is well below the 0.1% accuracy.

---

[2]This value is used for all the numerical results shown in the following, with the exception of the comparisons with `Prophecy4f`, where we use α_{G_μ} everywhere, to be consistent with the default choice of `Prophecy4f`.

[3]Analogous results are valid in the $H \to 4e$ channel, which coincides for the integrated partial width with the 4μ final state (apart from negligible mass effects).
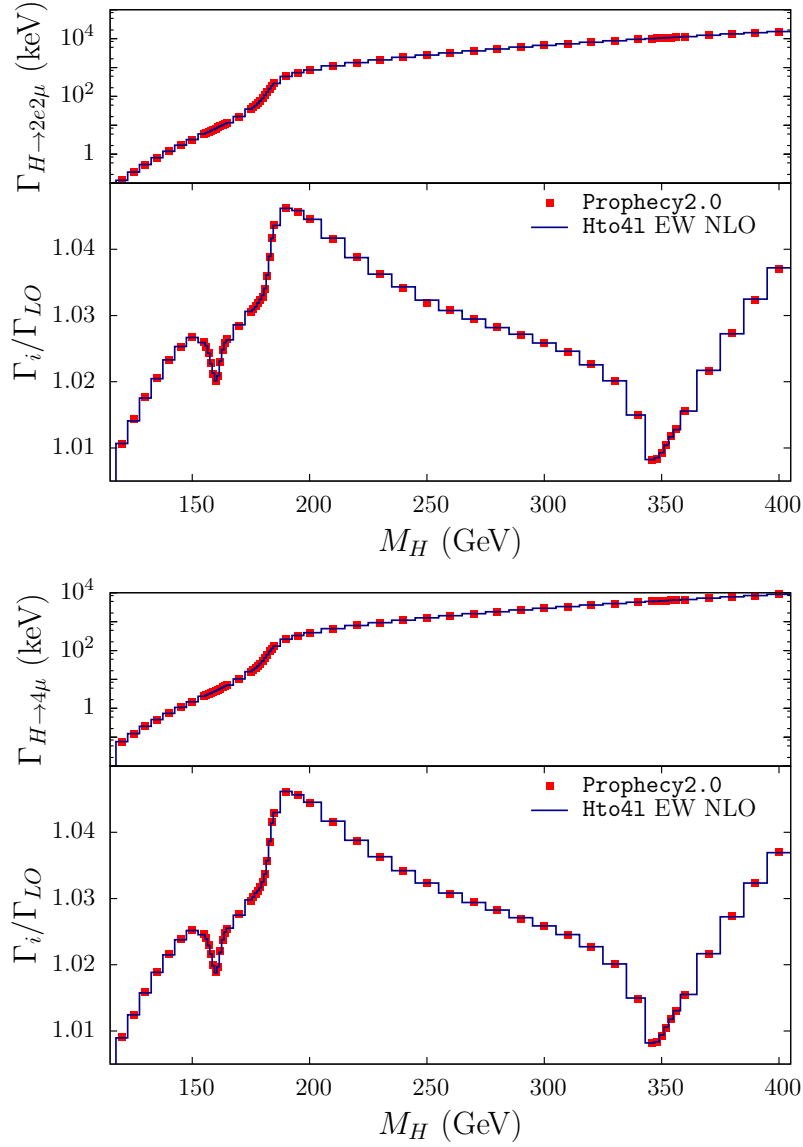
Figure 5.1: Comparison between the NLO electroweak calculation of `Prophecy4f` and `Hto4l` for the decay widths $H \to 2e2\mu$ (upper plot) and $H \to 4\mu$ (lower plot), as a function of the Higgs mass in the range [125, 400] GeV. For each plot, upper panel: absolute predictions in KeV; lower panel: ratio between LO width and NLO EW corrected width.

In Fig. 5.2 a comparison between `Prophecy4f` and `Hto4l` is shown for the e^+e^- invariant mass (in the Higgs rest frame), in the range [60, 100] GeV (upper plot) and in the range [85, 95] GeV (lower plot). The results refer to the decay channel $H \to 2e2\mu$ for $M_H = 125$ GeV. Also in this case, the

M_H/Final State	Prophecy4f	Hto4l
125 GeV/$H \to 2e2\mu$	0.24151(8)	0.24165(2)
140 GeV/$H \to 2e2\mu$	1.2672(2)	1.2667(1)
200 GeV/$H \to 2e2\mu$	825.9(1)	825.8(1)
125 GeV/$H \to 4\mu$	0.13324(2)	0.13325(2)
140 GeV/$H \to 4\mu$	0.6713(1)	0.6711(1)
200 GeV/$H \to 4\mu$	413.02(7)	412.98(2)

Table 5.2:   Comparison between the NLO electroweak predictions of `Prophecy4f` and our calculation (`Hto4l`) for the Higgs decay width (in KeV), for different values of the Higgs mass and final states. The numbers in parenthesis are the statistical uncertainty on the last digit due to MC integration.

agreement between the two codes is remarkable, in spite of the large effect due to the radiative corrections[4]. Actually, at and above the peak of the electron-pair invariant mass distribution the corrections are of the order of 30%, while for $M_{e^+e^-}$ below M_Z they can reach 50%. The lowering of the peak and the raising of a tail can be mainly ascribed to the photon radiation off the leptons, as typical final-state radiation (FSR) effect observed around the peak of resonant processes [192, 193, 194, 195].

A further comparison is given in Fig. 5.3 for the distribution of the angle between the decay planes of the virtual Z bosons in the H rest frame for the channels $H \to 2e2\mu$ (upper plot) and $H \to 4\mu$ (lower plot) for $M_H = 125$ GeV, which is the observable of main interest for spin-parity assignment. For the ϕ angle we use the definition

$$\cos\phi = \frac{(\mathbf{k}_{12} \times \mathbf{k}_1) \cdot (\mathbf{k}_{12} \times \mathbf{k}_3)}{|\mathbf{k}_{12} \times \mathbf{k}_1||\mathbf{k}_{12} \times \mathbf{k}_3|} \tag{5.2}$$

$$\mathrm{sgn}(\sin\phi) = \mathrm{sgn}\left\{\mathbf{k}_{12} \cdot [(\mathbf{k}_{12} \times \mathbf{k}_1) \times (\mathbf{k}_{12} \times \mathbf{k}_3)]\right\} \tag{5.3}$$

where $\mathbf{k}_{12} = \mathbf{k}_1 + \mathbf{k}_2$ and $\mathbf{k}_1$, $\mathbf{k}_2$, $\mathbf{k}_3$, $\mathbf{k}_4$ are the three-momenta of the final-state leptons.

Again the predictions of the two codes nicely agree. The contribution of the NLO corrections is particularly visible at the edges of the distribution, where it can reach the 5% level for both the decay channels.

---

[4]For simplicity, in the present Section we provide results for bare electrons only, *i.e.* in the absence of lepton-photon recombination effects.
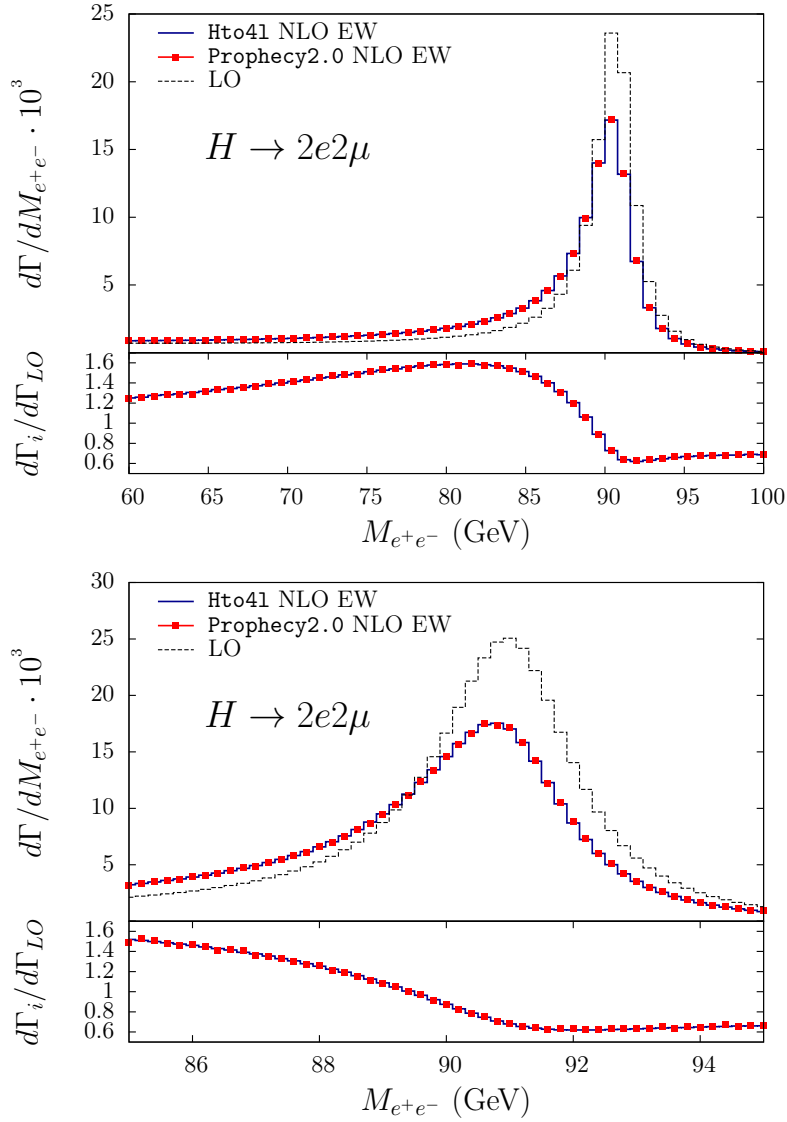
Figure 5.2: Comparison between the NLO electroweak calculation of `Prophecy4f` and `Hto4l` for the e^+e^- invariant mass (in the Higgs rest frame), in the range [60, 100] GeV (upper plot) and in the range [85, 95] GeV (lower plot). Predictions for the decay $H \to 2e2\mu$ at $M_H = 125$ GeV. Upper panels: absolute predictions for $d\Gamma/dM_{e^+e^-}$; lower panels: relative effect of the NLO corrections.

5.2 `Hto4l`: Predictions at NLOPS electroweak accuracy

Some illustrative results obtained according to a number of variants of the theoretical approach described in Chapter 4 are given in Figs. 5.4-5.6. In
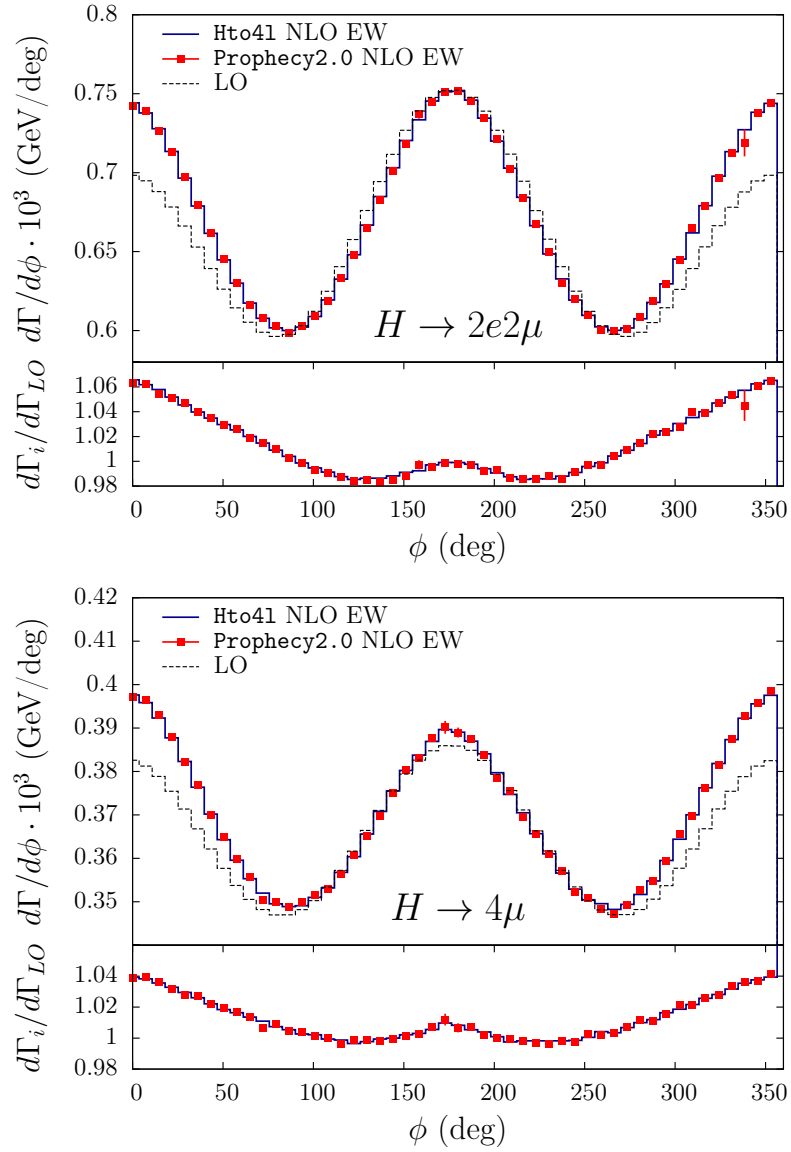
Figure 5.3: Comparison between the NLO electroweak calculation of `Prophecy4f` and `Hto4l` for the ϕ angle distribution (in the Higgs rest frame) for the decay channels $H \rightarrow 2e2\mu$ (upper plot) and $H \rightarrow 4\mu$ (lower plot) at $M_H = 125$ GeV. Upper panels: absolute predictions in GeV/deg; lower panels: relative effect of the NLO corrections.

order to disentangle the impact of the different sources of correction, we consider the results obtained according to the following levels of accuracy:

1. the pure PS approximation for the decay width as in Eq. (4.57), associated to multiple photon emission in the soft/collinear limit;

2. the $\mathcal{O}(\alpha)$ truncated approximation of Eq. (4.57), describing one photon radiation in the PS framework;

3. the complete NLO electroweak calculation;

4. the NLO QED calculation, given by the gauge-invariant subset of electromagnetic contributions within the full set of electroweak corrections;

5. the NLO electroweak corrections matched to the QED PS, as in Eq. (4.62);

6. the NLO QED corrections matched to the QED PS, *i.e.* the QED gauge-invariant realization of Eq. (4.62).

The comparison between approximations 1. and 2. is useful to quantify the higher-orders contribution due to photon emission beyond $\mathcal{O}(\alpha)$, while the difference between options 3. and 4. is a measure of pure weak loop corrections, the difference between approximations 2. and 3. is an estimate of non-logarithmic $\mathcal{O}(\alpha)$ QED terms plus pure weak loop corrections. The comparison between approximations 3. and 5., as well as between 4. and 6., allows us to check that the NLOPS matching procedure correctly preserves the effect of QED exponentiation as given by the difference between options 1. and 2. Moreover, the results of 1. vs. those of 5. and of 3. vs. those of 5. provide an estimate of the accuracy of the predictions available in the literature for Higgs physics at the LHC, in particular of the process-independent, widely used code `PHOTOS` [196], which describes multiple photon emission but does not include exact NLO electroweak corrections, and of `Prophecy4f`, that does not take into account the contribution of exclusive QED exponentiation.

In Fig. 5.4 we show the relative contribution of the different theoretical approximations discussed above for the e^+e^- (upper plot) and $\mu^+\mu^-$ (lower plot) invariant mass in the Higgs rest frame, in the range [85, 95] GeV. The results refer to the process $H \to 2e2\mu$ for $M_H = 125$ GeV, according to a bare lepton definition. By inspection of Fig. 5.4 we can draw the following conclusions: the NLO corrections to the lepton invariant masses are quite large, since they amount to about 50% (30%) to the e^+e^- ($\mu^+\mu^-$) invariant mass below the peak and about 30% (20%) at and above it. They are largely dominated by the enhanced leading logarithmic contributions of QED nature $\propto \alpha \log(M_Z^2/m_\ell^2)$, as can be inferred from the comparison between the results of the pure $\mathcal{O}(\alpha)$ PS algorithm and those of the NLO QED/electroweak calculations. From this comparison, one can also conclude that the $\mathcal{O}(\alpha)$ non-logarithmic QED terms contribute at the some per cent level, both for the e^+e^- and $\mu^+\mu^-$ invariant mass, whereas the pure weak loops have a much smaller effect, not exceeding the 1% level.
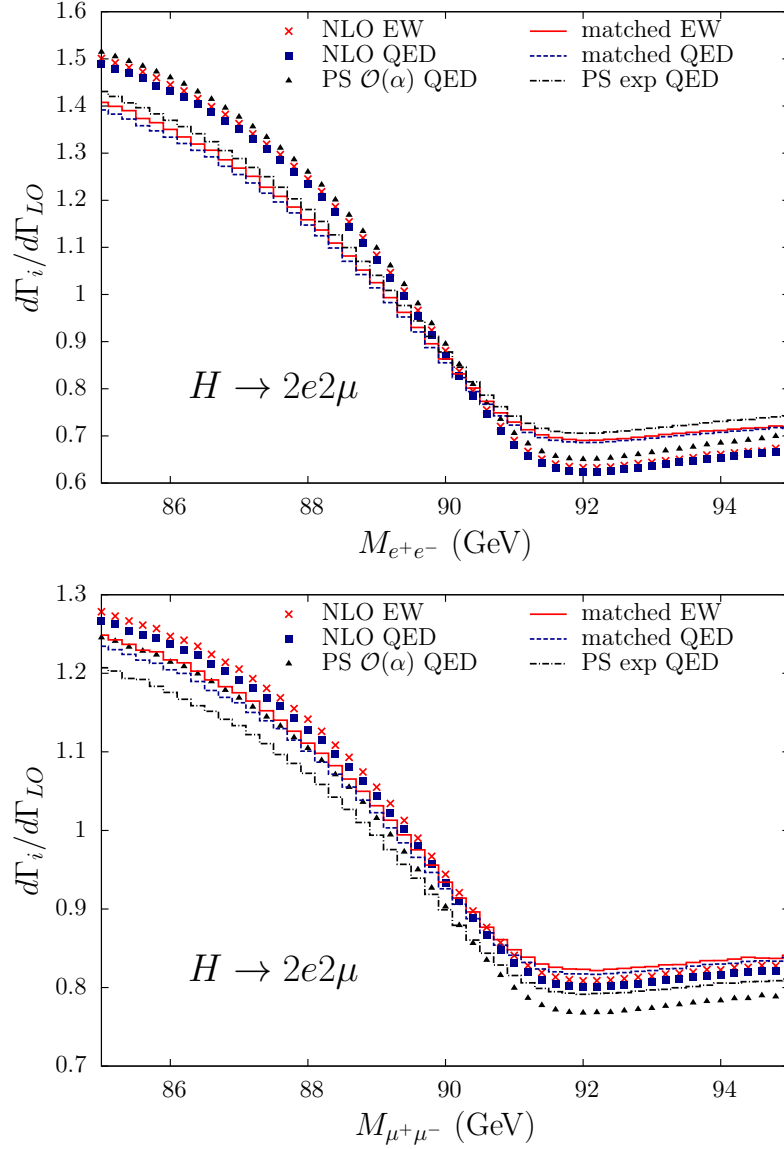
Figure 5.4: Relative contribution of the QED/electroweak corrections to the e^+e^- (upper plot) and $\mu^+\mu^-$ (lower plot) invariant mass in the Higgs rest frame, in the range [85, 95] GeV. Predictions for the decay $H \to 2e2\mu$ at $M_H = 125$ GeV. The theoretical approximations corresponding to the different lines are explained in the text.

The large impact of NLO QED corrections, which significantly modify the shape of the invariant mass distribution, translates in a relevant contribution due to higher-order photonic corrections. Multiple photon emission is of the order of 10% for the e^+e^- final-state and at the level of some per

cents for the $\mu^+\mu^-$ case, as a consequence of the different magnitude of the lepton-photon collinear logarithm. It can also be noticed that QED exponentiation reduces the impact of NLO corrections and that the NLOPS matching correctly preserves the size of multiple photon emission.
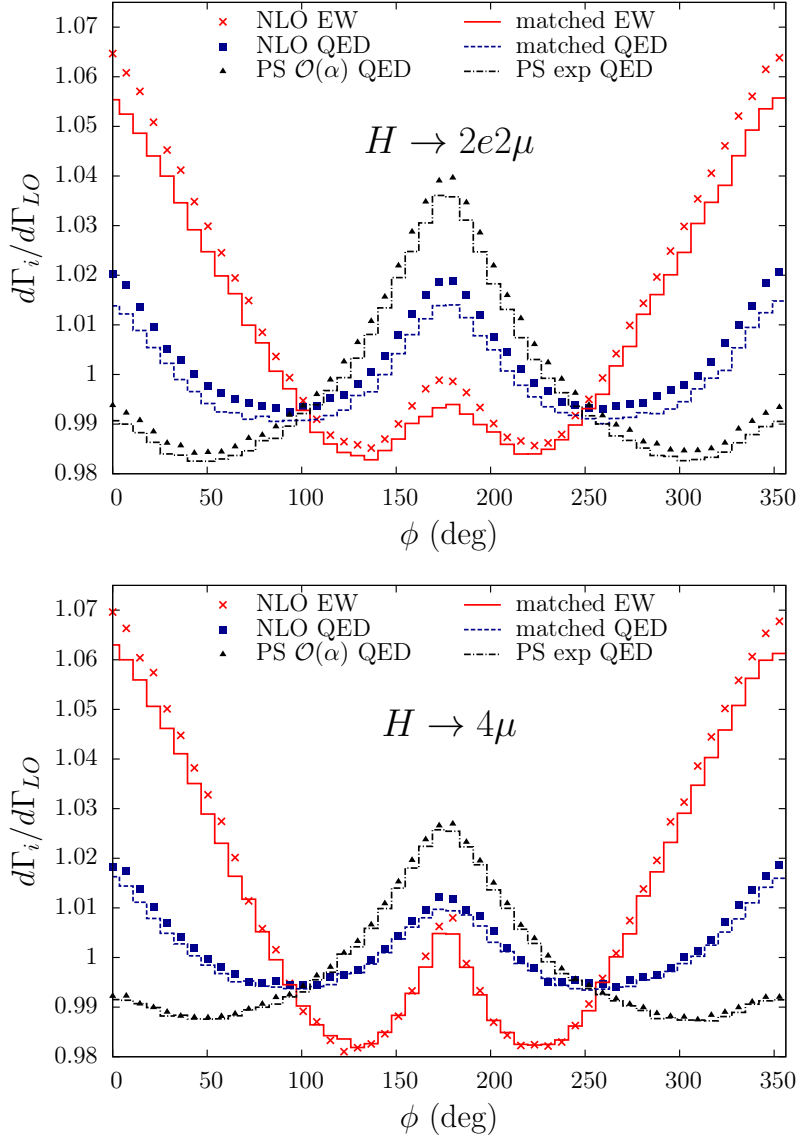

Figure 5.5: The same as Fig. 5.4 for the ϕ angle distribution in the decay channels $H \to 2e2\mu$ (upper plot) and $H \to 4\mu$ (lower plot) at $M_H = 125$ GeV.

Quite different conclusions derive from the analysis of Fig. 5.5, which shows the relative corrections of the different theoretical recipes on the ϕ

angle distribution for the $H \to 2e2\mu$ and $H \to 4\mu$ decays. For such an observable, the pure $\mathcal{O}(\alpha)$ PS approximation significantly underestimates the contribution of NLO EW corrections for ϕ close to 0° and 360°, while it provides an overestimate around 180°. Actually, it can be noticed that the ϕ angle distribution receives a non-negligible contribution from fixed-order non-logarithmic terms and that, more importantly, is particularly sensitive to pure weak corrections, which set the correct overall size and shape of the radiative corrections. On the other hand, the effect of QED exponentiation is moderate, varying between a few per mille to about 1%.

For completeness, we show in Fig. 5.6 results for the invariant mass of the e^+e^- pair and the ϕ angle distribution (for the process $H \to 2e2\mu$) under the more realistic experimental condition of calorimetric or recombined electrons and positrons. In this case, we replace the three-momentum of the $e^\pm$ with the effective momentum $\mathbf{p} = \mathbf{p_{e^\pm}} + \mathbf{p_\gamma}$ for each photon satisfying the condition $\Delta R_{e^\pm\gamma} = \left(\Delta\eta_{e^\pm\gamma}^2 + \Delta\phi_{e^\pm\gamma}^2\right)^{1/2} \leq 0.1$, as typically done by LHC experiments, where $\Delta\phi_{e^\pm\gamma}$ is the lepton-photon separation angle in the transverse plane. As can be seen from Fig. 5.6 in comparison to Fig. 5.4 and Fig. 5.5, the contribution of the radiative corrections is largely reduced, as expected, when switching from bare to recombined electrons/positrons. For the e^+e^- invariant mass, the corrections are reduced by about a factor of three, almost independently of the considered theoretical approximation, and preserve their shape. However, non-negligible corrections still remain under the calorimetric condition, of about +15% in the left tail of the invariant mass and of the order of -10% around the peak of the distribution, when considering the most accurate matched predictions. In comparison to the case of bare electrons, the effect of QED exponentiation for dressed electrons reduces to about 1% in the tail and at the per mille level at and above the peak.

More interestingly, the QED relative corrections to the ϕ angle distribution are substantially modified both in size and shape by the recombination effects, whereas the full electroweak predictions receive a slight size reduction and a less pronounced shape modification. In particular, we checked through detailed numerical inspections that the especially visible difference in shape between the pure PS and the diagrammatic QED predictions is of virtual origin and has to be ascribed to the QED pentagons, which are exactly included in the Feynman diagram calculation and only (crudely) approximated in the soft/collinear limit in the PS calculation. To some extent, we expect that the rich angular correlations introduced by pentagon diagrams are only poorly reproduced by the PS approximation. All in all, the results shown in the lower plot of Fig. 5.6 reinforce the already noticed particularly relevant
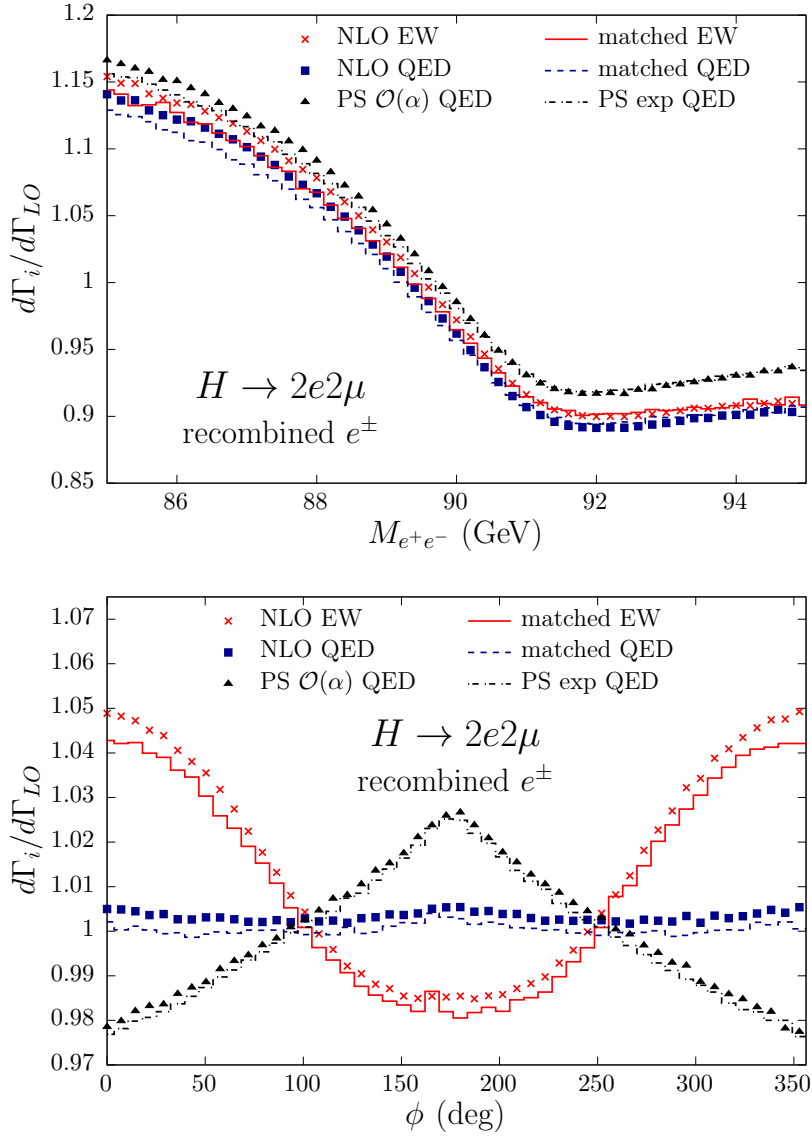
Figure 5.6:   Relative contribution of the QED/electroweak corrections to the e^+e^- invariant mass (upper plot) and the ϕ angle distribution (lower plot) for recombined electrons and positrons. Predictions for the decay $H \to 2e2\mu$ at $M_H = 125$ GeV in the Higgs rest frame. The theoretical approximations corresponding to the different lines are explained in the text.

rôle played by loop contributions with complex topology, both of QED and weak nature, to obtain reliable predictions for the ϕ angle observable.

To summarize, the main conclusion of this Section is that both NLO elec-

troweak and higher-order QED corrections, as well as their combination, are relevant for reliable simulations of the most important observables considered in precision studies of the Higgs sector at the LHC.

5.3 Interface to `POWHEG`: results for production and decay

In order to facilitate phenomenological studies of Higgs boson production and decay in the presence of both QCD and electroweak contributions, we have implemented an interface which allows to use our code in association with any event generator describing Higgs production. In Figs. 5.7-5.9 we show a sample of illustrative results obtained by interfacing `Hto4l` with `POWHEG` [120] for the simulation of Higgs boson production in gluon-gluon fusion. We use the `POWHEG` version with NLOPS accuracy in QCD [197] from the `POWHEG BOX` framework [198] and we consider Higgs production in proton-proton collisions at a c.m. energy of 8 TeV[5]. The events generated by `POWHEG` are interfaced to `Hto4l` according to the following procedure:

- generate unweighted events for the process $pp \rightarrow H(+j)$ in the Les Houches format using `POWHEG`, where H is an on-shell Higgs boson and j stands for the extra parton of the NLO QCD calculation;

- the Les Houches file is read event by event by `Hto4l` and the particles momenta are stored in the generic common block structure introduced in Ref. [199];

- each event is decayed into the selected channel in the H rest frame, using `Hto4l`. After boosting the decay products back to the laboratory frame, the events including production and decay are written in a file in the Les Houches format.

The Les Houches file can be finally passed to a shower event generator for QCD showering and hadronization. In our examples we use `PYTHIA v6.4` [200] as QCD PS. According to the above procedure, the $pp \rightarrow H \rightarrow 4\ell$ process is treated in narrow width approximation, as it is the case for a 125 GeV Higgs boson, and factorized in on-shell Higgs production and decay.

In our analysis we consider, for definiteness, the decay channel $H \rightarrow 2e2\mu$ and the following observables: the transverse momentum p_T^H and rapidity y_H

---

[5]However, as we are interested to study the relative impact of electroweak corrections dominated by contributions of the kind $\alpha^n \log^n(M_Z^2/m_\ell^2)$, the results shown in the following are in practice independent of the c.m. energy.
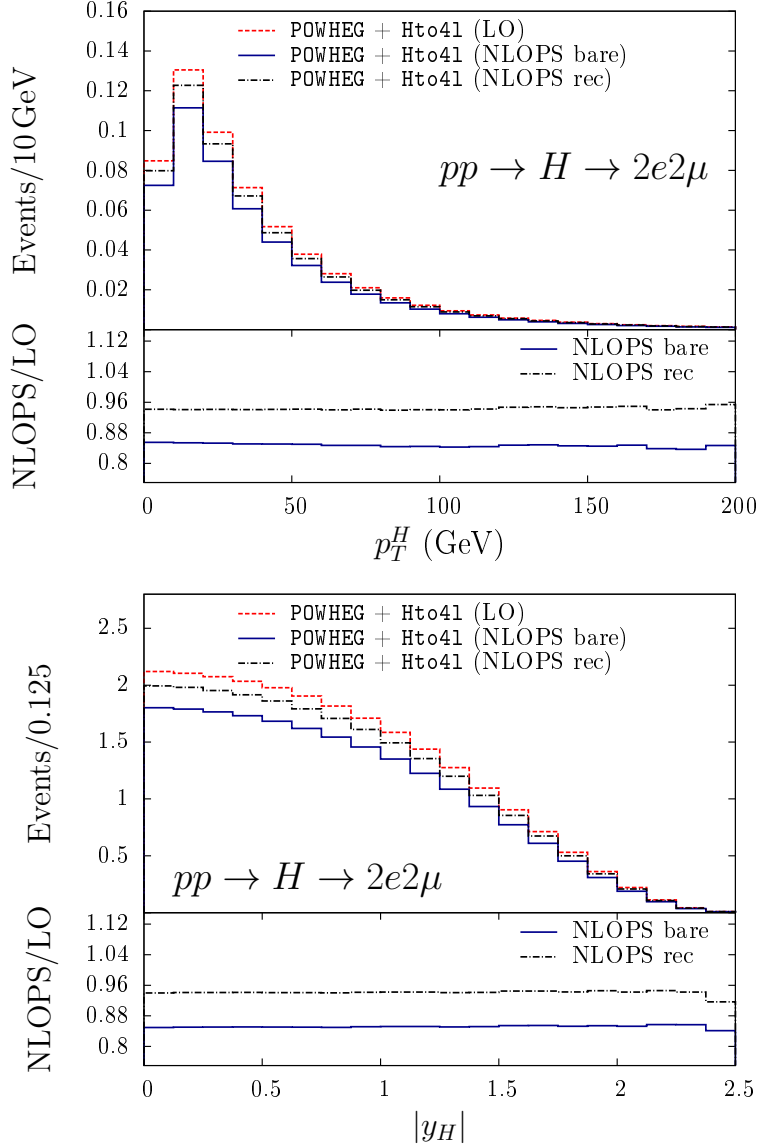
Figure 5.7: Comparison between the results obtained with `POWHEG` + `Hto4l` (Born) + `PYTHIA` v6 (red dashed line) and `POWHEG` + `Hto4l` (NLOPS) + `PYTHIA` v6 (blue solid and black dash-dotted lines) for the transverse momentum (upper plot) and rapidity (lower plot) of the Higgs boson. In the lower panels the relative contribution of NLOPS electroweak corrections for bare (solid line) and recombined (dash-dotted line) leptons is shown.
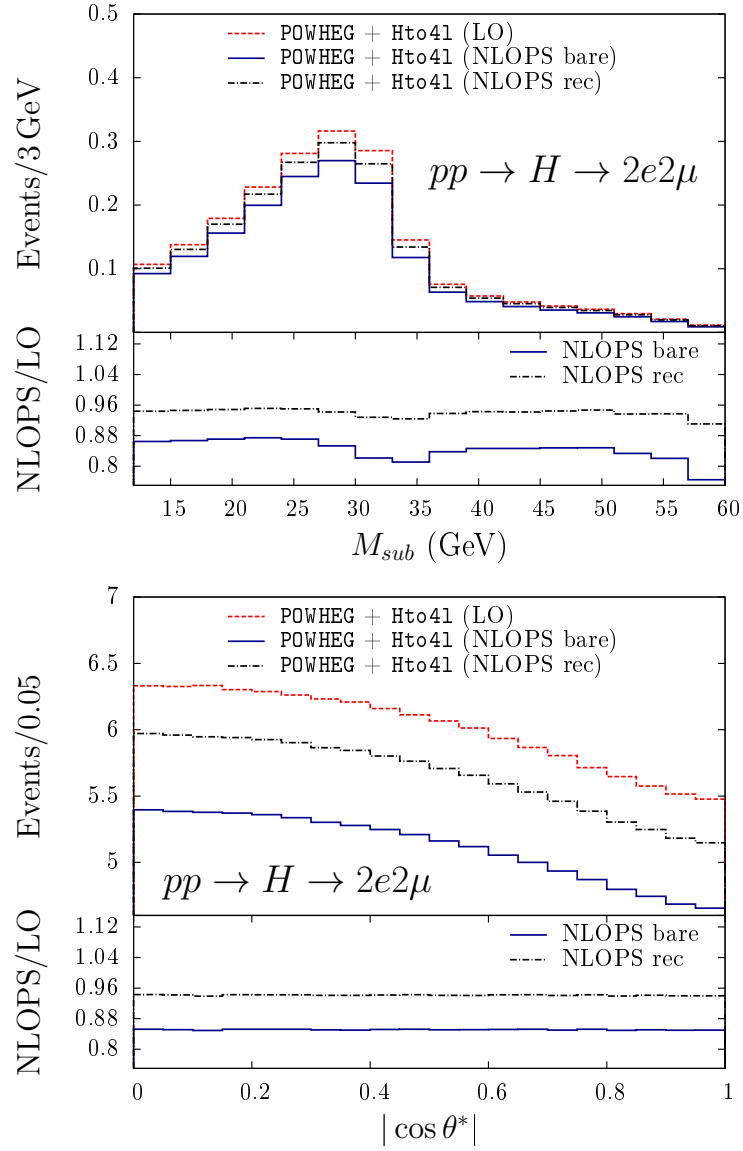
Figure 5.8: The same as in Fig. 5.7 for the invariant mass of the subleading lepton pair (upper plot) and the cosine of the angle of the leading lepton pair in the four-lepton rest frame with respect to the beam axis (lower plot).

of the Higgs boson (Fig. 5.7), the invariant mass of the subleading lepton pairs and the magnitude of the cosine of the decay angle of the leading lepton pair in the four-lepton rest frame with respect to the beam axis $|\cos\theta^*|$ (Fig. 5.8). The leading pair is defined as the lepton pair with invariant mass closest to the Z boson mass and its angle is obtained by summing the three-momenta of the two leptons. For the `POWHEG` calculation of Higgs production in gluon fusion, we use the PDF set `MSTW2008nlo68cl` [201] with factorization/renormalization scale $\mu_R = \mu_F = M_H$. The values of the other input parameters are the same as the ones given in Tab. 5.1.

The results shown in the following refer to a sample of $1, 2 \times 10^8$ un-weighted events and to the selection cuts adopted in Ref. [181]: each muon (electron) must satisfy transverse momenta $p_T > 6$ GeV (7 GeV) and be in the pseudorapidity range $|\eta| < 2.7$ (2.47). The highest-p_T lepton must satisfy the condition $p_T > 20$ GeV, while the subleading and the third leptons are respectively required to have $p_T > 15$ GeV and $p_T > 10$ GeV. The leptons are required to be separated by each other of $\Delta R = \sqrt{(\Delta\eta)^2 + (\Delta\phi)^2} > 0.1$ (0.2) when having same (different) flavors. The leading invariant mass M_{lead} is required to be in the range $50\,\mathrm{GeV} < M_{lead} < 106\,\mathrm{GeV}$, while the subleading one must be in the range $12\,\mathrm{GeV} < M_{sub} < 115\,\mathrm{GeV}$. Finally, the four momentum invariant mass has to be in the range $118\,\mathrm{GeV} < M_{1234} < 129\,\mathrm{GeV}$. We show the results for either bare leptons (blue solid line) and recombined leptons (black dash-dotted line) leptons. In the latter case, we recombine photons with both electrons and muons, if the condition $\Delta R_{\ell\gamma} \leq 0.1$ is satisfied, as in [181].

In Fig. 5.7 and Fig. 5.8 we show the comparison between the predictions obtained using `POWHEG` interfaced to our code at LO and NLOPS electroweak accuracy. It can be noticed that the contribution due to NLOPS electroweak corrections is almost flat and of about $-15\,(-5)\%$ for p_{T}^H, y_H and $|\cos\theta^*|$ when considering bare (recombined) leptons, while the invariant mass of the subleading lepton pairs receives a varying correction of size between $-20\,(-10)\%$ and $-10\,(-5)\%$ for bare (calorimetric) leptons, respectively.

In Fig. 5.9 we show the results for two observables which are fully exclusive over QED radiation and which can be easily treated in our approach. The results correspond to the process $pp \to H \to 2e2\mu + n\,\gamma$, with $E_\gamma^{\min} = 1$ GeV, for which we show the transverse momentum of the hardest photon and the angular separation between the hardest photon and the closest lepton, that exhibit the expected features of photon emission in radiative events.
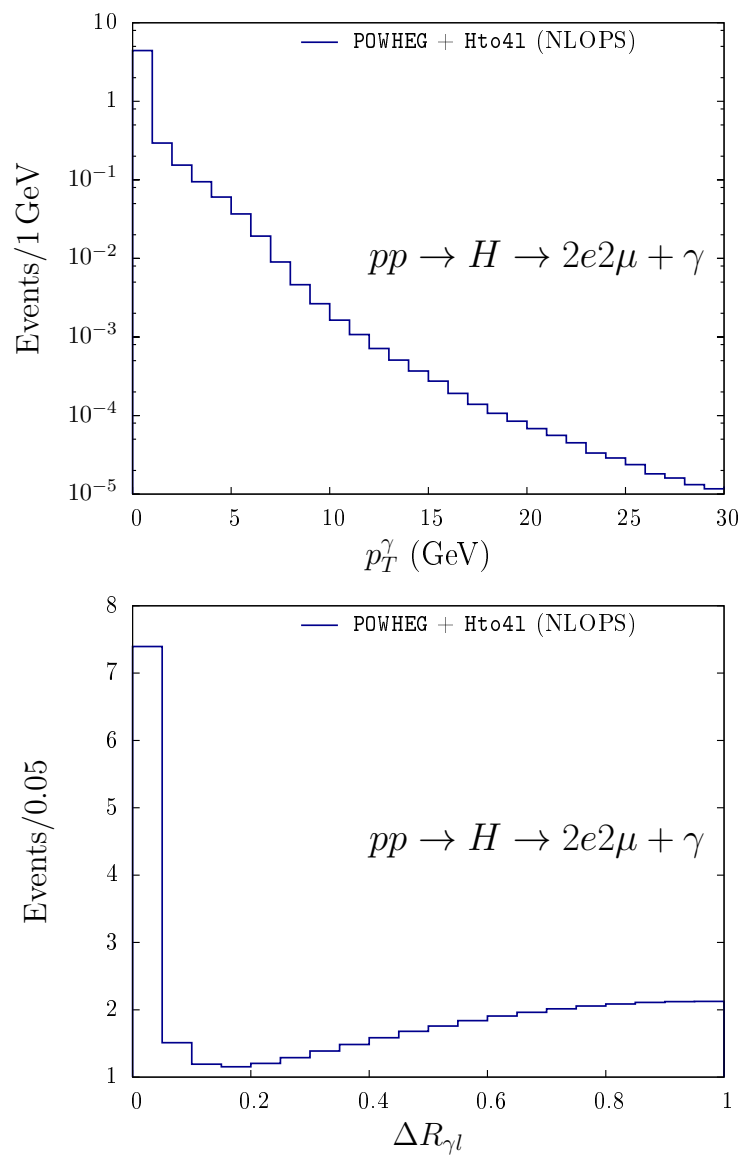
Figure 5.9: Distribution of the transverse momentum of the hardest photon (upper plot) and the angular separation between the hardest photon and the closest lepton (lower plot) obtained using `POWHEG + Hto4l` (NLOPS) + `PYTHIA v6`. The minimum photon energy is $E_\gamma^{\min} = 1$ GeV.

Chapter 6

New physics effects on Higgs decay into four charged leptons

The particularly clean signature and the non-trivial kinematics make the $H \to 4\ell$ decay an important channel for searching indirect evidence of new physics. Indeed, the presence of anomalous couplings in the Higgs sector would lead to unexpected deviations between theoretical predictions and experimental data. This motivates the recent developments of our study on the $H \to 4\ell$ decay channel. In this chapter we present some preliminary results on the impact of new physics effects on the Higgs decay into four charged leptons. To evaluate the deviations from SM predictions in a model-independent way, we adopt an Effective Field Theory (EFT) approach. Other studies on the BSM effects in the $H \to VV \to 4\ell$ have been published in the last years. In particular, in Refs. [202, 203, 204] new physics effects in $h \to 4\ell$ decays are parametrized in terms of specific anomalous Higgs vertices, while in Refs. [205, 206, 207] the language of pseudo-observables is adopted. Here we directly start from an EFT Lagrangian. In this framework the gauge invariance in preserved by construction. Moreover, since the EFT approach is widely used in the analysis of LHC data, the link with experimental constraints is more transparent. Our analysis is performed at the level of differential cross sections. In particular, we compare, for several kinematic observables, the effects of effective operators with respect to SM predictions at NLOPS accuracy. The results have been obtained with a new version of `Hto4l`, where new LO $H \to 2e2\mu$ matrix elements have been calculated from an effective Lagrangian that includes all the relevant dimension six operators to $H \to 4\ell$ decay channel.

The chapter is structured as follows: in Sec. 6.1 we introduce some generalities on the EFT approach, with particular emphasis on the connection

between EFT and LHC data; in Sec. 6.2 we describe the theoretical framework that we have adopted, while the implementation of the anomalous part in `Hto4l` is described in Sec. 6.3; finally in Sec. 6.4 we show and discuss some preliminary results for the $H \to 2e2\mu$ channel.

6.1   Introduction to Effective Field Theory

The discovery of the Higgs boson and the consistency of its measured properties with the SM ones have definitively promoted the SM as the appropriate theory for the unified description of fundamental interactions (with the remarkable exception of gravity), at least up to the EW scale. However, as we have mentioned in the introduction of this work, many arguments suggest that the SM cannot be the ultimate theory of fundamental interactions: it does not account for dark matter, neutrino masses and oscillations and matter/anti-matter asymmetry. Moreover, theoretical arguments based on a natural solution of the hierarchy problem suggest that at the TeV scale new degrees of freedom would eventually appear. On the other hand, the lack of direct signals of new physics is reinforcing the hypothesis that the scale of new physics could not be accessible at the LHC. In this unfavorable scenario the best chance for ATLAS and CMS to find hints of new physics would lie in the analysis of SM processes and in the discovery of unexpected discrepancies between theoretical SM predictions and experimental data. For instance, deviations from SM predictions could imply the presence of new particles in the loops, which could give rise to anomalous couplings between SM particles. From this point of view, the Effective Field Theory approach represents an important theoretical framework for the description of new interactions in a model independent way. On general grounds, the EFT approach is based on the hypothesis that the SM is suitable to describe strong and electroweak interactions at energy scales much lower than the scale Λ of new physics. If the mass of the lightest new particle is much larger than the SM ones, the low energy reduction of the complete theory at the EW scale proceeds through the decoupling of heavy particles. These heavy degrees of freedom are then integrated out according to the Appelquist-Carazzone theorem [208], giving rise to higher-dimensional operators which capture the low energy effects of new physics. It is important to stress that the basic features of the SM still hold in the EFT approximation: the effective Lagrangian has the same field content and it is invariant under the local $SU(3)_C \otimes SU(2)_L \otimes U(1)_Y$ symmetry group. Moreover, the spontaneous breaking of the $SU(2)_L \otimes U(1)_Y$ down to $U(1)_e$ is still due to the non vanishing vacuum expectation value of a complex scalar field transforming as $(1,2)_{1/2}$ under the local group. The

effective Lagrangian can be written in the following general form

$$\mathcal{L}_{\text{EFT}} = \mathcal{L}_{\text{SM}} + \frac{1}{\Lambda} \sum_i c_i^{(5)} \mathcal{O}_i^{(5)} + \frac{1}{\Lambda^2} \sum_i c_i^{(6)} \mathcal{O}_i^{(6)} + \cdots , \qquad (6.1)$$

where each $\mathcal{O}_i^{(D)}$ is a gauge invariant D-dimension operator suppressed by powers of Λ, while the parameters $c_i^{(D)}$ are the so-called Wilson coefficients. The main motivation to use an EFT approach lies in its generality. All decoupling BSM theories where new particles are much heavier than the SM ones and much heavier than the energy scale accessible by the experiments, can be mapped in such a Lagrangian. The constraints on the Wilson coefficients obtained by comparing experimental data with EFT predictions can be then interpreted in terms of any UV complete theory. In fact, once the underlying theory is specified, the dependence of the Wilson coefficients on the parameters of the complete theory can be recovered by integrating out the heavy degrees of freedom.

It is known from the first analysis of effective operators that the only gauge invariant dimension-five operator which can be built with a SM content leads to lepton number violation [209]. Since no dimension six operators can do the same job, the related Wilson coefficient is strongly constrained by the experiments and it is neglected in the analysis of LHC data. Then, the leading effects of new physics at the EW scale are expected to be parametrised by dimension six operators. The first complete set of 80 operators was derived in Ref. [210], assuming baryon and lepton number conservation, flavor universality, a linear realization of the EWSB, and a SM field content. However, it was soon noted that not all the operators of this set are independent: they can be linked through equations of motions of the SM fields, integration by parts, or field redefinitions. The first complete and non redundant set of 59 CP-even dimension six operators (the so-called Warsaw basis), was published only in 2010 [211]. It is worth mentioning that if one wants to include the low energy effects of CP violating models, other 6 CP-odd bosonic operators are necessary. Although the angle between the decay planes of the two intermediate gauge bosons is sensible to the CP properties of the Higgs boson, our analysis is restricted to CP-even operators, thus CP-odd operators will be not considered in the following. Since there are alternative choices in the redefinition of the fields and in the use of the equations of motion, different bases have been proposed in the literature. The most popular choices are the Warsaw basis [211] and the SILH (Strong Interacting Light Higgs) basis [212, 213]. The choice of the basis is usually led by the convenience to minimize the number of operators that are necessary to paramatrize the BSM effects on a given class of processes. Furthermore, the choice of the

basis can be also influenced by model dependent assumptions. For instance, the Warsaw basis is particularly appropriate for the low energy reduction of BSM theories that modify the interactions of the SM fermions. In contrast, the SILH basis has been designed to capture the effects of those theories in which new physics mostly couples to SM bosons. Regarding the application of EFT on Higgs physics, there is no theoretical obstacle to present the results of LHC analysis as constraints on the Wilson coefficients of the Warsaw or SILH basis. However this procedure can be rather cumbersome from the experimental point of view. The reason is that Wilson coefficients in either Warsaw and SILH basis enter the Higgs couplings to mass eigenstate in a rather complicated way. An alternative approach is represented by the BSM primaries basis [214], where the effective Lagrangian is written in terms of mass eigenstates, after electroweak symmetry breaking. Within this framework only the $SU(3)_C \otimes U(1)_e$ is manifest while the $SU(2)_L \otimes U(1)_Y$ is implicit, as it is encoded in the relations between different couplings in the Lagrangian. Following the same procedure, the so-called Higgs basis has been recently proposed to parametrize the space of $D = 6$ operators in a way that can be more directly connected to observable quantities in Higgs physics. On general grounds, the variables spanning the Higgs basis correspond to a subset of the couplings parametrizing new interactions in the mass-eigenstate effective Lagrangian. Since these couplings can be expressed as a linear combination of Wilson coefficients of any other basis, from a technical point of view the Higgs basis is nothing more than a linear transformation of the SILH or the Warsaw basis. The total number of independent couplings is the same of any other basis. The remaining dependent couplings are then expressed as a linear combination of the independent ones. Of course, the choice on which couplings are chosen as independent is free and is dictated by convenience. The algorithm for the construction of the complete $D = 6$ Lagrangian in terms of mass eigenstates is described in Ref. [215]. Here we limit to mention that in this formalism, by construction, all kinetic terms are canonically normalized, there is no kinetic mixing between the Z boson and the photon and there is no corrections to the Z boson mass. While, in general, dimension six operators give rise to mixing and mass corrections, the canonical form can always be recovered by using the equations of motions, integration by parts and a redefinition of the fields and couplings. Only the W mass receives a corrections from the term

$$\Delta \mathcal{L}_{\text{kinetic}}^{D=6} = 2\delta m \frac{g_2^2 v^2}{4} W_\mu^+ W_\mu^- \tag{6.2}$$

The independent coupling δm is a free parameter from the EFT point of view. However since it is very well constrained by electroweak precision

data ($\delta m = (2.6 \pm 1.9) \cdot 10^{-4}$) it is neglected in the analysis of Higgs data. Moreover, if custodial symmetry is preserved, $\delta m = 0$ by hypothesis.

6.2 $D = 6$ contributions to Higgs decay into four charged leptons

In order to include the effects of $D = 6$ operators in the decay of the Higgs boson into four charged leptons we adopt the Higgs basis, introduced in the previous section. For the full derivation of the effective Lagrangian in terms of mass eigenstate we refer to [215], limiting the discussion to the relevant CP-even couplings for our case of study. The operators contributing to this decay channel can be split into five classes. The first and most relevant class is given by the $D = 6$ contributions to anomalous HVV couplings

$$
\Delta\mathcal{L}_{HVV}^{D=6} = \frac{H}{v} \left[\delta c_Z M_Z^2 Z_\mu Z_\mu \right.
$$
$$
+ c_{\gamma\gamma} \frac{e^2}{4} A_{\mu\nu} A_{\mu\nu} + c_{Z\gamma} \frac{e\sqrt{g_1^2 + g_2^2}}{2} Z_{\mu\nu} A_{\mu\nu} + c_{ZZ} \frac{g_1^2 + g_2^2}{4} Z_{\mu\nu} Z_{\mu\nu} +
$$
$$
\left. + c_{z\square} g_2^2 Z_\mu \partial_\nu Z_{\mu\nu} + c_{\gamma\square} g_1 g_2 Z_\mu \partial_\nu A_{\mu\nu} \right],
$$
(6.3)

where we have adopted the convention to absorb the suppression factor $1/\Lambda$ in the effective coefficients. Of the six couplings in Eq. (6.3) only five are independent. We choose $c_{\gamma\square}$ as dependent coupling, which can be expressed as the following linear combination:

$$
c_{\gamma\square} = \frac{1}{g_2^2 - g_1^2} \left[2g_2^2 c_{Z\square} + (g_2^2 + g_1^2)c_{ZZ} - e^2 c_{\gamma\gamma} - (g_2^2 - g_1^2)c_{z\gamma} \right].
$$
(6.4)

The second class of operators is given by the anomalous contributions to $Z\ell\ell$ vertex

$$
\Delta\mathcal{L}_{Zff}^{D=6} = \sqrt{g_1^2 + g_2^2} Z_\mu \left[\sum_{\ell=e,\mu} \bar{\ell}_L \left(I_{W,\ell}^3 - s_W^2 Q_\ell + \gamma_\mu \delta g_L^{Z\ell} \right) \ell_L + \right.
$$
$$
\left. + \bar{\ell}_R \left(-s_W^2 Q_\ell + \gamma_\mu \delta g_R^{Z\ell} \right) \ell_R \right],
$$
(6.5)

while the third class gives rise to $HV\ell\ell$ contact interactions

$$
\Delta\mathcal{L}_{HV\ell\ell}^{D=6} = 2\frac{\sqrt{g_1^2 + g_2^2}}{v} \left[\sum_{\ell=e,\mu} \delta g_L^{HV\ell\ell} H Z_\mu \bar{\ell}_L \gamma_\mu \ell_L + \delta g_R^{HV\ell\ell} H Z_\mu \bar{\ell}_R \gamma_\mu \ell_R \right].
$$
(6.6)

In the Higgs basis the couplings of the contact terms are equal to the vertex corrections in Eq. (6.5)

$$\delta g_L^{Z\ell} = \delta g_L^{HV\ell\ell}, \qquad \delta g_R^{Z\ell} = \delta g_R^{HV\ell\ell}. \tag{6.7}$$

Given the constraints on the anomalous $Z\ell\ell$ couplings, the LHC Higgs studies cannot be sensitive to vertex corrections and contact interactions and therefore their effects are neglected in current analysis. The last two contributions involve the so-called dipole interactions. The first of these classes includes the dipole interactions between the Z boson and leptons

$$\Delta\mathcal{L}_{dZ\ell\ell}^{D=6} = -\frac{\sqrt{g_1^2 + g_2^2}}{4v} \sum_{\ell=e,\mu} \frac{\sqrt{m_i m_j}}{v} \bar{\ell}_{L,i}\sigma_{\mu\nu} \left[d_{Z\ell\ell}\right]_{ij} f_{R,j} Z_{\mu\nu} + \text{h.c.}, \tag{6.8}$$

while the second is related to the dipole-type contact interactions of the Higgs boson, parametrized by the following Lagrangian

$$\Delta\mathcal{L}_{dHZ\ell\ell}^{D=6} = -\frac{\sqrt{g_1^2 + g_2^2}}{4v^2} \sum_{\ell=e,\mu} \frac{\sqrt{m_i m_j}}{v} \bar{\ell}_{L,i}\sigma_{\mu\nu} \left[d_{ZH\ell\ell}\right]_{ij} f_{R,j} HZ_{\mu\nu} + \text{h.c.},. \tag{6.9}$$

As for the $HV\ell\ell$ contact interactions, the Higgs dipole couplings are equal to the $dV\ell\ell$ in Eq. (6.8). For Higgs decays into four light fermions, the dipole-like contributions do not interfere with the SM amplitudes due to the different helicity structure. Therefore, corrections to the decay width enter quadratically and should be then neglected. Moreover, as a consequence of the linearly realized electroweak symmetry in the $D = 6$ Lagrangian, the dipole parameters are proportional to the respective lepton dipole moments which are stringently constrained by experiment. For these two reasons, dipole interactions are always neglected in LHC analysis.

6.3   Calculation details

At this preliminary level we have considered the effective Lagrangian

$$\mathcal{L}^{D=6} = \mathcal{L}^{\text{SM}} + \mathcal{L}_{HVV}^{D=6}, \tag{6.10}$$

where $\mathcal{L}_{\text{SM}}$ is supplemented only by $D = 6$ contributions to HVV vertex described in Eq. (6.4). The master formula for the LO decay width, in presence of $D = 6$ operators reads

$$\Gamma_{\text{LO}}^{D=6}(H \to 2e2\mu) = \frac{1}{2M_H} \int \left\{ |\mathcal{M}_{\text{SM}}|^2 + 2\text{Re}\left(\mathcal{M}_{D=6}\mathcal{M}_{\text{SM}}^*\right) + |\mathcal{M}_{D=6}|^2 \right\} d\Phi_4, \tag{6.11}$$

An important remark is in order: the quadratic part $|\mathcal{M}_{D=6}|^2$ is suppressed by a factor $1/\Lambda^4$ in the scale of new physics. Then, from the point of view of the EFT expansion, it contributes at the same level of $D = 8$ operators. For this reason the quadratic part is usually neglected in the analysis. Nevertheless, we have included the quadratic contributions in our calculation, with the possibility to turn them off in the code. The reason is that for large values of the $D = 6$ coefficients which are allowed by present constraints, the leading anomalous contributions could be captured by the quadratic terms, indicating that the low-energy description of new physics restricted to $D = 6$ operators may not be sufficient. In addition to an anomalous part in the HZZ coupling, the presence of $D = 6$ operators gives rise to tree-level $H\gamma\gamma$ and $HZ\gamma$ vertexes which are not present in the SM Lagrangian. The Feynman rules for for the HVV vertexes couplings have been derived by implementing the effective Lagrangian of Eq. (6.10) in `FeynRules 2.0` [216], obtaining the following expressions:

$$V_{H\gamma\gamma}^{\mu_1\mu_2}(p_1, p_2) = \frac{ie^2 c_{\gamma\gamma}}{v} \left\{ p_1^{\mu_2} p_2^{\mu_1} - (p_1 \cdot p_2) \, g^{\mu_1\mu_2} \right\}, \tag{6.12}$$

$$V_{HZ\gamma}^{\mu_1\mu_2}(p_1, p_2) = \frac{ie^2}{c_W s_W v} \left\{ c_{z\gamma} \left[p_1^{\mu_2} p_2^{\mu_1} - (p_1 \cdot p_2) \, g^{\mu_1\mu_2} \right] + c_{\gamma\Box} \left[-p_1^{\mu_2} p_2^{\mu_1} + (p_1 \cdot p_2) \, g^{\mu_1\mu_2} \right] \right\}, \tag{6.13}$$

$$V_{HZZ}^{\mu_1\mu_2}(p_1, p_2) = \frac{2iM_Z^2 \delta c_Z}{v} g^{\mu_1\mu_2} + \frac{ie^2}{c_W^2 s_W^2 v} \left\{ c_{ZZ} \left[p_1^{\mu_2} p_2^{\mu_1} - (p_1 \cdot p_2) \, g^{\mu_1\mu_2} \right] + c_{Z\Box} \left[-p_1^{\mu_2} p_2^{\mu_1} + (p_1 \cdot p_2) \, g^{\mu_1\mu_2} \right] \right\}, \tag{6.14}$$

where p_1 and p_2 are the incoming momenta of the gauge bosons. Then, the new matrix elements have been carried out by means of the symbolic manipulation program `FORM` [183], and they have been included in a new version of `Hto4l` which will be publicly available soon. In order to make the code more flexible we have implemented a mapping from the SILH basis to the Higgs one. The relations between the two basis are reported in Appendix B. As a consistency check we have compared the value of the matrix elements implemented in `Hto4l` with the one generated with `MadGraph5` [217] for several phase-space points, finding an excellent agreement.

6.4 Numerical results

In this section we show the results obtained for the $H \to 2e2\mu$ decay channel in presence of $D = 6$ operators. As a benchmark for the values of the Higgs coefficients we use the constraints given in Ref. [218]:

$$\begin{pmatrix} \delta c_Z \\ c_{ZZ} \\ c_{Z\square} \\ c_{\gamma\gamma} \\ c_{Z\gamma} \end{pmatrix} = \begin{pmatrix} -0.12 \pm 0.20 \\ 0.5 \pm 1.8 \\ -0.21 \pm 0.82 \\ 0.014 \pm 0.029 \\ 0.01 \pm 0.10 \end{pmatrix} . \tag{6.15}$$

Higgs coefficient		$\Gamma_{h \to 2e2\mu} \times 10^{-4}$ [MeV]	$\Gamma_{\rm BSM}/\Gamma_{\rm SM}$
δc_Z	$+0.2$	3.33	1.39
	-0.2	1.43	0.61
c_{ZZ}	1.0	1.87	0.76
	-1.0	2.88	1.21
$c_{Z\square}$	$+0.5$	2.73	1.14
	-0.5	2.02	0.84
$c_{\gamma\gamma}$	$+0.015$	2.38	-
	-0.015	2.38	-
$c_{Z\gamma}$	$+0.05$	2.40	1.008
	-0.05	2.36	0.983

Table 6.1: Higgs decay width in the $2e2\mu$ channel in presence of $D = 6$ operators. The values are within the constraints of ref. [218].

In Table 6.1 we report the LO results for the decay width $\Gamma_{h \to 2e2\mu}$, obtained by switching one coefficient at a time and for a choice of coefficients allowed by the constraints reported in (6.15). The results have been obtained by neglecting the quadratic contributions in Eq. (6.11) As it can be seen, δc_Z, c_{ZZ}, $c_{Z\square}$ are very weakly constrained by present data and large deviation from the SM are allowed.

As already mentioned, in a linear EFT some of the parameters enetering to Higgs observables also contribute to EW observables and thus get constrained by the LEP data. As a benchmark for the values of the Higgs coefficients we use the constraints given in Ref. [218]. The analyses carried out in this Ref. provides constraints on the five CP-even paramaters except on the paramaters of the contact interaction. The parameters δc_Z and $c_{\gamma\gamma}$ are severaly constrained by the LHC data. δc_Z multiplies a SM-like effective operator and it does not change the shape of the distributions. On the other hand, for numerical values within the present constraints, the effect of $c_{\gamma\gamma}$

on the $H \to 4\ell$ channel is negligible and it has been omitted in the analysis. The constraint on $c_{Z\gamma}$, on the other hand, has large uncertainty. Therefore, at the differential level we restrict our analysis to $c_{Z\gamma}, c_{ZZ}$ and $c_{Z\Box}$, where sizeable effects are expected.

As it can be seen from Eq. (6.13) c_{ZZ}, $c_{Z\Box}$ enter the anomalous vertex $V_{HZ\gamma}$ (we remind that $c_{\gamma\Box}$ is a dependent coupling, see Eq. (6.4)). Therefore, the kinematic configurations with one of the invariant lepton pairs mass close to zero could lead to an important contribution to the $H \to 2e2\mu$ partial width. Therefore, in order to get rid of these large contributions which would be rejected in the event selection, we have implemented a lower cut of 15 GeV on the invariant mass of electrons and muons pairs.

In Figs. 6.1-6.6 we show the effects of $c_{Z\gamma}$, c_{ZZ} and $c_{Z\Box}$ by switching one coefficient at a time for benchmark values of $c_{Z\gamma} = \pm 0.05$, $c_{ZZ} = \pm 1.0$ and $c_{Z\Box} = \pm 0.5$. We consider the following observables:

- the leading (M_{lead}) and the subleading (M_{sub}) lepton pair invariant mass, with M_{lead} defined as the same-flavor opposite-sign (SFOS) lepton pair invariant mass closest to the Z boson mass;

- ϕ is the angle between two intermediate gauge-bosons decay plane;

- $\Delta\theta_{e^-\mu^-}$ is the relative angle between the electron and the muon.

Since the constraints quoted in [218] have been derived in the linear approximation, the results in Figs. 6.1-6.6 have been obtained by switching off the $1/\Lambda^4$ contributions. In these figures we show the effect of the $D = 6$ operators on the distributions of the kinematic observables described above (upper panels).

It appears that although the global effects are comparable or even larger than the higher-order EW corrections, the angular observables are the most sensitive to BSM kinematic effects, while for invariant mass and lepton transverse momenta distributions the largest modifications on the shape occur in the tails, where the local significance is rather small. However, looking at the M_{sub} distributions in Figs. 6.3 and 6.5 we can see that for the adopted values of c_{ZZ} and $c_{Z\Box}$ the effect on the shape is of the same order of the higher-order SM contributions.
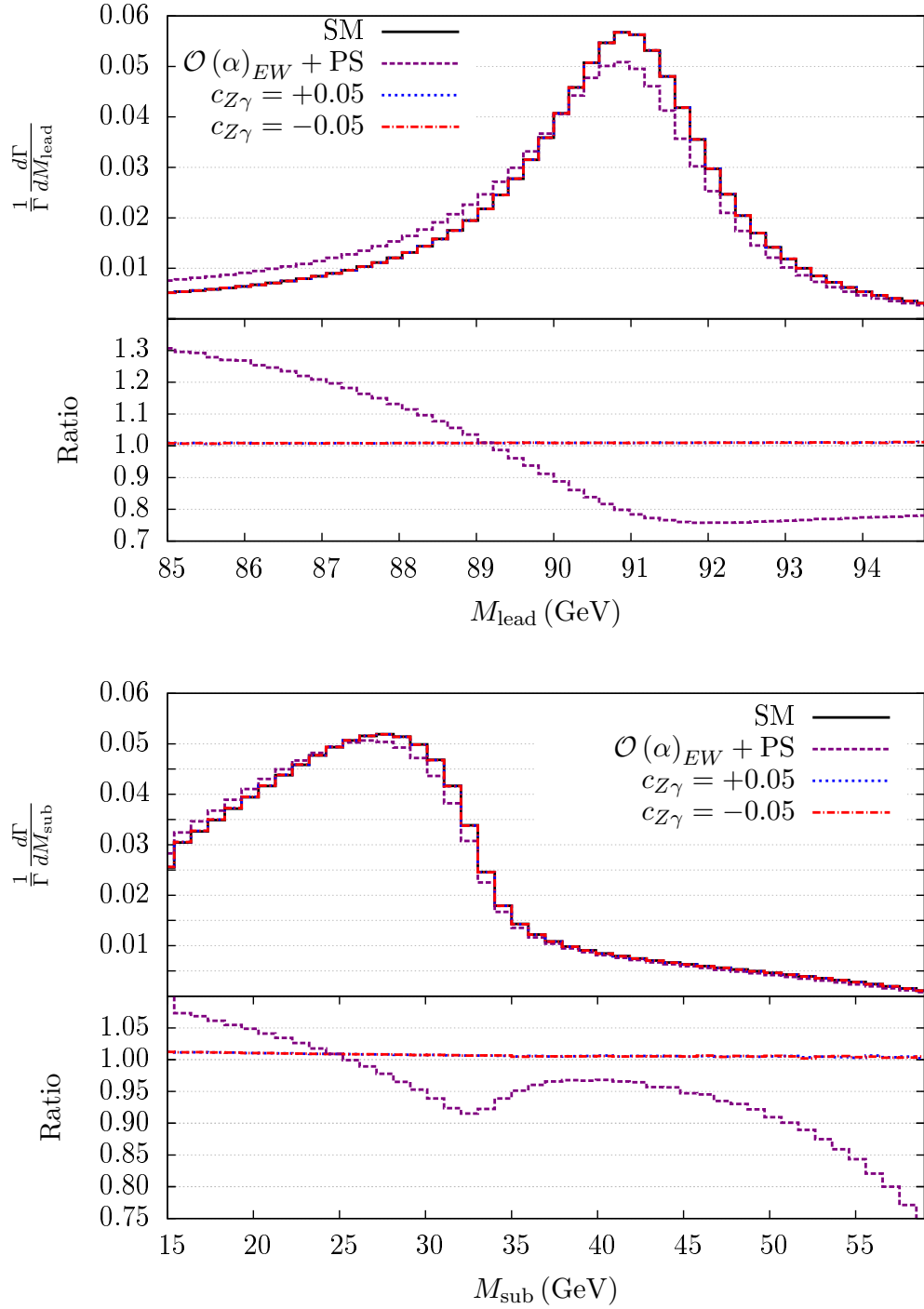
Figure 6.1: upper panels: differential distributions of the leading (M_{lead}) and the sub-leading (M_{sub}) SFOS invariant mass for the SM case at LO (black line), at NLOPS EW accuracy (violet line), and for $c_{Z\gamma} = \pm 0.05$ (blue and red lines). Lower panels: ratio between the normalized BSM and SM distributions and the SM one. (blue and red lines); ratio between the normalized SM distribution at NLOPS accuracy and the LO one (violet line).
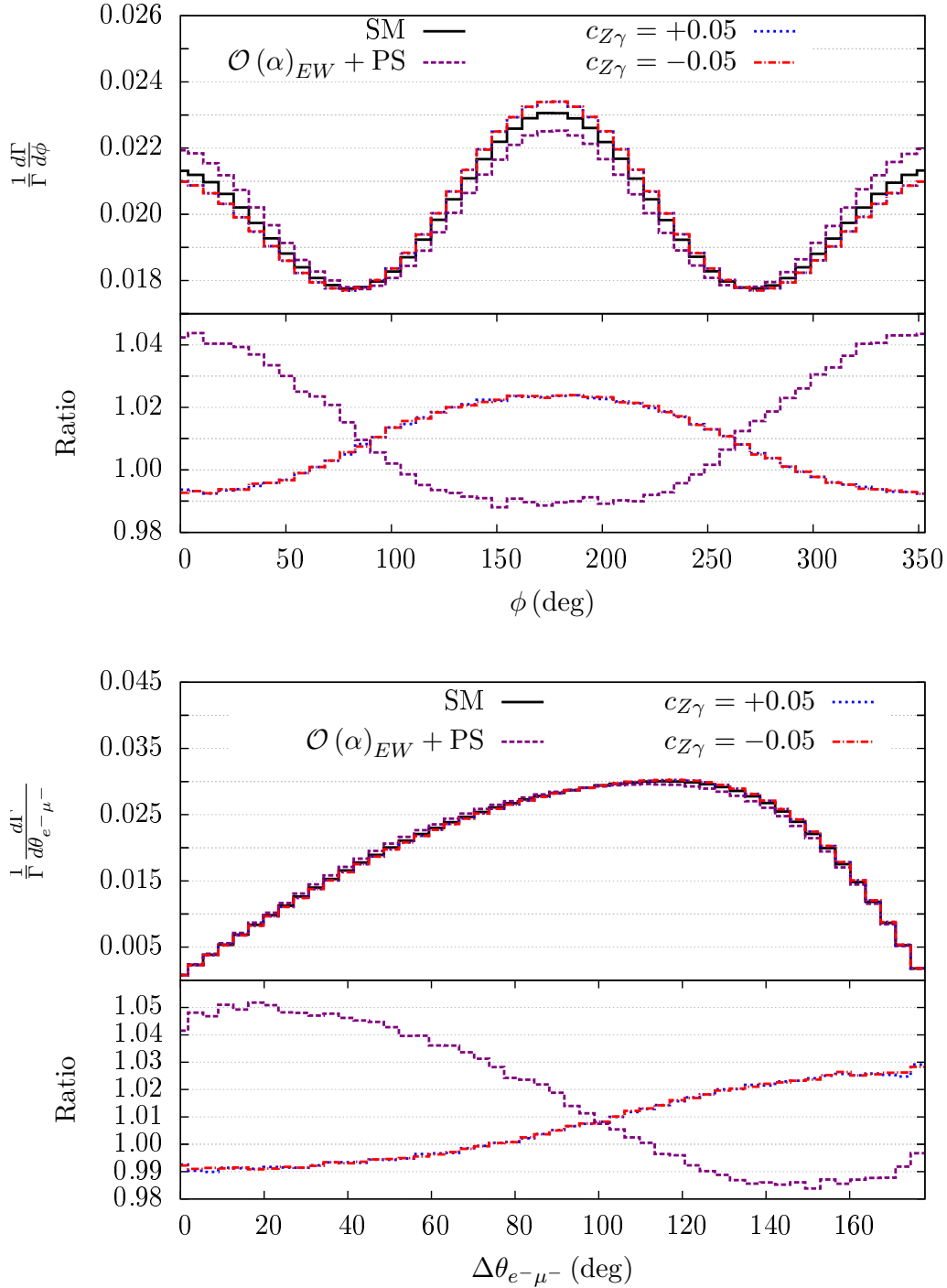
Figure 6.2: left panel: differential distributions of the angle between two intermediate gauge-bosons decay plane and of the relative angle between the electron and the muon for the SM case at LO (black line), at NLOPS EW accuracy (violet line), and for $c_{ZZ} = \pm 1$ (blue and red lines). Lower panels: ratio between the normalized BSM and SM distributions and the SM one. (blue and red lines); ratio between the normalized SM distribution at NLOPS accuracy and the LO one (violet line).
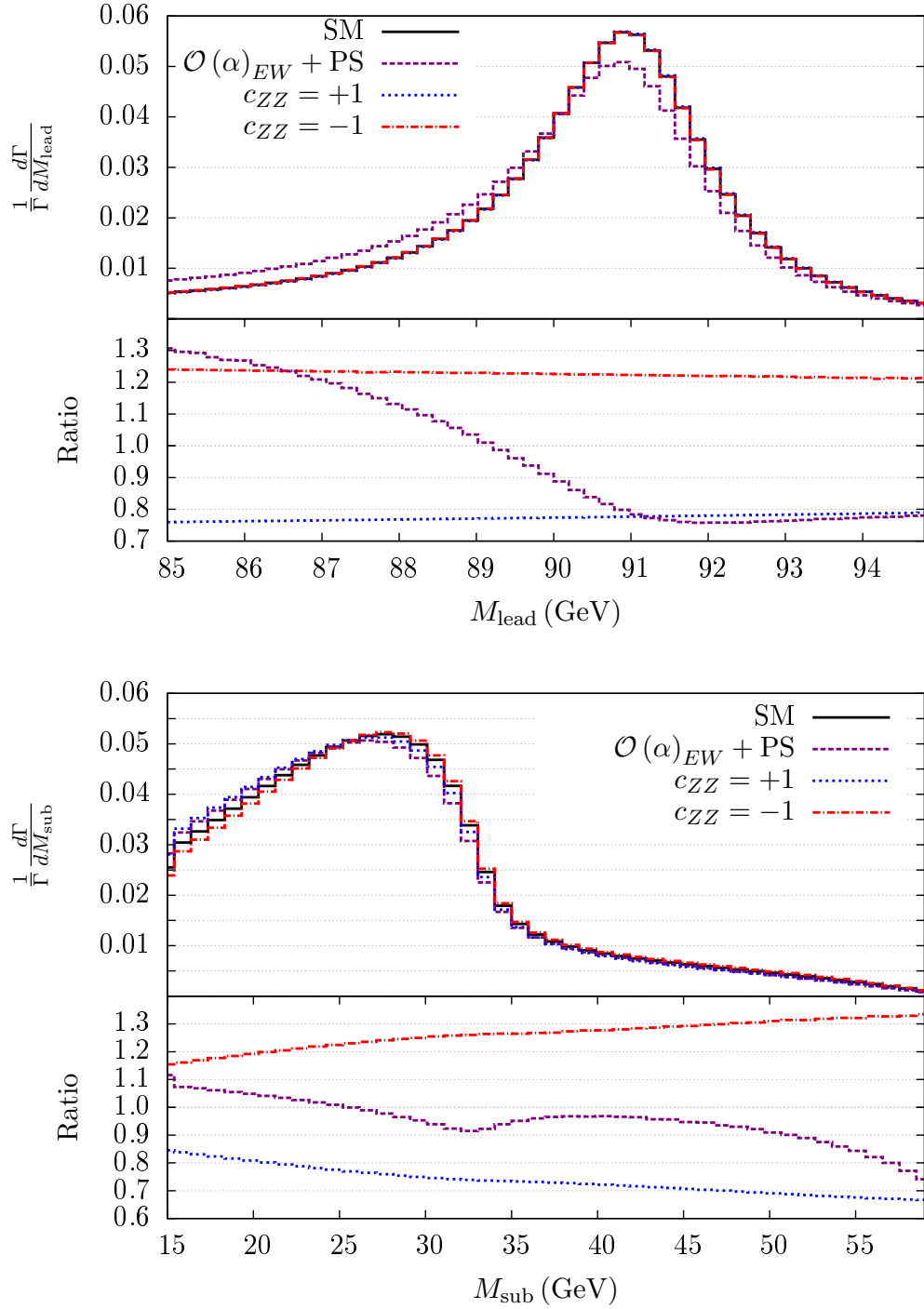
Figure 6.3: upper panels: differential distributions of the leading (M_{lead}) and the sub-leading (M_{sub}) SFOS invariant mass for the SM case at LO (black line), at NLOPS EW accuracy (violet line), and for $c_{ZZ} = \pm 1$ (blue and red lines). Lower panels: ratio between the normalized BSM and SM distributions and the SM one. (blue and red lines); ratio between the normalized SM distribution at NLOPS accuracy and the LO one (violet line).
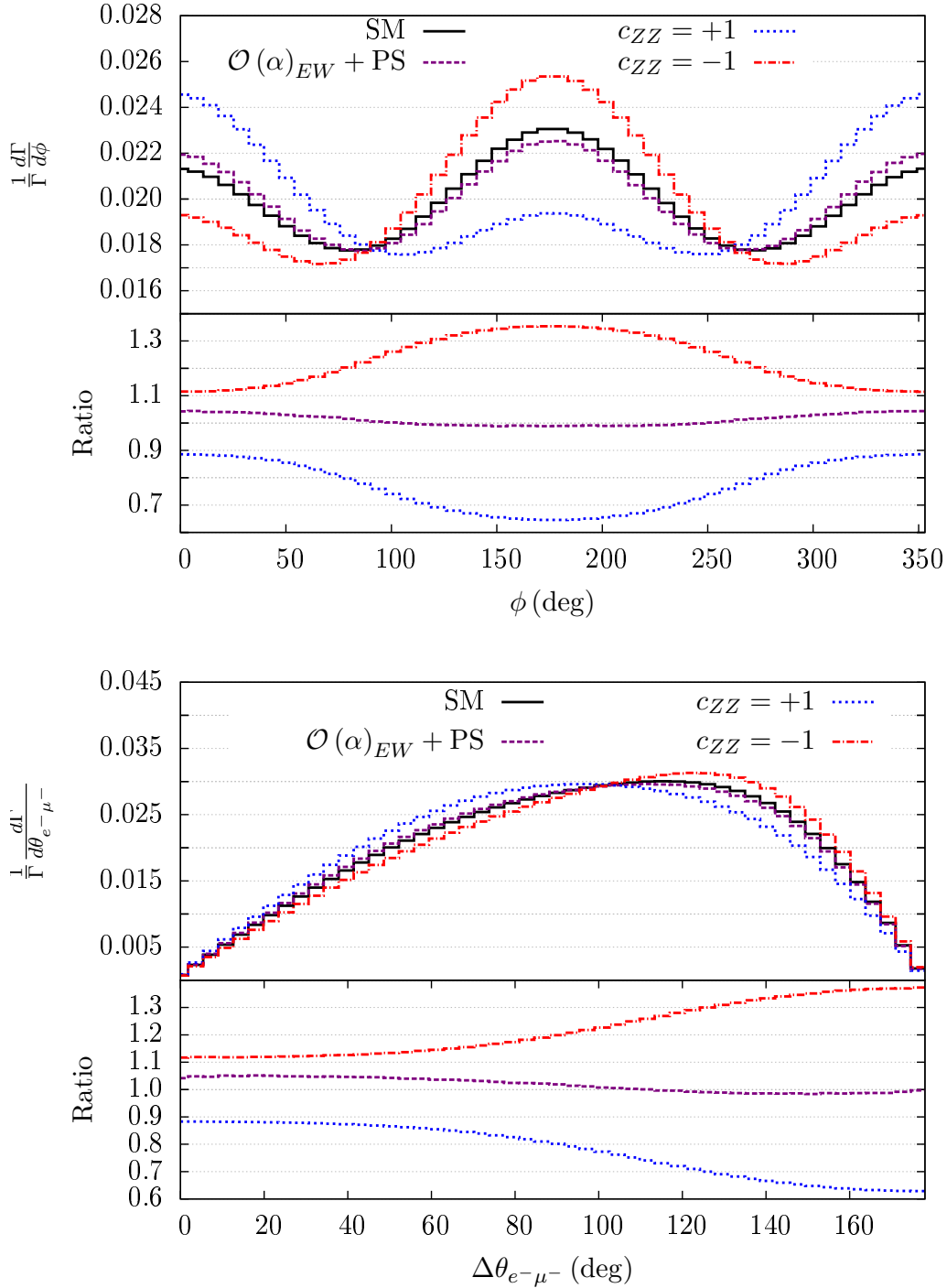
Figure 6.4: upper panels: differential distributions of the angle between two intermediate gauge-bosons decay plane and of the relative angle between the electron and the muon for the SM case at LO (black line), at NLOPS EW accuracy (violet line), and for $c_{ZZ} = \pm 1$ (blue and red lines). Lower panels: ratio between the normalized BSM and SM distributions and the SM one. (blue and red lines); ratio between the normalized SM distribution at NLOPS accuracy and the LO one (violet line).
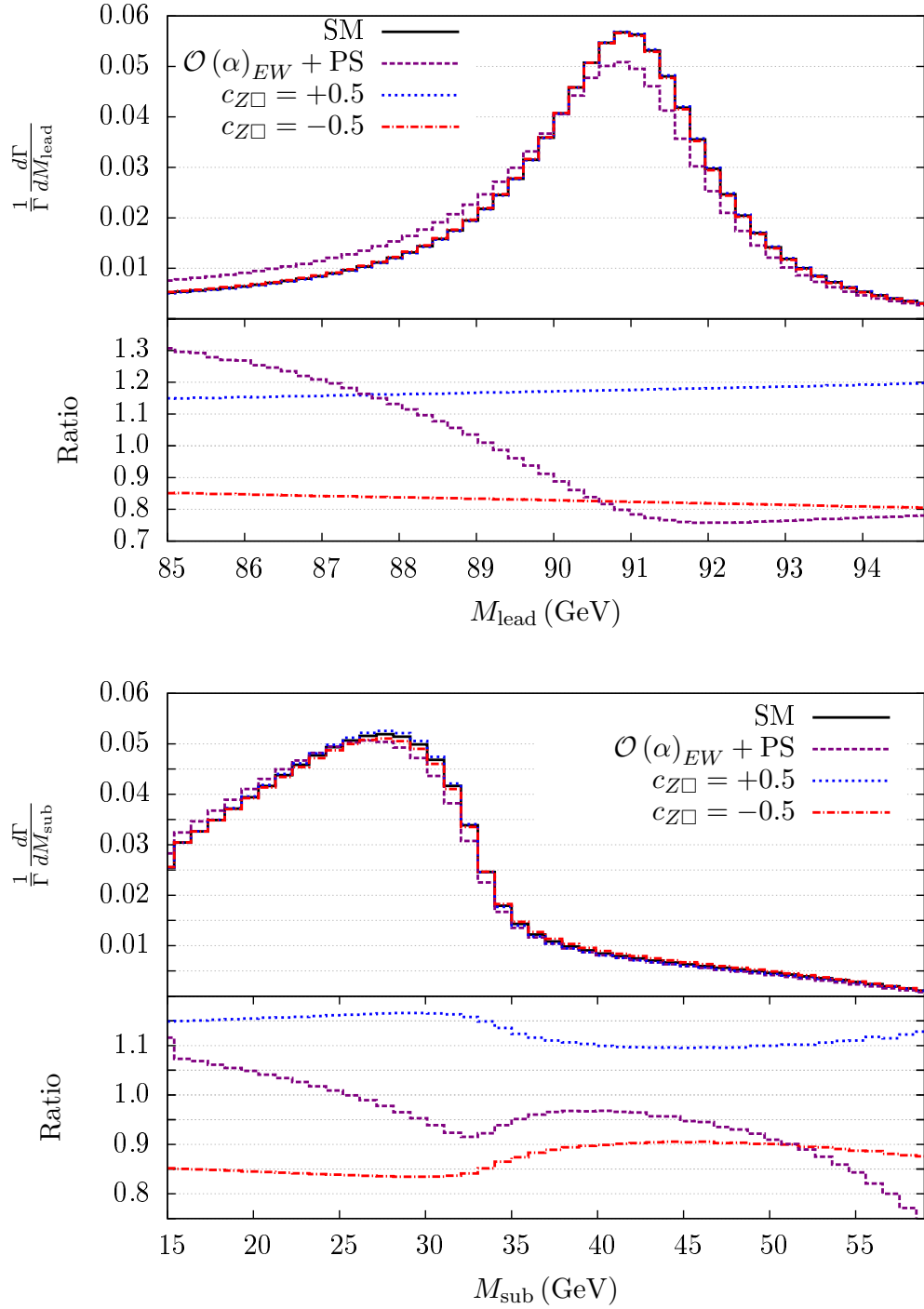
Figure 6.5: upper panels: differential distributions of the leading (M_{lead}) and the sub-leading (M_{sub}) SFOS invariant mass for the SM case at LO (black line), at NLOPS EW accuracy (violet line), and for $c_{Z\square} = \pm 0.5$ (blue and red lines). Lower panels: ratio between the normalized BSM and SM distributions and the SM one. (blue and red lines); ratio between the normalized SM distribution at NLOPS accuracy and the LO one (violet line).
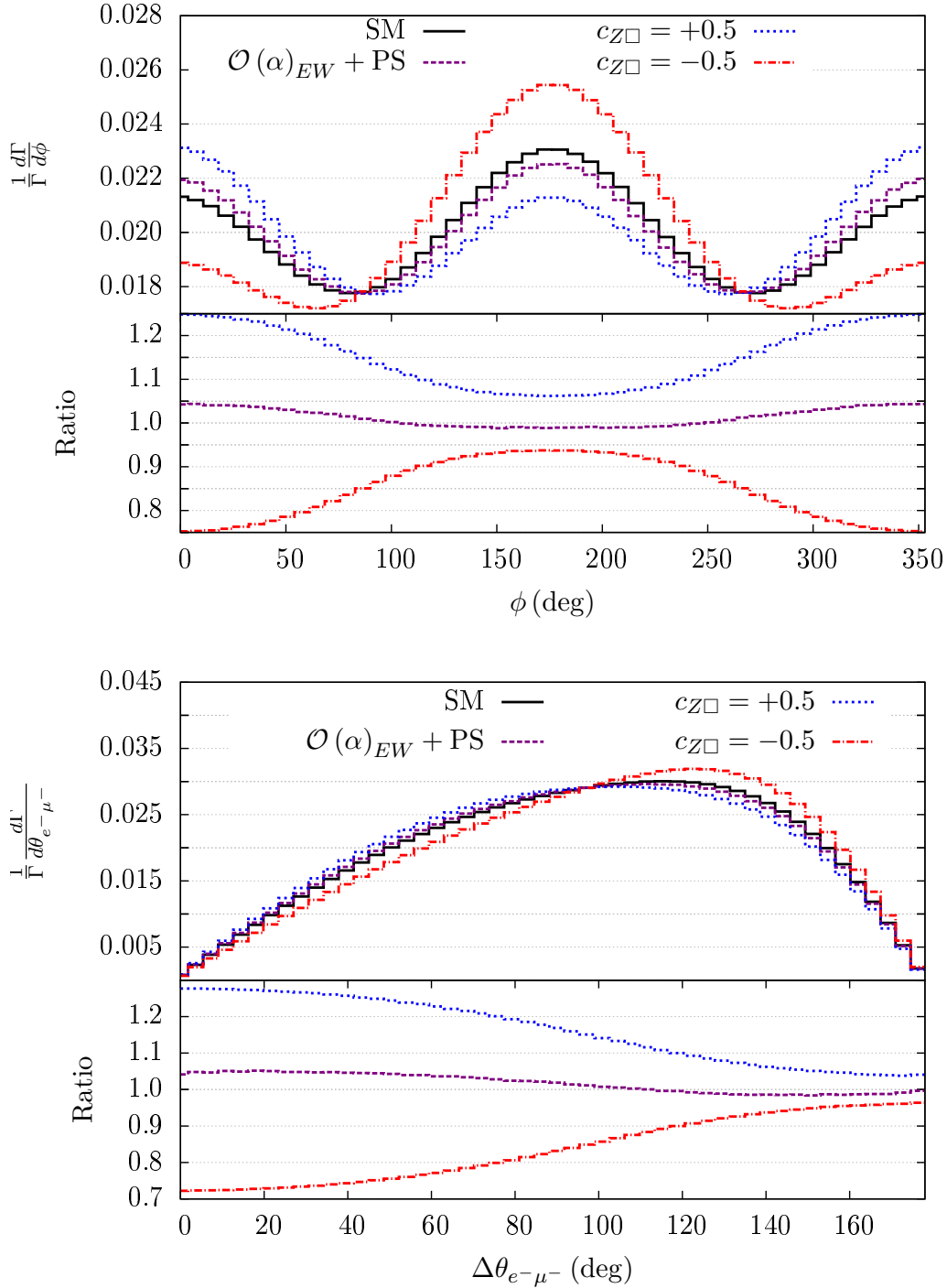
Figure 6.6: upper panels: differential distributions of the angle between two intermediate gauge-bosons decay plane and of the relative angle between the electron and the muon for the SM case at LO (black line), at NLOPS EW accuracy (violet line), and for $c_{Z\square} = \pm 0.5$ (blue and red lines). Lower panels: ratio between the normalized BSM and SM distributions and the SM one. (blue and red lines); ratio between the normalized SM distribution at NLOPS accuracy and the LO one (violet line).

Conclusions

In this thesis we have presented novel results on the Higgs decay into four charged leptons ($H \to 4e, 4\mu, 2e2\mu$), including complete NLO EW corrections matched with a QED PS algorithm for the exclusive description of multiple photon effects. For inclusive partial widths at NLO EW accuracy without multiple photon emission, `Hto4l` and `Prophecy4f` [41, 42] must agree for the leptonic final states included in `Hto4l`. In order to emphasize the reliability of our calculation, a comparison of the two codes has been carried out at differential and integrated level, finding, in both cases, perfect agreement. Going beyond the NLO EW accuracy, `Hto4l` includes also the possibility to simulate multiphoton emissions in a QED PS approach, consistently matched to the NLO calculation. In order to asses the effects of different sources of higher-order corrections we have compared NLOPS distributions with the ones obtained by considering only fixed-order corrections and in the pure PS approximation. In this way we have shown that the relative impact of different sources of corrections at the level of differential distributions strongly depends on the kinematic observable considered in the analysis. For instance, the NLO corrections on the invariant masses of leptons pairs are dominated by the leading logarithmic contributions of QED nature, which then translate in relevant contributions of higher-order QED corrections. On the other hand, angular variables, such as the relative angle between the two intermediate Z bosons decay planes, are particularly sensitive to pure weak corrections, while the pure PS approximation gives an inaccurate description of this distributions. In conclusion, our code combines, for $H \to 4\ell$ channels, the virtues of NLO corrections implemented in `Prophecy4f` with the ones of a QED PS algorithm. `Hto4l` can be used in combination of any event generator for Higgs production, and it will be useful for present and future phenomenological studies.

Given the importance of the $H \to 4\ell$ channel in the searches of indirect

evidence of new physics, we are now studying the possible BSM effects with a new version of `Hto4l` which will be publicly available soon. In particular, we have derived the anomalous couplings which could affect the $H \to 2e2\mu$ channel in an EFT framework, adopting the Higgs basis of $D = 6$ operators, whose coefficients can be easily related to observable quantities. To make the code more flexible we have also implemented a mapping from the SILH basis to the Higgs one. In this work we presented some preliminary results, showing the effects of $D = 6$ operators for values of the coefficients allowed by present constraints. We have considered the effects both at the integrated and differential level, considering a certain number of kinematic observables. To highlight the effects on the shape we have considered the ratio between the BSM normalized distributions with respect to the SM ones. Given the weak constraints on some of the coefficients, large deviations from the SM predictions are allowed at the integrated level. Moreover, it appears that the angular variables are the most sensitive to BSM kinematic effects. In the next future we expect to include the anomalous couplings also in the $H \to 4e, 4\mu$ channels and to provide the possibility to include the anomalous contributions as a part of a calculation which includes both LO BSM effects and NLOPS SM corrections.

Appendix A

Phase-space parameterisation and integration

The $4 + n$ bodies phase space as in Eq. (4.58) is integrated according to standard multi-channel MC techniques, combined with importance sampling to reduce the variance of the integral and help event generation[1]. The first step is to generate a photon multiplicity n and associate n_1 (n_2) photons to the electron (muon) current $(n_1 + n_2 = n)$, defining the channel of the multi-channel integration. The phase space is then conveniently split into two decaying objects to follow the Z propagators, namely

$$\mathrm{d}\Phi(P_H; p_1, \cdots, p_4, k_1, \cdots, k_n) = (2\pi)^6 \mathrm{d}Q_{Z_1}^2 \mathrm{d}Q_{Z_2}^2 \mathrm{d}\Phi(P_H; P_{Z_1}, P_{Z_2}) \times$$
$$\mathrm{d}\Phi(P_{Z_1}; p_1, p_2, k_1, \cdots, k_{n_1}) \, \mathrm{d}\Phi(P_{Z_2}; p_3, p_4, k_{n_1+1}, \cdots, k_{n_1+n_2}) \quad \text{(A.1)}$$

where P_{Z_i} $(P_{Z_i}^2 = Q_{Z_i}^2)$ are the momenta of the virtual Z bosons.

We refrain from writing explicitly the simple $1 \to 2$ decay phase spaces of Eq. (A.1) and we focus instead on the case where at least one photon is present. The efficient sampling of photons collinear to final state leptons is a non trivial task, because the directions of the leptons are known only after all the momenta are generated. Instead of adopting a solution based on a properly chosen multi-channel strategy (see for instance Ref. [190]), we adopt a different and elegant solution, which consists in writing the phase space in the frame where the leptons are back-to-back, $i.e.$ $\vec{p_a} = -\vec{p_b}$ (see for example [219, 220, 221]).

Omitting overall numerical factors for brevity, the building block we are

---

[1]Here we consider only the decay $H \to 2e2\mu$, the generalization to 4 identical leptons being straightforward.

interested in is

$$
\begin{aligned}
\mathrm{d}\Phi(P; p_a, p_b, k_1, \cdots, k_r) &= \delta^{(4)}\left(P - p_a - p_b - \sum_{i=1}^{r} k_i\right) \frac{\mathrm{d}^3\vec{p}_a}{p_a^0} \frac{\mathrm{d}^3\vec{p}_b}{p_b^0} \prod_{i=1}^{r} \frac{\mathrm{d}^3\vec{k}_i}{k_i^0} \\
&\equiv \delta^{(4)}(P - Q - K)\, \delta\Phi
\end{aligned}
$$

where we defined $Q = p_a + p_b$, $K = \sum_{i=1}^{r} k_i$ and $\delta\Phi$ contains the infinitesimal phase space element divided by the final state particle energies. It is usually understood that all the variables are expressed in the frame where P is at rest, but we want to express them where Q is at rest. In order to do that, the previous equation can be further manipulated by inserting the following identities

$$
\begin{aligned}
&\mathrm{d}^4 Q\, \delta^{(4)}(Q - p_a - p_b) = 1 \\
&\mathrm{d}s'\, \delta(Q^2 - s') = 1 \\
&\mathrm{d}^4 P\, \delta^{(3)}(\vec{P})\, \delta(P^0 - \sqrt{s}) = 2\sqrt{s}\, \mathrm{d}^4 P\, \delta^{(3)}(\vec{P})\, \delta(P^2 - s) = 1 \quad \text{(A.2)}
\end{aligned}
$$

which help to make explicit the Lorentz invariance of the phase space element.

With the help of Eq. (A.2) and appropriately rearranging the terms, we can write

$$
\begin{aligned}
\mathrm{d}\Phi(P; p_a, p_b, k_1, \cdots, k_r) &= \delta\Phi\, \mathrm{d}^3\vec{Q}\delta^{(4)}(Q - p_a - p_b)\delta^{(3)}(\vec{P}) \\
2\sqrt{s}\, \mathrm{d}^4 P\delta^{(4)}(P - Q - K)\delta(P^2 - s)\mathrm{d}s'\mathrm{d}Q^0\delta(Q^2 - s') &= \\
&= \delta\Phi\sqrt{\frac{s}{s'}}\, \delta^{(3)}(\vec{P})\delta^{(4)}(Q - p_a - p_b)\delta((Q + K)^2 - s)\mathrm{d}^3\vec{Q}\mathrm{d}s' = \\
&= \mathrm{d}s'\frac{s}{s'}\delta^{(4)}(Q - p_a - p_b)\delta((Q + K)^2 - s)\frac{\mathrm{d}^3\vec{p}_a}{p_a^0}\frac{\mathrm{d}^3\vec{p}_b}{p_b^0}\prod_{i=1}^{r}\frac{\mathrm{d}^3\vec{k}_i}{k_i^0} = \\
&= \frac{s'}{2s}\beta_a\mathrm{d}\Omega_a\frac{1}{1 + \frac{\sum_{i=1}^{r} k_i^0}{\sqrt{s'}}}\prod_{i=1}^{r}\frac{\mathrm{d}^3\vec{k}_i}{k_i^0} \quad \text{(A.3)}
\end{aligned}
$$

In the cascade of identities (A.3) we used the result $\mathrm{d}^3\vec{Q}\, \delta^{(3)}(\vec{P}) = (s'/s)^{\frac{3}{2}}$ (see [220]) and we made use of Lorentz invariance. In the last identity it is understood that all the variables are expressed in the frame where $Q = p_a + p_b$ is at rest and $s' = Q^2$, $s = P^2$, β_a is the speed of particle a and $\mathrm{d}\Omega_a = \mathrm{d}\cos\theta_a \mathrm{d}\phi_a$. The big advantage of the last equation is that the lepton momenta p_a and p_b lie on the same direction defined by $\cos\theta_a$ and ϕ_a, hence all photons can be generated along this direction to sample the collinear singularities. Once all particle momenta are generated, they can be boosted back to the rest frame of the decaying Higgs boson.

One last remark concerns the integration limits of the phase space. As mentioned in Sec. 4.4.2, photon energies should be generated larger than the infrared cut-off ϵ in the Higgs frame, which is a non Lorentz invariant cut. Since the minimum photon energy can not be determined *a priori* in the frame where Q is at rest (because Q itself depends on the photons momenta), we decide to generate photon energies starting from 0 to cover the whole phase space and then, once boosted back, cut the event if a photon enegy falls below ϵ. Finally, in order to flatten the infrared divergence, we choose to sample the photon energies according to the function

$$f(\omega) \propto \begin{cases} \frac{1}{\omega} & \omega \geq \epsilon' \\ \frac{1}{\epsilon'} & \omega < \epsilon' \end{cases}$$

where ϵ' is a guessed (and tuned for efficiency) minimum energy.

The Higgs basis

In Chapter 6 we have introduced the Higgs basis as a new choice for the parametrization of the space of dimension-six operators. In this basis the dimension-six operators affecting the Higgs sector of the SM are explicitly separated by the ones constrained by other experiments. For this reason, the Higgs basis turns out to be particularly convenient for the analysis of LHC Higgs data. In this Appendix, we limit ourselves to report the expressions for the effective coefficients taken into account in Sec. 6.2, written in terms of the SILH Wilson coefficients. The reader can refer to [215] for the derivation of the remaining relations for the mapping between the two basis. The list of bosonic dimension-six operators of the SILH basis is given in Table B.1, while the list of two-fermion dimension-six operators is given in Tables B.2 and B.3. We omit to list the four-fermion operators because they do not play any role in the Higgs decay into four fermions. The symbol $\overleftrightarrow{D}_\mu$ states for the so-called Hermitian derivative defined as

$$\varphi^\dagger i \overleftrightarrow{D}_\mu \varphi = i\varphi^\dagger \left(D_\mu - \overleftarrow{D}_\mu \right) \varphi,$$

where $\varphi^\dagger \overleftarrow{D}_\mu \varphi = (D_\mu \varphi)^\dagger \phi$. Let us start by considering the operators giving rise to anomalous contributions to the HVV vertex. The relations among the effective coefficients of Eq. 6.3 and the Wilson coefficients of the SILH basis are

$$\delta c_Z = -\frac{1}{2}\bar{c}_H - \frac{3}{2}\left[\bar{c}'_{H\ell}\right]_{22}, \tag{B.1}$$

$$c_{\gamma\gamma} = \frac{16}{g_2^2}\bar{c}_\gamma \tag{B.2}$$

$$c_{ZZ} = -\frac{4}{g_1^2 + g_2^2}\left[\bar{c}_{HW} + \frac{g_1^2}{g_2^2}\bar{c}_{HB} - 4\frac{g_1^2}{g_2^2}s_W^2\bar{c}_\gamma\right], \tag{B.3}$$

$$c_{z\gamma} = \frac{2}{g_2^2} \left[\bar{c}_{HB} - \bar{c}_{HW} - 8s_W^2 \bar{c}_\gamma \right], \tag{B.4}$$

$$c_{z\square} = \frac{2}{g_2^2} \left[\bar{c}_W + \bar{c}_{HW} + \bar{c}_{2W} + \frac{g_1^2}{g_2^2} \left(\bar{c}_B + \bar{c}_{HB} + \bar{c}_{2B} \right) - \frac{1}{2} \bar{c}_T + \frac{1}{2} [\bar{c}'_{H\ell}]_{22} \right], \tag{B.5}$$

$$c_{\gamma\square} = \frac{2}{g_2^2} \left(\bar{c}_{HW} - \bar{c}_{HB} \right) + \frac{4}{g_2^2 - g_1^2} \left[\bar{c}_W + \bar{c}_{2W} \frac{g_1^2}{g_2^2} \left(\bar{c}_B + \bar{c}_{2B} \right) - \frac{1}{2} \bar{c}_T + \frac{1}{2} [\bar{c}'_{H\ell}]_{22} \right], \tag{B.6}$$

Regarding the anomalous interactions of the Z boson with leptons, the relations among the coefficients of the Higgs basis and SILH ones are given by the following relations:

$$\delta g_L^{Z\ell} = -\frac{1}{2} \bar{c}'_{H\ell} - \frac{1}{2} \bar{c}_{H\ell} + \hat{f} \left(-\frac{1}{2}, -1 \right), \tag{B.7}$$

$$\delta g_R^{Z\ell} = -\frac{1}{2} \bar{c}'_{He} + \hat{f} \left(0, -1 \right), \tag{B.8}$$

where

$$\hat{f} \left(T_f^3, Q_f \right) = \left[\bar{c}_{2W} + \frac{g_1^2}{g_2^2} \bar{c}_{2B} + \frac{1}{2} \bar{c}_T - [\bar{c}'_{H\ell}]_{22} \right] T_f^3$$
$$- \frac{g_1^2}{g_2^2 - g_1^2} \left[\frac{(2g_2^2 - g_1^2)}{g_2^2} \bar{c}_{2B} + \bar{c}_{2W} + \bar{c}_W + \bar{c}_B - \frac{1}{2} \bar{c}_T + \frac{1}{2} [\bar{c}'_{H\ell}]_{22} \right] Q_f \tag{B.9}$$

The same relations hold for the contact terms of Eq. (6.6). Finally, we have to consider the dipole interactions, which do not occur in the SM but may appear in the EFT with $D = 6$ operators. For the dipole interaction of the Z boson with leptons we get

$$[d_{Z\ell\ell}]_{ij} = \frac{16}{g_2^2} (c_W^2 \bar{c}_{eW} + s_W^2 \bar{c}_{eB}). \tag{B.10}$$

As in the previous case, the same combinations give also rise to contact interactions in the among the Higgs, weak bosons and fermions.

Bosonic CP-even

$\mathcal{O}_H$	$\frac{1}{2v^2}\left[\partial_\mu\left(H^\dagger H\right)\right]^2$
$\mathcal{O}_T$	$\frac{1}{2v^2}\left(H^\dagger\overleftrightarrow{D}_\mu H\right)^2$
$\mathcal{O}_6$	$-\frac{\lambda}{v^2}\left(H^\dagger H\right)^3$
$\mathcal{O}_\gamma$	$\frac{g_1^2}{M_W^2}H^\dagger H B_{\mu\nu}B_{\mu\nu}$
$\mathcal{O}_W$	$\frac{ig_2^2}{2M_W^2}\left(H^\dagger\sigma^i\overleftrightarrow{D}_\mu H\right)D_\nu W_{\mu\nu}^i$
$\mathcal{O}_B$	$\frac{ig_1^2}{2M_W^2}\left(H^\dagger\overleftrightarrow{D}_\mu H\right)\partial_\nu B_{\mu\nu}$
$\mathcal{O}_{HW}$	$\frac{ig_2}{M_W}\left(D_\mu H^\dagger\sigma^i D_\nu H\right)W_{\mu\nu}^i$
$\mathcal{O}_{HB}$	$\frac{ig_1}{M_W}\left(D_\mu H^\dagger D_\nu H\right)B_{\mu\nu}$
$\mathcal{O}_{2W}$	$\frac{1}{M_W^2}D_\mu W_{\mu\nu}^i D_\rho W_{\rho\nu}^i$
$\mathcal{O}_{2B}$	$\frac{1}{M_W^2}\partial_\mu W_{\mu\nu}\partial_\rho B_{\rho\nu}$
$\mathcal{O}_{3W}$	$\frac{g_2^3}{M_W^2}\epsilon^{ijk}W_{\mu\nu}^i W_{\nu\rho}^j W_{\rho\mu}^k$

Table B.1: bosonic CP-even operators of the SILH basis

Vertex and contact operators

$[\mathcal{O}_{H\ell}]_{ij}$	$\frac{i}{v^2}\bar{\ell}_i\gamma_\mu\ell_j H^\dagger\overleftrightarrow{D}_\mu H$
$[\mathcal{O}'_{H\ell}]_{ij}$	$\frac{i}{v^2}\bar{\ell}_i\sigma^k\gamma_\mu\ell_j H^\dagger\sigma^k\overleftrightarrow{D}_\mu H$
$[\mathcal{O}_{He}]_{ij}$	$\frac{i}{v^2}\bar{e}_i\gamma_\mu e_j H^\dagger\overleftrightarrow{D}_\mu H$
$[\mathcal{O}_{Hq}]_{ij}$	$\frac{i}{v^2}\bar{q}_i\gamma_\mu q_j H^\dagger\overleftrightarrow{D}_\mu H$
$\left[\mathcal{O}'_{Hq}\right]_{ij}$	$\frac{i}{v^2}\bar{q}_i\sigma^k\gamma_\mu q_j H^\dagger\sigma^k\overleftrightarrow{D}_\mu H$
$[\mathcal{O}_{Hu}]_{ij}$	$\frac{i}{v^2}\bar{u}_i\gamma_\mu u_j H^\dagger\overleftrightarrow{D}_\mu H$
$[\mathcal{O}_{Hd}]_{ij}$	$\frac{i}{v^2}\bar{d}_i\gamma_\mu d_j H^\dagger\overleftrightarrow{D}_\mu H$
$[\mathcal{O}_{Hud}]_{ij}$	$\frac{i}{v^2}\bar{u}_i\gamma_\mu d_j H^\dagger\overleftrightarrow{D}_\mu H$

Table B.2: Two-fermion operators of the SILH basis

Dipole operators

$[\mathcal{O}_{eW}]_{ij}$	$\frac{g_2}{M_W^2}\frac{\sqrt{2m_{e_i}m_{e_j}}}{v}\bar{\ell}_i\sigma^k H\sigma_{\mu\nu}e_j W^k_{\mu\nu}$
$[\mathcal{O}_{eB}]_{ij}$	$\frac{g_1}{M_W^2}\frac{\sqrt{2m_{e_i}m_{e_j}}}{v}\bar{\ell}_i H\sigma_{\mu\nu}e_j B_{\mu\nu}$
$[\mathcal{O}_{uW}]_{ij}$	$\frac{g_2}{M_W^2}\frac{\sqrt{2m_{u_i}m_{u_j}}}{v}\bar{q}_i\sigma^k \tilde{H}\sigma_{\mu\nu}u_j W^k_{\mu\nu}$
$[\mathcal{O}_{uB}]_{ij}$	$\frac{g_1}{M_W^2}\frac{\sqrt{2m_{u_i}m_{u_j}}}{v}\bar{q}_i\tilde{H}\sigma_{\mu\nu}u_j B_{\mu\nu}$
$[\mathcal{O}_{dW}]_{ij}$	$\frac{g_2}{M_W^2}\frac{\sqrt{2m_{d_i}m_{d_j}}}{v}\bar{q}_i\sigma^k H\sigma_{\mu\nu}d_j W^k_{\mu\nu}$
$[\mathcal{O}_{dB}]_{ij}$	$\frac{g_1}{M_W^2}\frac{\sqrt{2m_{d_i}m_{d_j}}}{v}\bar{q}_i H\sigma_{\mu\nu}d_j B_{\mu\nu}$

Table B.3: Two-fermion operators of the SILH basis which give rise to dipole interactions

Acknowledgments

- I am very greatful to Fulvio for the opportunity to work under his guidance over the last three year. I am also greatful to Guido and Oreste for the academic and non academic support and for they patience when I came to them in the search of suggestions.

- I want to thank Carlo and Ambresh for the fruitful collaboration and for being not only extraordinary colleagues but also very good friends.

- A necessary thanks goes to Mauro Chiesa for the stimulating discussions and to Anastasija for the final proof reading.

- I want also to offer my special thanks to Valeria and Homero simply because they have been very special friends.

- I would like to extend my deepest gratitude to my family. Without their encouragement and support, this work would have not been possible.

- Last but not least I want to thank Gaia because she is part of my life.

Bibliography

[1] S. L. Glashow, *Partial Symmetries of Weak Interactions*, *Nucl. Phys.*
22 (1961) 579–588.

[2] A. Salam, *Weak and Electromagnetic Interactions*, *Conf. Proc.*
C680519 (1968) 367–377.

[3] S. Weinberg, *A Model of Leptons*, *Phys. Rev. Lett.* **19** (1967)
1264–1266.

[4] H. Fritzsch, M. Gell-Mann, and H. Leutwyler, *Advantages of the
Color Octet Gluon Picture*, *Phys. Lett.* **B47** (1973) 365–368.

[5] D. J. Gross and F. Wilczek, *Ultraviolet Behavior of Nonabelian Gauge
Theories*, *Phys. Rev. Lett.* **30** (1973) 1343–1346.

[6] H. D. Politzer, *Reliable Perturbative Results for Strong Interactions?*,
Phys. Rev. Lett. **30** (1973) 1346–1349.

[7] F. Englert and R. Brout, *Broken symmetry and the mass of gauge
vector mesons*, *Phys. Rev. Lett.* **13** (Aug, 1964) 321–323.

[8] P. Higgs, *Broken symmetries, massless particles and gauge fields*,
Physics Letters **12** (1964), no. 2 132 – 133.

[9] P. W. Higgs, *Broken symmetries and the masses of gauge bosons*,
Phys. Rev. Lett. **13** (Oct, 1964) 508–509.

[10] G. S. Guralnik, C. R. Hagen, and T. W. B. Kibble, *Global
conservation laws and massless particles*, *Phys. Rev. Lett.* **13** (Nov,
1964) 585–587.

[11] P. W. Higgs, *Spontaneous symmetry breakdown without massless bosons*, Phys. Rev. **145** (May, 1966) 1156–1163.

[12] T. W. B. Kibble, *Symmetry breaking in non-abelian gauge theories*, Phys. Rev. **155** (Mar, 1967) 1554–1561.

[13] G. 't Hooft, *Renormalization of Massless Yang-Mills Fields*, Nucl. Phys. **B33** (1971) 173–199.

[14] G. 't Hooft, *Renormalizable Lagrangians for Massive Yang-Mills Fields*, Nucl. Phys. **B35** (1971) 167–188.

[15] G. 't Hooft and M. J. G. Veltman, *Regularization and Renormalization of Gauge Fields*, Nucl. Phys. **B44** (1972) 189–213.

[16] C. H. Llewellyn Smith, *High-Energy Behavior and Gauge Symmetry*, Phys. Lett. **B46** (1973) 233–236.

[17] J. S. Bell, *HIGH-ENERGY BEHAVIOR OF TREE DIAGRAMS IN GAUGE THEORIES*, Nucl. Phys. **B60** (1973) 427–436.

[18] J. M. Cornwall, D. N. Levin, and G. Tiktopoulos, *Uniqueness of spontaneously broken gauge theories*, Phys. Rev. Lett. **30** (1973) 1268–1270. [Erratum: Phys. Rev. Lett.31,572(1973)].

[19] J. M. Cornwall, D. N. Levin, and G. Tiktopoulos, *Derivation of Gauge Invariance from High-Energy Unitarity Bounds on the s Matrix*, Phys. Rev. **D10** (1974) 1145. [Erratum: Phys. Rev.D11,972(1975)].

[20] **Gargamelle Neutrino** Collaboration, F. J. Hasert et al., *Observation of Neutrino Like Interactions Without Muon Or Electron in the Gargamelle Neutrino Experiment*, Phys. Lett. **B46** (1973) 138–140.

[21] **Gargamelle Neutrino** Collaboration, F. J. Hasert et al., *Observation of Neutrino Like Interactions without Muon or Electron in the Gargamelle Neutrino Experiment*, Nucl. Phys. **B73** (1974) 1–22.

[22] T. Eichten et al., *Measurement of the Neutrino - Nucleon Anti-neutrino - Nucleon Total Cross-sections*, Phys. Lett. **B46** (1973) 274–280.

[23] **ATLAS Collaboration** Collaboration, G. Aad et al., *Observation of a new particle in the search for the Standard Model Higgs boson with the ATLAS detector at the LHC, Phys.Lett.* **B716** (2012) 1–29, [`arXiv:1207.7214`].

[24] **CMS Collaboration** Collaboration, S. Chatrchyan et al., *Observation of a new boson at a mass of 125 GeV with the CMS experiment at the LHC, Phys.Lett.* **B716** (2012) 30–61, [`arXiv:1207.7235`].

[25] **LHC Higgs Cross Section Working Group** Collaboration, S. Dittmaier et al., *Handbook of LHC Higgs Cross Sections: 1. Inclusive Observables,* `arXiv:1101.0593`.

[26] S. Dittmaier, S. Dittmaier, C. Mariotti, G. Passarino, R. Tanaka, et al., *Handbook of LHC Higgs Cross Sections: 2. Differential Distributions,* `arXiv:1201.3084`.

[27] **LHC Higgs Cross Section Working Group** Collaboration, S. Heinemeyer et al., *Handbook of LHC Higgs Cross Sections: 3. Higgs Properties,* `arXiv:1307.1347`.

[28] D. E. De Florian Sabaris, C. Grojean, F. Maltoni, C. Mariotti, A. Nikitenko, M. Pieri, P. Savard, M. Schumacher, and R. Tanaka, *Handbook of LHC Higgs cross sections: 4. Deciphering the nature of the Higgs sector,* .

[29] **ATLAS, CMS** Collaboration, G. Aad et al., *Combined Measurement of the Higgs Boson Mass in pp Collisions at $\sqrt{s} = 7$ and 8 TeV with the ATLAS and CMS Experiments, Phys. Rev. Lett.* **114** (2015) 191803, [`arXiv:1503.07589`].

[30] **CMS** Collaboration, V. Khachatryan et al., *Constraints on the spin-parity and anomalous HVV couplings of the Higgs boson in proton collisions at 7 and 8 TeV, Phys. Rev.* **D92** (2015), no. 1 012004, [`arXiv:1411.3441`].

[31] **ATLAS** Collaboration, G. Aad et al., *Study of the spin and parity of the Higgs boson in diboson decays with the ATLAS detector, Eur. Phys. J.* **C75** (2015), no. 10 476, [`arXiv:1506.05669`]. [Erratum: Eur. Phys. J.C76,no.3,152(2016)].

[32] **ATLAS, CMS** Collaboration, G. Aad et al., *Measurements of the Higgs boson production and decay rates and constraints on its*

couplings from a combined ATLAS and CMS analysis of the LHC pp collision data at $\sqrt{s}$ = *7 and 8 TeV*, `arXiv:1606.02266`.

[33] S. Dawson et al., *Working Group Report: Higgs Boson*, in *Community Summer Study 2013: Snowmass on the Mississippi (CSS2013) Minneapolis, MN, USA, July 29-August 6, 2013*, 2013. `arXiv:1310.8361`.

[34] **ATLAS** Collaboration, *Physics at a High-Luminosity LHC with ATLAS*, in *Community Summer Study 2013: Snowmass on the Mississippi (CSS2013) Minneapolis, MN, USA, July 29-August 6, 2013*, 2013. `arXiv:1307.7292`.

[35] **CMS** Collaboration, *Projected Performance of an Upgraded CMS Detector at the LHC and HL-LHC: Contribution to the Snowmass Process*, in *Community Summer Study 2013: Snowmass on the Mississippi (CSS2013) Minneapolis, MN, USA, July 29-August 6, 2013*, 2013. `arXiv:1307.7135`.

[36] S. Boselli, C. M. Carloni Calame, G. Montagna, O. Nicrosini, and F. Piccinini, *Higgs boson decay into four leptons at NLOPS electroweak accuracy*, *JHEP* **06** (2015) 023, [`arXiv:1503.07394`].

[37] F. Piccinini, C. Carloni Calame, G. Montagna, O. Nicrosini, M. Moretti, et al., *QED corrections to Higgs boson decay into four leptons at the LHC*, *PoS* **HEP2005** (2006) 307.

[38] C. Carloni Calame, M. Moretti, G. Montagna, O. Nicrosini, F. Piccinini, et al., *Impact of QED corrections to Higgs decay into four leptons at the LHC*, *Nucl.Phys.Proc.Suppl.* **157** (2006) 73–77, [`hep-ph/0604033`].

[39] A. Bredenstein, A. Denner, S. Dittmaier, and M. Weber, *Precise predictions for the Higgs-boson decay* $H \to WW/ZZ \to 4$ *leptons*, *Phys.Rev.* **D74** (2006) 013004, [`hep-ph/0604011`].

[40] A. Bredenstein, A. Denner, S. Dittmaier, and M. Weber, *Radiative corrections to the semileptonic and hadronic Higgs-boson decays* $H \to WW/ZZ \to 4$ *fermions*, *JHEP* **0702** (2007) 080, [`hep-ph/0611234`].

[41] A. Bredenstein, A. Denner, S. Dittmaier, and M. Weber, *Precision calculations for the Higgs decays* $H \to ZZ/WW \to 4$ *leptons*, *Nucl.Phys.Proc.Suppl.* **160** (2006) 131–135, [`hep-ph/0607060`].

[42] A. Bredenstein, A. Denner, S. Dittmaier, and M. Weber, *Precision calculations for $H \to WW/ZZ \to 4$ fermions with PROPHECY4f*, `arXiv:0708.4123`.

[43] A. Denner, S. Dittmaier, M. Roth, and L. Wieders, *Electroweak corrections to charged-current $e^+e^- \to 4$ fermion processes: Technical details and further results*, Nucl.Phys. **B724** (2005) 247–294, [`hep-ph/0505042`].

[44] L. D. Faddeev and V. N. Popov, *Feynman Diagrams for the Yang-Mills Field*, Phys. Lett. **B25** (1967) 29–30.

[45] D. A. Ross and J. C. Taylor, *Renormalization of a unified theory of weak and electromagnetic interactions*, Nucl. Phys. **B51** (1973) 125–144. [Erratum: Nucl. Phys.B58,643(1973)].

[46] N. Cabibbo, *Unitary Symmetry and Leptonic Decays*, Phys. Rev. Lett. **10** (1963) 531–533. [,648(1963)].

[47] M. Kobayashi and T. Maskawa, *CP Violation in the Renormalizable Theory of Weak Interaction*, Prog. Theor. Phys. **49** (1973) 652–657.

[48] A. Denner, *Techniques for calculation of electroweak radiative corrections at the one loop level and results for W physics at LEP-200*, Fortsch. Phys. **41** (1993) 307–420, [`arXiv:0709.1075`].

[49] R. E. Behrends, R. J. Finkelstein, and A. Sirlin, *Radiative corrections to decay processes*, Phys. Rev. **101** (1956) 866–873.

[50] T. Kinoshita and A. Sirlin, *Radiative corrections to Fermi interactions*, Phys. Rev. **113** (1959) 1652–1660.

[51] A. Denner and S. Dittmaier, *The Complex-mass scheme for perturbative calculations with unstable particles*, Nucl.Phys.Proc.Suppl. **160** (2006) 22–26, [`hep-ph/0605312`].

[52] A. Denner, S. Dittmaier, M. Roth, and L. Wieders, *Erratum to "complete electroweak corrections to charged-current fermion processes" [phys. lett. b 612 (2005) 223]*, Physics Letters B **704** (2011), no. 5 667 – 668.

[53] W. Beenakker, *Restoring gauge invariance in gauge boson production processes*, Acta Phys. Polon. **B28** (1997) 679–682, [`hep-ph/9612296`].

[54] J. R. Andersen et al., *Les Houches 2013: Physics at TeV Colliders: Standard Model Working Group Report*, `arXiv:1405.1067`.

[55] R. G. Stuart, *Gauge invariance, analyticity and physical observables at the Z0 resonance*, *Phys. Lett.* **B262** (1991) 113–119.

[56] A. Aeppli, G. J. van Oldenborgh, and D. Wyler, *Unstable particles in one loop calculations*, *Nucl. Phys.* **B428** (1994) 126–146, [`hep-ph/9312212`].

[57] M. Beneke, A. P. Chapovsky, A. Signer, and G. Zanderighi, *Effective theory approach to unstable particle production*, *Phys. Rev. Lett.* **93** (2004) 011602, [`hep-ph/0312331`].

[58] M. Beneke, A. P. Chapovsky, A. Signer, and G. Zanderighi, *Effective theory calculation of resonant high-energy scattering*, *Nucl. Phys.* **B686** (2004) 205–247, [`hep-ph/0401002`].

[59] A. Denner, S. Dittmaier, M. Roth, and D. Wackeroth, *Predictions for all processes e+ e- —> 4 fermions + gamma*, *Nucl. Phys.* **B560** (1999) 33–65, [`hep-ph/9904472`].

[60] A. Sirlin, *Theoretical considerations concerning the Z0 mass*, *Phys. Rev. Lett.* **67** (1991) 2127–2130.

[61] P. Gambino and P. A. Grassi, *The Nielsen identities of the SM and the definition of mass*, *Phys. Rev.* **D62** (2000) 076002, [`hep-ph/9907254`].

[62] **Particle Data Group** Collaboration, K. A. Olive et al., *Review of Particle Physics*, *Chin. Phys.* **C38** (2014) 090001.

[63] M. Böhm, A. Denner, and H. Joos, *Gauge Theories of the Strong and Electroweak Interaction*. Teubner, Stuttgart and Leipzig and Wiesbaden, 3rd ed., 2001.

[64] D. R. Yennie, S. C. Frautschi, and H. Suura, *The infrared divergence phenomena and high-energy processes*, *Annals Phys.* **13** (1961) 379–452.

[65] S. Weinberg, *Infrared photons and gravitons*, *Phys. Rev.* **140** (1965) B516–B524.

[66] F. Bloch and A. Nordsieck, *Note on the Radiation Field of the electron*, *Phys. Rev.* **52** (1937) 54–59.

[67] T. Kinoshita, *Mass singularities of Feynman amplitudes, J. Math. Phys.* **3** (1962) 650–677.

[68] T. D. Lee and M. Nauenberg, *Degenerate Systems and Mass Singularities, Phys. Rev.* **133** (1964) B1549–B1562. [,25(1964)].

[69] V. N. Gribov and L. N. Lipatov, *Deep inelastic e p scattering in perturbation theory, Sov. J. Nucl. Phys.* **15** (1972) 438–450. [Yad. Fiz.15,781(1972)].

[70] Y. L. Dokshitzer, *Calculation of the Structure Functions for Deep Inelastic Scattering and e+ e- Annihilation by Perturbation Theory in Quantum Chromodynamics., Sov. Phys. JETP* **46** (1977) 641–653. [Zh. Eksp. Teor. Fiz.73,1216(1977)].

[71] G. Altarelli and G. Parisi, *Asymptotic Freedom in Parton Language, Nucl. Phys.* **B126** (1977) 298–318.

[72] G. Montagna, O. Nicrosini, and F. Piccinini, *Precision physics at LEP, Riv. Nuovo Cim.* **21N9** (1998) 1–162, [`hep-ph/9802302`].

[73] C. M. Carloni Calame, *An Improved parton shower algorithm in QED, Phys. Lett.* **B520** (2001) 16–24, [`hep-ph/0103117`].

[74] **SLD Electroweak Group, DELPHI, LEP, ALEPH, SLD Heavy Flavour Group, OPAL, LEP Electroweak Working Group, L3** Collaboration, *A Combination of preliminary electroweak measurements and constraints on the standard model,* `hep-ex/0412015`.

[75] **OPAL, DELPHI, LEP Working Group for Higgs boson searches, ALEPH, L3** Collaboration, R. Barate et al., *Search for the standard model Higgs boson at LEP, Phys. Lett.* **B565** (2003) 61–75, [`hep-ex/0306033`].

[76] **CDF, D0** Collaboration, T. Aaltonen et al., *Higgs Boson Studies at the Tevatron, Phys. Rev.* **D88** (2013), no. 5 052014, [`arXiv:1303.6346`].

[77] J. Goldstone, A. Salam, and S. Weinberg, *Broken Symmetries, Phys. Rev.* **127** (1962) 965–970.

[78] M. S. Chanowitz and M. K. Gaillard, *The TeV Physics of Strongly Interacting W's and Z's, Nucl. Phys.* **B261** (1985) 379–431.

[79] B. W. Lee, C. Quigg, and H. B. Thacker, *Weak Interactions at Very High-Energies: The Role of the Higgs Boson Mass*, Phys. Rev. **D16** (1977) 1519.

[80] A. Djouadi, *The Anatomy of electro-weak symmetry breaking. I: The Higgs boson in the standard model*, Phys. Rept. **457** (2008) 1–216, [hep-ph/0503172].

[81] T. Hambye and K. Riesselmann, *Matching conditions and Higgs mass upper bounds revisited*, Phys. Rev. **D55** (1997) 7255–7262, [hep-ph/9610272].

[82] G. Degrassi, S. Di Vita, J. Elias-Miro, J. R. Espinosa, G. F. Giudice, G. Isidori, and A. Strumia, *Higgs mass and vacuum stability in the Standard Model at NNLO*, JHEP **08** (2012) 098, [arXiv:1205.6497].

[83] H. M. Georgi, S. L. Glashow, M. E. Machacek, and D. V. Nanopoulos, *Higgs Bosons from Two Gluon Annihilation in Proton Proton Collisions*, Phys. Rev. Lett. **40** (1978) 692.

[84] A. Djouadi, M. Spira, and P. M. Zerwas, *Production of Higgs bosons in proton colliders: QCD corrections*, Phys. Lett. **B264** (1991) 440–446.

[85] D. Graudenz, M. Spira, and P. M. Zerwas, *QCD corrections to Higgs boson production at proton proton colliders*, Phys. Rev. Lett. **70** (1993) 1372–1375.

[86] M. Spira, A. Djouadi, D. Graudenz, and P. M. Zerwas, *Higgs boson production at the LHC*, Nucl. Phys. **B453** (1995) 17–82, [hep-ph/9504378].

[87] R. V. Harlander and W. B. Kilgore, *Next-to-next-to-leading order Higgs production at hadron colliders*, Phys. Rev. Lett. **88** (2002) 201801, [hep-ph/0201206].

[88] C. Anastasiou and K. Melnikov, *Higgs boson production at hadron colliders in NNLO QCD*, Nucl. Phys. **B646** (2002) 220–256, [hep-ph/0207004].

[89] V. Ravindran, J. Smith, and W. L. van Neerven, *NNLO corrections to the total cross-section for Higgs boson production in hadron hadron collisions*, Nucl. Phys. **B665** (2003) 325–366, [hep-ph/0302135].

[90] C. Anastasiou, C. Duhr, F. Dulat, F. Herzog, and B. Mistlberger, *Higgs Boson Gluon-Fusion Production in QCD at Three Loops*, Phys. Rev. Lett. **114** (2015) 212001, [arXiv:1503.06056].

[91] C. Anastasiou, C. Duhr, F. Dulat, E. Furlan, T. Gehrmann, F. Herzog, A. Lazopoulos, and B. Mistlberger, *High precision determination of the gluon fusion Higgs boson cross-section at the LHC*, JHEP **05** (2016) 058, [arXiv:1602.00695].

[92] R. V. Harlander and K. J. Ozeren, *Finite top mass effects for hadronic Higgs production at next-to-next-to-leading order*, JHEP **11** (2009) 088, [arXiv:0909.3420].

[93] A. Pak, M. Rogal, and M. Steinhauser, *Finite top quark mass effects in NNLO Higgs boson production at LHC*, JHEP **02** (2010) 025, [arXiv:0911.4662].

[94] R. V. Harlander and K. J. Ozeren, *Top mass effects in Higgs production at next-to-next-to-leading order QCD: Virtual corrections*, Phys. Lett. **B679** (2009) 467–472, [arXiv:0907.2997].

[95] R. V. Harlander, H. Mantler, S. Marzani, and K. J. Ozeren, *Higgs production in gluon fusion at next-to-next-to-leading order QCD for finite top mass*, Eur. Phys. J. **C66** (2010) 359–372, [arXiv:0912.2104].

[96] U. Aglietti, R. Bonciani, G. Degrassi, and A. Vicini, *Two loop light fermion contribution to Higgs production and decays*, Phys. Lett. **B595** (2004) 432–441, [hep-ph/0404071].

[97] S. Actis, G. Passarino, C. Sturm, and S. Uccirati, *NLO Electroweak Corrections to Higgs Boson Production at Hadron Colliders*, Phys. Lett. **B670** (2008) 12–17, [arXiv:0809.1301].

[98] S. Actis, G. Passarino, C. Sturm, and S. Uccirati, *NNLO Computational Techniques: The Cases H —> gamma gamma and H —> g g*, Nucl. Phys. **B811** (2009) 182–273, [arXiv:0809.3667].

[99] C. Anastasiou, R. Boughezal, and F. Petriello, *Mixed QCD-electroweak corrections to Higgs boson production in gluon fusion*, JHEP **04** (2009) 003, [arXiv:0811.3458].

[100] J. Butterworth et al., *PDF4LHC recommendations for LHC Run II*, J. Phys. **G43** (2016) 023001, [arXiv:1510.03865].

[101] M. Bonvini, S. Marzani, C. Muselli, and L. Rottoli, *On the Higgs cross section at N^3LO+N^3LL and its uncertainty*, *JHEP* **08** (2016) 105, [arXiv:1603.08000].

[102] D. de Florian, G. Ferrera, M. Grazzini, and D. Tommasini, *Higgs boson production at the LHC: transverse momentum resummation effects in the H->2gamma, H->WW->lnu lnu and H->ZZ->4l decay modes*, *JHEP* **06** (2012) 132, [arXiv:1203.6321].

[103] T. Becher, M. Neubert, and D. Wilhelm, *Higgs-Boson Production at Small Transverse Momentum*, *JHEP* **05** (2013) 110, [arXiv:1212.2621].

[104] M. Grazzini and H. Sargsyan, *Heavy-quark mass effects in Higgs boson production at the LHC*, *JHEP* **09** (2013) 129, [arXiv:1306.4581].

[105] X. Chen, T. Gehrmann, E. W. N. Glover, and M. Jaquier, *Precise QCD predictions for the production of Higgs + jet final states*, *Phys. Lett.* **B740** (2015) 147–150, [arXiv:1408.5325].

[106] D. Neill, I. Z. Rothstein, and V. Vaidya, *The Higgs Transverse Momentum Distribution at NNLL and its Theoretical Errors*, *JHEP* **12** (2015) 097, [arXiv:1503.00005].

[107] A. Banfi, F. Caola, F. A. Dreyer, P. F. Monni, G. P. Salam, G. Zanderighi, and F. Dulat, *Jet-vetoed Higgs cross section in gluon fusion at $N^3LO+NNLL$ with small-R resummation*, *JHEP* **04** (2016) 049, [arXiv:1511.02886].

[108] G. Cullen, H. van Deurzen, N. Greiner, G. Luisoni, P. Mastrolia, E. Mirabella, G. Ossola, T. Peraro, and F. Tramontano, *Next-to-Leading-Order QCD Corrections to Higgs Boson Production Plus Three Jets in Gluon Fusion*, *Phys. Rev. Lett.* **111** (2013), no. 13 131801, [arXiv:1307.4737].

[109] H. van Deurzen, N. Greiner, G. Luisoni, P. Mastrolia, E. Mirabella, G. Ossola, T. Peraro, J. F. von Soden-Fraunhofen, and F. Tramontano, *NLO QCD corrections to the production of Higgs plus two jets at the LHC*, *Phys. Lett.* **B721** (2013) 74–81, [arXiv:1301.0493].

[110] J. Alwall, R. Frederix, S. Frixione, V. Hirschi, F. Maltoni, O. Mattelaer, H. S. Shao, T. Stelzer, P. Torrielli, and M. Zaro, *The automated computation of tree-level and next-to-leading order*

differential cross sections, and their matching to parton shower simulations, *JHEP* **07** (2014) 079, [arXiv:1405.0301].

[111] K. Hamilton, P. Nason, and G. Zanderighi, *Finite quark-mass effects in the NNLOPS POWHEG+MiNLO Higgs generator*, *JHEP* **05** (2015) 140, [arXiv:1501.04637].

[112] V. D. Barger, R. J. N. Phillips, and D. Zeppenfeld, *Mini - jet veto: A Tool for the heavy Higgs search at the LHC*, *Phys. Lett.* **B346** (1995) 106–114, [hep-ph/9412276].

[113] V. Del Duca, G. Klamke, D. Zeppenfeld, M. L. Mangano, M. Moretti, F. Piccinini, R. Pittau, and A. D. Polosa, *Monte Carlo studies of the jet activity in Higgs + 2 jet events*, *JHEP* **10** (2006) 016, [hep-ph/0608158].

[114] M. Ciccolini, A. Denner, and S. Dittmaier, *Strong and electroweak corrections to the production of Higgs + 2jets via weak interactions at the LHC*, *Phys. Rev. Lett.* **99** (2007) 161803, [arXiv:0707.0381].

[115] M. Ciccolini, A. Denner, and S. Dittmaier, *Electroweak and QCD corrections to Higgs production via vector-boson fusion at the LHC*, *Phys. Rev.* **D77** (2008) 013002, [arXiv:0710.4749].

[116] K. Arnold et al., *VBFNLO: A Parton level Monte Carlo for processes with electroweak bosons*, *Comput. Phys. Commun.* **180** (2009) 1661–1670, [arXiv:0811.4559].

[117] K. Arnold et al., *VBFNLO: A Parton Level Monte Carlo for Processes with Electroweak Bosons – Manual for Version 2.5.0*, arXiv:1107.4038.

[118] J. Baglio et al., *Release Note - VBFNLO 2.7.0*, arXiv:1404.3940.

[119] P. Nason and C. Oleari, *NLO Higgs boson production via vector-boson fusion matched with shower in POWHEG*, *JHEP* **02** (2010) 037, [arXiv:0911.5299].

[120] S. Frixione, P. Nason, and C. Oleari, *Matching NLO QCD computations with Parton Shower simulations: the POWHEG method*, *JHEP* **0711** (2007) 070, [arXiv:0709.2092].

[121] B. Jäger, F. Schissler, and D. Zeppenfeld, *Parton-shower effects on Higgs boson production via vector-boson fusion in association with three jets*, *JHEP* **07** (2014) 125, [arXiv:1405.6950].

[122] S. Frixione, P. Torrielli, and M. Zaro, *Higgs production through vector-boson fusion at the NLO matched with parton showers, Phys. Lett.* **B726** (2013) 273–282, [`arXiv:1304.7927`].

[123] F. Maltoni, K. Mawatari, and M. Zaro, *Higgs characterisation via vector-boson fusion and associated production: NLO and parton-shower effects, Eur. Phys. J.* **C74** (2014), no. 1 2710, [`arXiv:1311.1829`].

[124] P. Bolzoni, F. Maltoni, S.-O. Moch, and M. Zaro, *Higgs production via vector-boson fusion at NNLO in QCD, Phys. Rev. Lett.* **105** (2010) 011801, [`arXiv:1003.4451`].

[125] P. Bolzoni, F. Maltoni, S.-O. Moch, and M. Zaro, *Vector boson fusion at NNLO in QCD: SM Higgs and beyond, Phys. Rev.* **D85** (2012) 035002, [`arXiv:1109.3717`].

[126] A. Stange, W. J. Marciano, and S. Willenbrock, *Associated production of Higgs and weak bosons, with H —> b anti-b, at hadron colliders, Phys. Rev.* **D50** (1994) 4491–4498, [`hep-ph/9404247`].

[127] M. L. Ciccolini, S. Dittmaier, and M. Kramer, *Electroweak radiative corrections to associated WH and ZH production at hadron colliders, Phys. Rev.* **D68** (2003) 073003, [`hep-ph/0306234`].

[128] A. Denner, S. Dittmaier, S. Kallweit, and A. Muck, *Electroweak corrections to Higgs-strahlung off W/Z bosons at the Tevatron and the LHC with HAWK, JHEP* **03** (2012) 075, [`arXiv:1112.5142`].

[129] R. Hamberg, W. L. van Neerven, and T. Matsuura, *A complete calculation of the order $\alpha - s^2$ correction to the Drell-Yan K factor, Nucl. Phys.* **B359** (1991) 343–405. [Erratum: Nucl. Phys.B644,403(2002)].

[130] O. Brein, A. Djouadi, and R. Harlander, *NNLO QCD corrections to the Higgs-strahlung processes at hadron colliders, Phys. Lett.* **B579** (2004) 149–156, [`hep-ph/0307206`].

[131] L. Altenkamp, S. Dittmaier, R. V. Harlander, H. Rzehak, and T. J. E. Zirke, *Gluon-induced Higgs-strahlung at next-to-leading order QCD, JHEP* **02** (2013) 078, [`arXiv:1211.5015`].

[132] O. Brein, R. Harlander, M. Wiesemann, and T. Zirke, *Top-Quark Mediated Effects in Hadronic Higgs-Strahlung, Eur. Phys. J.* **C72** (2012) 1868, [`arXiv:1111.0761`].

[133] R. Frederix and S. Frixione, *Merging meets matching in MC@NLO*, *JHEP* **12** (2012) 061, [arXiv:1209.6215].

[134] R. Boughezal, J. M. Campbell, R. K. Ellis, C. Focke, W. Giele, X. Liu, F. Petriello, and C. Williams, *Color Singlet Production at NNLO in MCFM, Submitted to: JHEP* (2016) [arXiv:1605.08011].

[135] M. C. Kumar, M. K. Mandal, and V. Ravindran, *Associated production of Higgs boson with vector boson at threshold N^3LO in QCD*, *JHEP* **03** (2015) 037, [arXiv:1412.3357].

[136] O. Brein, R. V. Harlander, and T. J. E. Zirke, *vh@nnlo - Higgs Strahlung at hadron colliders*, *Comput. Phys. Commun.* **184** (2013) 998–1003, [arXiv:1210.5347].

[137] R. Raitio and W. W. Wada, *Higgs Boson Production at Large Transverse Momentum in QCD*, *Phys. Rev.* **D19** (1979) 941.

[138] J. N. Ng and P. Zakarauskas, *A QCD Parton Calculation of Conjoined Production of Higgs Bosons and Heavy Flavors in $p\bar{p}$ Collision*, *Phys. Rev.* **D29** (1984) 876.

[139] J. F. Gunion, *Associated top anti-top Higgs production as a large source of W H events: Implications for Higgs detection in the lepton neutrino gamma gamma final state*, *Phys. Lett.* **B261** (1991) 510–517.

[140] W. J. Marciano and F. E. Paige, *Associated production of Higgs bosons with t anti-t pairs*, *Phys. Rev. Lett.* **66** (1991) 2433–2435.

[141] W. Beenakker, S. Dittmaier, M. Kramer, B. Plumper, M. Spira, and P. M. Zerwas, *Higgs radiation off top quarks at the Tevatron and the LHC*, *Phys. Rev. Lett.* **87** (2001) 201805, [hep-ph/0107081].

[142] L. Reina and S. Dawson, *Next-to-leading order results for t anti-t h production at the Tevatron*, *Phys. Rev. Lett.* **87** (2001) 201804, [hep-ph/0107101].

[143] L. Reina, S. Dawson, and D. Wackeroth, *QCD corrections to associated t anti-t h production at the Tevatron*, *Phys. Rev.* **D65** (2002) 053017, [hep-ph/0109066].

[144] S. Dawson, L. H. Orr, L. Reina, and D. Wackeroth, *Associated top quark Higgs boson production at the LHC*, *Phys. Rev.* **D67** (2003) 071503, [hep-ph/0211438].

[145] W. Beenakker, S. Dittmaier, M. Kramer, B. Plumper, M. Spira, and P. M. Zerwas, *NLO QCD corrections to t anti-t H production in hadron collisions, Nucl. Phys.* **B653** (2003) 151–203, [hep-ph/0211352].

[146] R. Frederix, S. Frixione, V. Hirschi, F. Maltoni, R. Pittau, and P. Torrielli, *Scalar and pseudoscalar Higgs production in association with a top–antitop pair, Phys. Lett.* **B701** (2011) 427–433, [arXiv:1104.5613].

[147] M. V. Garzelli, A. Kardos, C. G. Papadopoulos, and Z. Trocsanyi, *Standard Model Higgs boson production in association with a top anti-top pair at NLO with parton showering, Europhys. Lett.* **96** (2011) 11001, [arXiv:1108.0387].

[148] H. B. Hartanto, B. Jager, L. Reina, and D. Wackeroth, *Higgs boson production in association with top quarks in the POWHEG BOX, Phys. Rev.* **D91** (2015), no. 9 094003, [arXiv:1501.04498].

[149] F. Cascioli, P. Maierhofer, and S. Pozzorini, *Scattering Amplitudes with Open Loops, Phys. Rev. Lett.* **108** (2012) 111601, [arXiv:1111.5206].

[150] F. Cascioli, S. Höche, F. Krauss, P. Maierhöfer, S. Pozzorini, and F. Siegert, *Precise Higgs-background predictions: merging NLO QCD and squared quark-loop corrections to four-lepton + 0,1 jet production, JHEP* **01** (2014) 046, [arXiv:1309.0500].

[151] Y. Zhang, W.-G. Ma, R.-Y. Zhang, C. Chen, and L. Guo, *QCD NLO and EW NLO corrections to $t\bar{t}H$ production with top quark decays at hadron collider, Phys. Lett.* **B738** (2014) 1–5, [arXiv:1407.1110].

[152] S. Frixione, V. Hirschi, D. Pagani, H. S. Shao, and M. Zaro, *Weak corrections to Higgs hadroproduction in association with a top-quark pair, JHEP* **09** (2014) 065, [arXiv:1407.0823].

[153] S. Frixione, V. Hirschi, D. Pagani, H. S. Shao, and M. Zaro, *Electroweak and QCD corrections to top-pair hadroproduction in association with heavy bosons, JHEP* **06** (2015) 184, [arXiv:1504.03446].

[154] P. Ciafaloni and D. Comelli, *Sudakov enhancement of electroweak corrections, Phys. Lett.* **B446** (1999) 278–284, [hep-ph/9809321].

[155] G. Degrassi, P. P. Giardino, F. Maltoni, and D. Pagani, *Probing the Higgs self coupling via single Higgs production at the LHC*, `arXiv:1607.04251`.

[156] A. Denner, S. Heinemeyer, I. Puljak, D. Rebuzzi, and M. Spira, *Standard Model Higgs-Boson Branching Ratios with Uncertainties*, *Eur. Phys. J.* **C71** (2011) 1753, [`arXiv:1107.5909`].

[157] A. Djouadi, J. Kalinowski, and M. Spira, *HDECAY: A Program for Higgs boson decays in the standard model and its supersymmetric extension, Comput. Phys. Commun.* **108** (1998) 56–74, [`hep-ph/9704448`].

[158] J. M. Butterworth et al., *THE TOOLS AND MONTE CARLO WORKING GROUP Summary Report from the Les Houches 2009 Workshop on TeV Colliders*, in *Physics at TeV colliders. Proceedings, 6th Workshop, dedicated to Thomas Binoth, Les Houches, France, June 8-26, 2009*, 2010. `arXiv:1003.1643`.

[159] P. A. Baikov, K. G. Chetyrkin, and J. H. Kuhn, *Scalar correlator at O(alpha(s)**4), Higgs decay into b-quarks and bounds on the light quark masses, Phys. Rev. Lett.* **96** (2006) 012003, [`hep-ph/0511063`].

[160] E. Braaten and J. P. Leveille, *Higgs Boson Decay and the Running Mass, Phys. Rev.* **D22** (1980) 715.

[161] N. Sakai, *Perturbative QCD Corrections to the Hadronic Decay Width of the Higgs Boson, Phys. Rev.* **D22** (1980) 2220.

[162] T. Inami and T. Kubota, *Renormalization Group Estimate of the Hadronic Decay Width of the Higgs Boson, Nucl. Phys.* **B179** (1981) 171–188.

[163] S. G. Gorishnii, A. L. Kataev, and S. A. Larin, *The Width of Higgs Boson Decay Into Hadrons: Three Loop Corrections of Strong Interactions, Sov. J. Nucl. Phys.* **40** (1984) 329–334. [Yad. Fiz.40,517(1984)].

[164] M. Drees and K.-i. Hikasa, *Heavy Quark Thresholds in Higgs Physics, Phys. Rev.* **D41** (1990) 1547.

[165] M. Drees and K.-i. Hikasa, *NOTE ON QCD CORRECTIONS TO HADRONIC HIGGS DECAY, Phys. Lett.* **B240** (1990) 455. [Erratum: Phys. Lett.B262,497(1991)].

[166] P. A. Baikov and K. G. Chetyrkin, *Top Quark Mediated Higgs Boson Decay into Hadrons to Order α_s^5*, Phys. Rev. Lett. **97** (2006) 061803, [hep-ph/0604194].

[167] U. Aglietti, R. Bonciani, G. Degrassi, and A. Vicini, *Master integrals for the two-loop light fermion contributions to gg —> H and H —> gamma gamma*, Phys. Lett. **B600** (2004) 57–64, [hep-ph/0407162].

[168] G. Degrassi and F. Maltoni, *Two-loop electroweak corrections to Higgs production at hadron colliders*, Phys. Lett. **B600** (2004) 255–260, [hep-ph/0407249].

[169] G. Degrassi and F. Maltoni, *Two-loop electroweak corrections to the Higgs-boson decay H —> gamma gamma*, Nucl. Phys. **B724** (2005) 183–196, [hep-ph/0504137].

[170] M. Spira, A. Djouadi, and P. M. Zerwas, *QCD corrections to the H Z gamma coupling*, Phys. Lett. **B276** (1992) 350–353.

[171] A. Ghinculov, *Two loop heavy Higgs correction to Higgs decay into vector bosons*, Nucl. Phys. **B455** (1995) 21–38, [hep-ph/9507240].

[172] A. Frink, B. A. Kniehl, D. Kreimer, and K. Riesselmann, *Heavy Higgs lifetime at two loops*, Phys. Rev. **D54** (1996) 4548–4560, [hep-ph/9606310].

[173] N. Kauer and G. Passarino, *Inadequacy of zero-width approximation for a light Higgs boson signal*, JHEP **08** (2012) 116, [arXiv:1206.4803].

[174] **ATLAS** Collaboration, G. Aad et al., *Constraints on the off-shell Higgs boson signal strength in the high-mass ZZ and WW final states with the ATLAS detector*, Eur. Phys. J. **C75** (2015), no. 7 335, [arXiv:1503.01060].

[175] **CMS** Collaboration, V. Khachatryan et al., *Constraints on the Higgs boson width from off-shell production and decay to Z-boson pairs*, Phys. Lett. **B736** (2014) 64–85, [arXiv:1405.3455].

[176] T. Plehn, D. L. Rainwater, and D. Zeppenfeld, *Determining the structure of Higgs couplings at the LHC*, Phys. Rev. Lett. **88** (2002) 051801, [hep-ph/0105325].

[177] **ATLAS** Collaboration, G. Aad et al., *Test of CP Invariance in vector-boson fusion production of the Higgs boson using the Optimal Observable method in the ditau decay channel with the ATLAS detector*, `arXiv:1602.04516`.

[178] T. Binoth, S. Karg, N. Kauer, and R. Ruckl, *Multi-Higgs boson production in the Standard Model and beyond, Phys. Rev.* **D74** (2006) 113008, [`hep-ph/0608057`].

[179] T. Plehn and M. Rauch, *The quartic higgs coupling at hadron colliders, Phys. Rev.* **D72** (2005) 053008, [`hep-ph/0507321`].

[180] F. Maltoni, E. Vryonidou, and M. Zaro, *Top-quark mass effects in double and triple Higgs production in gluon-gluon fusion at NLO, JHEP* **11** (2014) 079, [`arXiv:1408.6542`].

[181] **ATLAS** Collaboration, G. Aad et al., *Fiducial and differential cross sections of Higgs boson production measured in the four-lepton decay channel in pp collisions at $\sqrt{s}$=8 TeV with the ATLAS detector, Phys.Lett.* **B738** (2014) 234–253, [`arXiv:1408.3226`].

[182] G. 't Hooft and M. J. Veltman, *Scalar One Loop Integrals, Nucl.Phys.* **B153** (1979) 365–401.

[183] J. Vermaseren, *New features of FORM*, `math-ph/0010025`.

[184] G. Montagna, O. Nicrosini, and G. Passarino, *Analytic final state corrections to $e^+e^- \rightarrow f\bar{f}$ with realistic cuts, Phys.Lett.* **B309** (1993) 436–442.

[185] T. Hahn and M. Perez-Victoria, *Automatized one loop calculations in four-dimensions and D-dimensions, Comput.Phys.Commun.* **118** (1999) 153–165, [`hep-ph/9807565`].

[186] T. Hahn, *Automatic loop calculations with FeynArts, FormCalc, and LoopTools, Nucl.Phys.Proc.Suppl.* **89** (2000) 231–236, [`hep-ph/0005029`].

[187] A. Denner and S. Dittmaier, *Reduction of one loop tensor five point integrals, Nucl.Phys.* **B658** (2003) 175–202, [`hep-ph/0212259`].

[188] A. Denner and S. Dittmaier, *Scalar one-loop 4-point integrals, Nucl.Phys.* **B844** (2011) 199–242, [`arXiv:1005.2076`].

[189] G. Passarino and M. Veltman, *One Loop Corrections for e^+e^- Annihilation Into $\mu^+\mu^-$ in the Weinberg Model*, Nucl.Phys. **B160** (1979) 151.

[190] G. Balossini, C. M. Carloni Calame, G. Montagna, O. Nicrosini, and F. Piccinini, *Matching perturbative and parton shower corrections to Bhabha process at flavour factories*, Nucl.Phys. **B758** (2006) 227–253, [hep-ph/0607181].

[191] G. Balossini, C. Bignamini, C. C. Calame, G. Montagna, O. Nicrosini, et al., *Photon pair production at flavour factories with per mille accuracy*, Phys.Lett. **B663** (2008) 209–213, [arXiv:0801.3360].

[192] C. Carloni Calame, G. Montagna, O. Nicrosini, and A. Vicini, *Precision electroweak calculation of the charged current Drell-Yan process*, JHEP **0612** (2006) 016, [hep-ph/0609170].

[193] C. Carloni Calame, G. Montagna, O. Nicrosini, and A. Vicini, *Precision electroweak calculation of the production of a high transverse-momentum lepton pair at hadron colliders*, JHEP **0710** (2007) 109, [arXiv:0710.1722].

[194] L. Barze, G. Montagna, P. Nason, O. Nicrosini, and F. Piccinini, *Implementation of electroweak corrections in the POWHEG BOX: single W production*, JHEP **04** (2012) 037, [arXiv:1202.0465].

[195] L. Barze, G. Montagna, P. Nason, O. Nicrosini, F. Piccinini, and A. Vicini, *Neutral current Drell-Yan with combined QCD and electroweak corrections in the POWHEG BOX*, Eur. Phys. J. **C73** (2013), no. 6 2474, [arXiv:1302.4606].

[196] E. Barberio and Z. Was, *PHOTOS: A Universal Monte Carlo for QED radiative corrections. Version 2.0*, Comput.Phys.Commun. **79** (1994) 291–308.

[197] S. Alioli, P. Nason, C. Oleari, and E. Re, *NLO Higgs boson production via gluon fusion matched with shower in POWHEG*, JHEP **0904** (2009) 002, [arXiv:0812.0578].

[198] S. Alioli, P. Nason, C. Oleari, and E. Re, *A general framework for implementing NLO calculations in shower Monte Carlo programs: the POWHEG BOX*, JHEP **1006** (2010) 043, [arXiv:1002.2581].

[199] E. Boos, M. Dobbs, W. Giele, I. Hinchliffe, J. Huston, et al., *Generic user process interface for event generators*, `hep-ph/0109068`.

[200] T. Sjostrand, S. Mrenna, and P. Z. Skands, *PYTHIA 6.4 Physics and Manual*, *JHEP* **0605** (2006) 026, [`hep-ph/0603175`].

[201] A. Martin, W. Stirling, R. Thorne, and G. Watt, *Parton distributions for the LHC*, *Eur.Phys.J.* **C63** (2009) 189–285, [`arXiv:0901.0002`].

[202] D. Stolarski and R. Vega-Morales, *Directly Measuring the Tensor Structure of the Scalar Coupling to Gauge Bosons*, *Phys. Rev.* **D86** (2012) 117504, [`arXiv:1208.4840`].

[203] Y. Chen, N. Tran, and R. Vega-Morales, *Scrutinizing the Higgs Signal and Background in the $2e2\mu$ Golden Channel*, *JHEP* **01** (2013) 182, [`arXiv:1211.1959`].

[204] Y. Chen and R. Vega-Morales, *Extracting Effective Higgs Couplings in the Golden Channel*, *JHEP* **04** (2014) 057, [`arXiv:1310.2893`].

[205] M. Gonzalez-Alonso, A. Greljo, G. Isidori, and D. Marzocca, *Pseudo-observables in Higgs decays*, *Eur. Phys. J.* **C75** (2015) 128, [`arXiv:1412.6038`].

[206] M. Gonzalez-Alonso, A. Greljo, G. Isidori, and D. Marzocca, *Electroweak bounds on Higgs pseudo-observables and $h \to 4\ell$ decays*, *Eur. Phys. J.* **C75** (2015) 341, [`arXiv:1504.04018`].

[207] M. Bordone, A. Greljo, G. Isidori, D. Marzocca, and A. Pattori, *Higgs Pseudo Observables and Radiative Corrections*, *Eur. Phys. J.* **C75** (2015), no. 8 385, [`arXiv:1507.02555`].

[208] T. Appelquist and J. Carazzone, *Infrared Singularities and Massive Fields*, *Phys. Rev.* **D11** (1975) 2856.

[209] S. Weinberg, *Baryon and Lepton Nonconserving Processes*, *Phys. Rev. Lett.* **43** (1979) 1566–1570.

[210] W. Buchmuller and D. Wyler, *Effective Lagrangian Analysis of New Interactions and Flavor Conservation*, *Nucl. Phys.* **B268** (1986) 621–653.

[211] B. Grzadkowski, M. Iskrzynski, M. Misiak, and J. Rosiek, *Dimension-Six Terms in the Standard Model Lagrangian*, *JHEP* **10** (2010) 085, [`arXiv:1008.4884`].

[212] G. F. Giudice, C. Grojean, A. Pomarol, and R. Rattazzi, *The Strongly-Interacting Light Higgs*, *JHEP* **06** (2007) 045, [hep-ph/0703164].

[213] R. Contino, M. Ghezzi, C. Grojean, M. Muhlleitner, and M. Spira, *Effective Lagrangian for a light Higgs-like scalar*, *JHEP* **07** (2013) 035, [arXiv:1303.3876].

[214] R. S. Gupta, A. Pomarol, and F. Riva, *BSM Primary Effects*, *Phys. Rev.* **D91** (2015), no. 3 035001, [arXiv:1405.0181].

[215] A. Falkowski, A. T. Mendes, A. Falkowski, and G. Isidori, *Higgs Basis: Proposal for an EFT basis choice for LHC HXSWG*, .

[216] A. Alloul, N. D. Christensen, C. Degrande, C. Duhr, and B. Fuks, *FeynRules 2.0 - A complete toolbox for tree-level phenomenology*, *Comput. Phys. Commun.* **185** (2014) 2250–2300, [arXiv:1310.1921].

[217] J. Alwall, M. Herquet, F. Maltoni, O. Mattelaer, and T. Stelzer, *MadGraph 5: Going Beyond*, *JHEP* **1106** (2011) 128, [arXiv:1106.0522].

[218] A. Falkowski, *Effective field theory approach to LHC Higgs data*, *Pramana* **87** (2016), no. 3 39, [arXiv:1505.00046].

[219] M. Schonherr and F. Krauss, *Soft Photon Radiation in Particle Decays in SHERPA*, *JHEP* **0812** (2008) 018, [arXiv:0810.5071].

[220] S. Jadach, *Monte-Carlo Methods for High-Energy Phyiscs*, Lectures at the Torino School of Physics, .

[221] S. Jadach, B. Ward, and Z. Was, *The Precision Monte Carlo event generator K K for two fermion final states in e+ e- collisions*, *Comput.Phys.Commun.* **130** (2000) 260–325, [hep-ph/9912214].